Calibrating the Iowa Pore Index with Mercury Intrusion Porosimetry and Petrography – Phase II

Final Report
October 2019

IOWA STATE UNIVERSITY
Institute for Transportation

Sponsored by
Federal Highway Administration
Iowa Department of Transportation
(Intrans Project 15-553)

About the Institute for Transportation

The mission of the Institute for Transportation (InTrans) at Iowa State University is to develop and implement innovative methods, materials, and technologies for improving transportation efficiency, safety, reliability, and sustainability while improving the learning environment of students, faculty, and staff in transportation-related fields.

Iowa State University Nondiscrimination Statement

Iowa State University does not discriminate on the basis of race, color, age, ethnicity, religion, national origin, pregnancy, sexual orientation, gender identity, genetic information, sex, marital status, disability, or status as a US veteran. Inquiries regarding nondiscrimination policies may be directed to Office of Equal Opportunity, 3410 Beardshear Hall, 515 Morrill Road, Ames, Iowa 50011, telephone: 515-294-7612, hotline: 515-294-1222, email: eooffice@iastate.edu.

Disclaimer Notice

The contents of this report reflect the views of the authors, who are responsible for the facts and the accuracy of the information presented herein. The opinions, findings and conclusions expressed in this publication are those of the authors and not necessarily those of the sponsors.

The sponsors assume no liability for the contents or use of the information contained in this document. This report does not constitute a standard, specification, or regulation.

The sponsors do not endorse products or manufacturers. Trademarks or manufacturers' names appear in this report only because they are considered essential to the objective of the document.

Quality Assurance Statement

The Federal Highway Administration (FHWA) provides high-quality information to serve Government, industry, and the public in a manner that promotes public understanding. Standards and policies are used to ensure and maximize the quality, objectivity, utility, and integrity of its information. The FHWA periodically reviews quality issues and adjusts its programs and processes to ensure continuous quality improvement.

Iowa DOT Statements

Federal and state laws prohibit employment and/or public accommodation discrimination on the basis of age, color, creed, disability, gender identity, national origin, pregnancy, race, religion, sex, sexual orientation or veteran's status. If you believe you have been discriminated against, please contact the Iowa Civil Rights Commission at 800-457-4416 or the Iowa Department of Transportation affirmative action officer. If you need accommodations because of a disability to access the Iowa Department of Transportation's services, contact the agency's affirmative action officer at 800-262-0003.

The preparation of this report was financed in part through funds provided by the Iowa Department of Transportation through its "Second Revised Agreement for the Management of Research Conducted by Iowa State University for the Iowa Department of Transportation" and its amendments.

The opinions, findings, and conclusions expressed in this publication are those of the authors and not necessarily those of the Iowa Department of Transportation or the U.S. Department of Transportation Federal Highway Administration.

Technical Report Documentation Page

1. Report No. InTrans Project 15-553	**2. Government Accession No.**	**3. Recipient's Catalog No.**	
4. Title and Subtitle Calibrating the Iowa Pore Index with Mercury Intrusion Porosimetry and Petrography – Phase II		**5. Report Date** October 2019 **6. Performing Organization Code**	
7. Author(s) Joseph F. Orso IV (orcid.org/0000-0003-4613-0276) and Franciszek Hasiuk (orcid.org/0000-0002-6531-1710)		**8. Performing Organization Report No.** InTrans Project 15-553	
9. Performing Organization Name and Address Geological and Atmospheric Sciences Iowa State University 253 Science Ames, IA 50011		**10. Work Unit No. (TRAIS)** **11. Contract or Grant No.**	
12. Sponsoring Organization Name and Address Iowa Department of Transportation 800 Lincoln Way Ames, IA 50010	Federal Highway Administration 1200 New Jersey Avenue, SE Washington, DC 20590	**13. Type of Report and Period Covered** Final Report **14. Sponsoring Agency Code** 18-SPR0-010	
15. Supplementary Notes Visit https://intrans.iastate.edu/ for color pdfs of this and other research reports.			

16. Abstract

Coarse aggregate, depending on intended usage, constitutes roughly 20–45% of portland cement concrete as well as being a major component in the construction of granular surface roads and shoulders for paved roads. However, coarse aggregate quality greatly varies among sources based on its petrophysical properties. Therefore, it is important to understand how these properties emerge from the depositional and diagenetic history of a deposit in order to accurately predict pavement durability, which can be negatively impacted by oscillating freeze/thaw cycles. To derive more information about a coarse aggregate's pore system, this study used a "third generation" Iowa Pore Index (IPI) device capable of measuring the volume of intruded water at various time intervals ranging from 0.1–2.0 seconds, as well as measuring intrusion at variable pressures up to 70 psi (480 kPa). Using this new device, 21 carbonate samples (10 dolostones and 11 limestones) were compared to "traditional" IPI measurements. The new method gave slightly higher primary loads.

Additionally, with cumulative volume plotted for the first five minutes of intrusion, dolostones and limestones with elevated primary loads stood apart from the remaining, less macroporous limestone sources. By decreasing apparatus chamber size, higher total intrusion was recorded and IPI values were more correlative with traditional measurements. However, by analyzing the effect of variable pressure intrusion (15, 35, and 60 psi), it was observed that the transition point between intrusion of macropores and micropores was sample-dependent based on lithological properties (i.e., porosity, connectivity of pores, and pore-throat sizes). Although prior methods utilized 60 seconds as this transition point, incremental intrusion data suggest most samples complete macropore intrusion within the first 12 seconds. Therefore, by assessing the incremental intrusion of each source, new primary and secondary loads were calculated, which may be more characteristic of individual lithologies. As a result, secondary load values increased as more intrusion was accounted to micropores than through utilization of the previous method.

With further study, this method could better predict the longevity and overall durability of coarse aggregate based on pore structure in a more individualized fashion than the previous IPI method.

17. Key Words aggregates—coarse aggregates—dolostones—Iowa Pore Index—limestones—portland cement concrete—rock typing—water intrusion device		**18. Distribution Statement** No restrictions.	
19. Security Classification (of this report) Unclassified.	**20. Security Classification (of this page)** Unclassified.	**21. No. of Pages** 91	**22. Price** NA

Form DOT F 1700.7 (8-72) **Reproduction of completed page authorized**

CALIBRATING THE IOWA PORE INDEX WITH MERCURY INTRUSION POROSIMETRY AND PETROGRAPHY – PHASE II

Final Report
October 2019

Principal Investigator
Franciszek "Franek" Hasiuk, Associate Scientist
Kansas Geological Survey, University of Kansas

Research Assistant
Joseph F. Orso IV

Authors
Joseph F. Orso IV and Franciszek "Franek" Hasiuk

Sponsored by
Iowa Department of Transportation

Preparation of this report was financed in part
through funds provided by the Iowa Department of Transportation
through its Research Management Agreement with the
Institute for Transportation
(InTrans Project 15-553)

A report from
Institute for Transportation
Iowa State University
2711 South Loop Drive, Suite 4700
Ames, IA 50010-8664
Phone: 515-294-8103 / Fax: 515-294-0467
www.intrans.iastate.edu

TABLE OF CONTENTS

LIST OF FIGURES

LIST OF TABLES

ACKNOWLEDGMENTS

We thank the Iowa Department of Transportation for sponsoring this study. Their support, including their supplying the necessary funds and equipment for experimentation, have allowed us to uncover more information regarding the lithological factors that govern the Iowa Pore Index.

EXECUTIVE SUMMARY

Coarse aggregate, depending on intended usage, constitutes roughly 20–45% of portland cement concrete as well as being a major component in the construction of granular surface roads and shoulders for paved roads. However, coarse aggregate quality greatly varies among sources based on its petrophysical properties. Therefore, it is important to understand how these properties emerge from the depositional and diagenetic history of a deposit in order to accurately predict pavement durability, which can be negatively impacted by oscillating freeze/thaw cycles.

The Iowa Pore Index (IPI) test, which involves a device and a procedure for measuring the volume ratio of macropores to micropores of coarse aggregate via water intrusion, was initially developed by the Iowa Department of Transportation (DOT) in the 1980s. Among the numerous methods for characterizing the porosity of coarse aggregates, water intrusion is most advantageous because it is inexpensive, non-destructive, and quick. With the IPI, water intrudes a 4,500 g sample of oven-dried coarse aggregate over the span of 15 minutes at a constant pressure of 35 psi (240 kPa). Although the device has been automated since, the basic idea has remained unchanged and has been adopted by other states and accepted as a national standard. With prior devices, two volumes of intrusion were measured: the primary load and secondary load, which relate to macropores and micropores, respectively. A high secondary load (i.e., high microporosity) has been correlated with shorter pavement service life.

To derive more information about a coarse aggregate's pore system, this study used a "third generation" Iowa Pore Index device capable of measuring the volume of intruded water at various time intervals ranging from 0.1–2.0 seconds, as well as measuring intrusion at variable pressures up to 70 psi (480 kPa). Using this new device, 21 carbonate samples (10 dolostones and 11 limestones) were compared to "traditional" IPI measurements. The new method gave slightly higher primary loads.

Additionally, with cumulative volume plotted for the first five minutes of intrusion, dolostones and limestones with elevated primary loads stood apart from the remaining, less macroporous limestone sources. By decreasing apparatus chamber size, higher total intrusion was recorded and IPI values were more correlative with traditional measurements. However, by analyzing the effect of variable pressure intrusion (15, 35, and 60 psi), it was observed that the transition point between intrusion of macropores and micropores was sample-dependent based on lithological properties (i.e., porosity, connectivity of pores, and pore-throat sizes).

Although prior methods utilized 60 seconds as this transition point, incremental intrusion data suggest most samples complete macropore intrusion within the first 12 seconds. Therefore, by assessing the incremental intrusion of each source, new primary and secondary loads were calculated, which may be more characteristic of individual lithologies. As a result, secondary load values increased as more intrusion was accounted to micropores than through utilization of the previous method.

With further study, this method could better predict the longevity and overall durability of coarse aggregate based on pore structure in a more individualized fashion than the previous IPI method.

INTRODUCTION

Concrete Deterioration: Exerted Stress at Aggregate/Paste Interface

Within numerous Midwestern states, concrete durability is significantly tested during winter months with oscillating freeze/thaw cycles. Iowa, for instance, can experience over 20 freeze/thaw cycles within a given year (Dubberke 2002). Specifically, freeze/thaw cycles have been associated with premature aggregate deterioration. Initially identified in the 1930s, D-cracking (Figure 1), or deterioration cracking, is a problem recognized not only in the US, but also in a number of other countries located within temperate climate zones (e.g., Canada, China, and India) (Detwiler et al. 2001, Drumm and Meier 2003, Schwartz 1987).

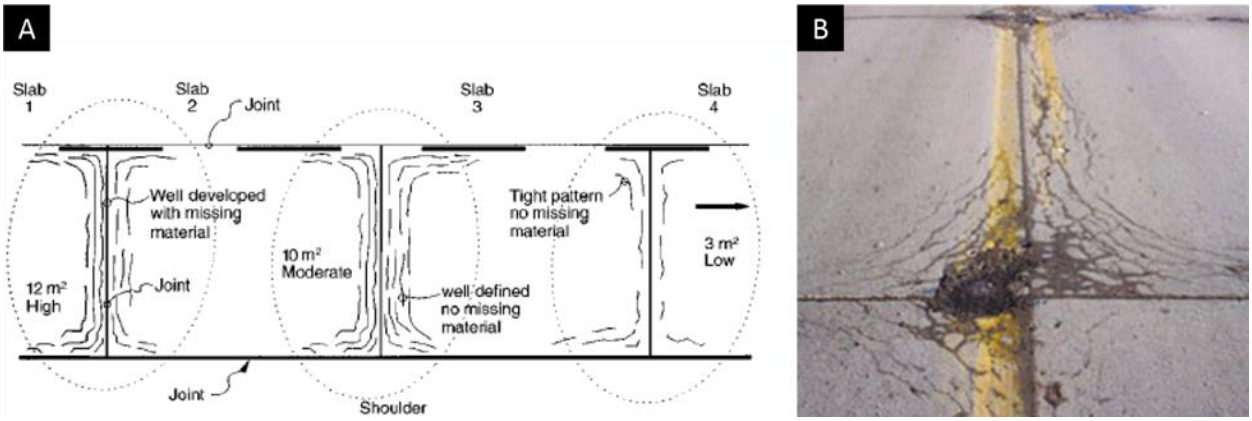

(a) Miller and Bellinger 2003 and (b) Jim Grove, ATI Inc./FHWA

Figure 1. (a) Succession of varying intensities of D-cracks on a pavement surface and (b) D-cracking near the intersection of joints

The intensity of D-cracking is generally classified as high, moderate, or low (Figure 1a), with a high spatial density of D-cracks often increasing deterioration near joint intersections (Figure 1b).This deterioration has been suggested to be the product of the use of non-ideal coarse aggregate (CA) (Schwartz 1987). D-cracks typically originate in the lower levels of pavement where water saturation is most frequent and common (Stark 1976). This saturation, paired with cyclic transitions, or oscillations, of above freezing and sub-freezing temperatures, causes this problem to occur (Stark 1976).

The root cause of D-cracks is created by implied stress from cyclic freezing and thawing events resulting in reduced tensile strength of aggregate and associated concrete paste (Stark 1976). Within most portland cement concrete (PCC) mixes, the total composition is roughly two-thirds by weight fine and coarse aggregate. As a result, within Iowa, 20–45 wt% of PCC mixes are composed of coarse aggregate. Depending on the coarse aggregate utilized, as well as the number of freeze/thaw cycles, D-cracking may occur in less than a year (Stark 1976), presenting a significant cost to the Iowa Department of Transportation (DOT) and Iowa taxpayers alike (Iowa DOT 2015).

It is important to note that the volumetric expansion of water is roughly 9% and occurs as water reaches 0°C. However, although many argue that this volumetric expansion is the sole driver of this occurrence, this expansion only accounts for a small fraction of D-cracks (Hallet 2006). Therefore, porous particles, such as aggregates that cause D-cracking, may be saturated with water at levels less than 91% (Murton et al. 2006). As a result, this mechanism can drive a thermomechanical pressure gradient that exerts stresses that cause the aggregate/paste interface to deteriorate (Dash et al. 2006).

In other words, D-cracks are not strictly an effect of the formation of ice, but are evidence of large temperature gradients that occur on short timescales. These large temperature fluctuations facilitate water migration and the growth of ice through a process known as "ice segregation" (Hallet 2006). Ice segregation (Figure 2) occurs when unfrozen water is forced by suction into capillary pores (those with openings between 50 nm to 10 μm) because of pressure gradients caused by sub-zero temperatures (Murton et al. 2006, Dong et al. 2017).

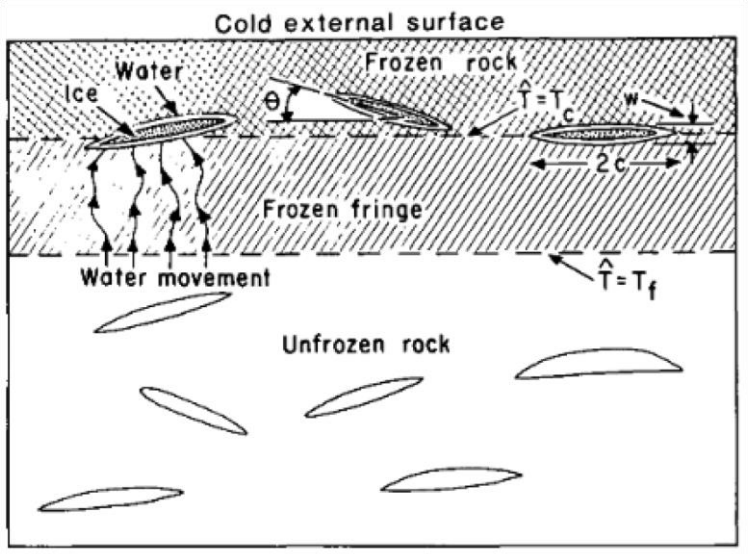

Walder and Hallet 1985, Geological Society of America

Figure 2. Deterioration cracking known as "ice segregation"

The lenses represent pores with the pavement or underlying substrate (Figure 2). Water intrudes the outer portion of the material and freezes due to temperature. Water within the outer pores freezes and creates a temperature gradient that draws water from the surrounding aggregate. This pressure causes the material to expand and apply stress onto the surrounding paste. Therefore, the daily temperature gradients that persist throughout much of the Midwestern US during winter months result in premature deterioration of pavements.

Additionally, it has been identified that as water is promptly discharged upon ice melt, the dissolution of certain paste components is expedited (Van Dam et al. 2002). As time elapses, this occurrence propagates upward through the entirety of the pavement layer (Stark 1976). Due to the nature of D-cracks, early diagnosis is dependent on concrete core analysis. On the other hand,

when visible at the pavement surface (Figure 3), the deterioration might already be too extensive for any sort of repair short of full-depth patching or total reconstruction (Schwartz 1987).

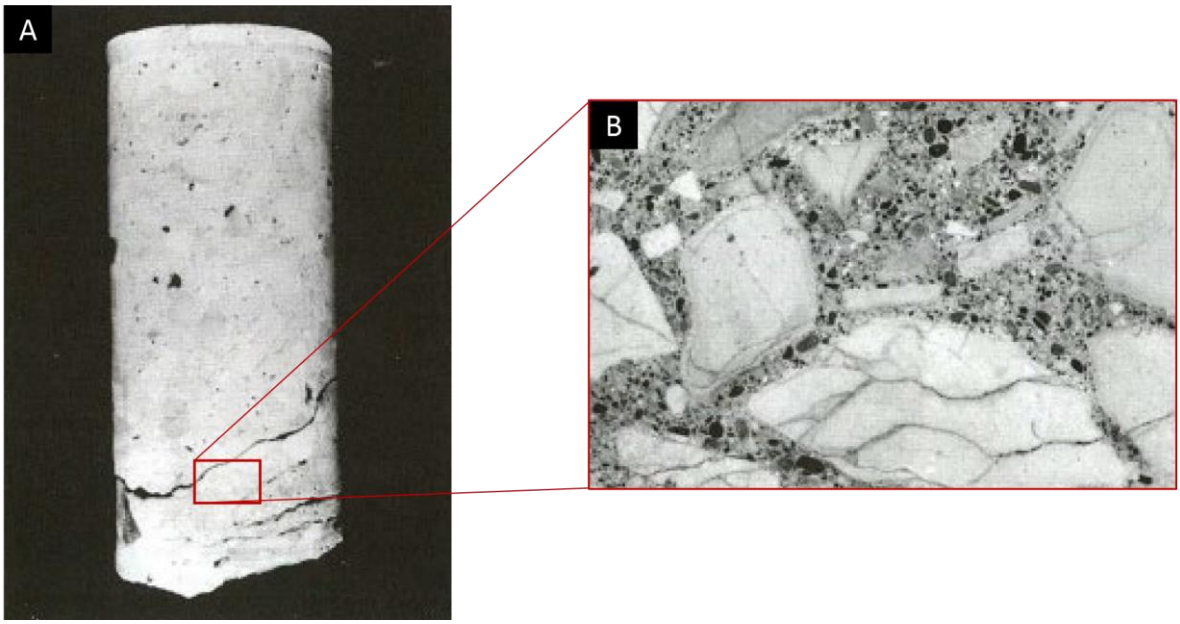

Klieger et al. 1978, PCA

Figure 3. (a) D-cracking prior to signs on pavement surface and (b) aggregate deterioration

Although the National Cooperative Highway Research Program (NCHRP) identified D-cracking as only one of the several deterioration issues arising from the aggregate/mortar interface (e.g., blow ups, spalling, punch outs, alkali-aggregate reactivity, etc.), D-cracking is more frequently investigated than these other pathologies due to its extensive occurrence, which results in more significant remediation costs (Hanna 2003).

Iowa DOT CA Testing

As with most state departments of transportation, locally sourced aggregates are most often utilized due to cost-effectiveness and logistical efficiency. As a result, within Iowa, native carbonate lithologies (i.e., limestones and dolostones) are most often utilized for PCC. The Iowa DOT currently grades aggregates based on durability as derived from field performance and laboratory testing. X-ray diffraction, X-ray fluorescence, and the Iowa Pore Index (IPI) test are the three primary laboratory tests indicating the durability of a CA. Through utilizing these tests, chemistry, mineralogy, and petrophysical properties are combined to generate an aggregate durability value (Ridzuan et al. 2017). The durability classifications for CA can be divided into three categories (Iowa DOT 2019) as follows:

- Class 2 are the most likely to suffer from freeze/thaw deterioration and show minimal deterioration in the first 20 years of pavement service.
- Class 3 show less than 5% deterioration of joints in the first 25 years of service.
- Class 3i possess the highest durability with only 5% deterioration of the joints in the first 35

years of service.

Although these durability classifications seem to effectively differentiate CA, this has not always been the case. Specifically, highly microporous CA has been associated with a greater propensity for D-cracking (Ridzuan et al. 2017).

IPI Origin and Evolution

Wendell Dubberke, an Iowa DOT materials geologist, developed a protocol for testing CA pore size distributions in the late 1970s and 1980s (Hanson 2009). Before this, aggregate durability was graded solely on observed field performance and durability beam testing (ASTM C666). Dubberke recognized the relationship between petrophysical properties and aggregate durability. Therefore, he developed a test method and a device utilizing pressurized water intrusion to quantify aggregate and the ratio of micropores to macropores in a CA sample. Using water intrusion in the test was sought to mimic the water that any pavement is exposed to during its service life. As a result, Dubberke's intended purpose for this test was to determine an aggregate's freeze/thaw susceptibility or durability based on aggregate porosity. Dubberke named this test the Iowa Pore Index (IPI).

The initial IPI procedure involved measuring pressurized water intrusion within a 9,000 g sample of coarse aggregate of a specific particle size. Dubberke's original device incorporated a modified Watts Press-Ur-Meter to force water into a CA's pore systems (Figure 4).

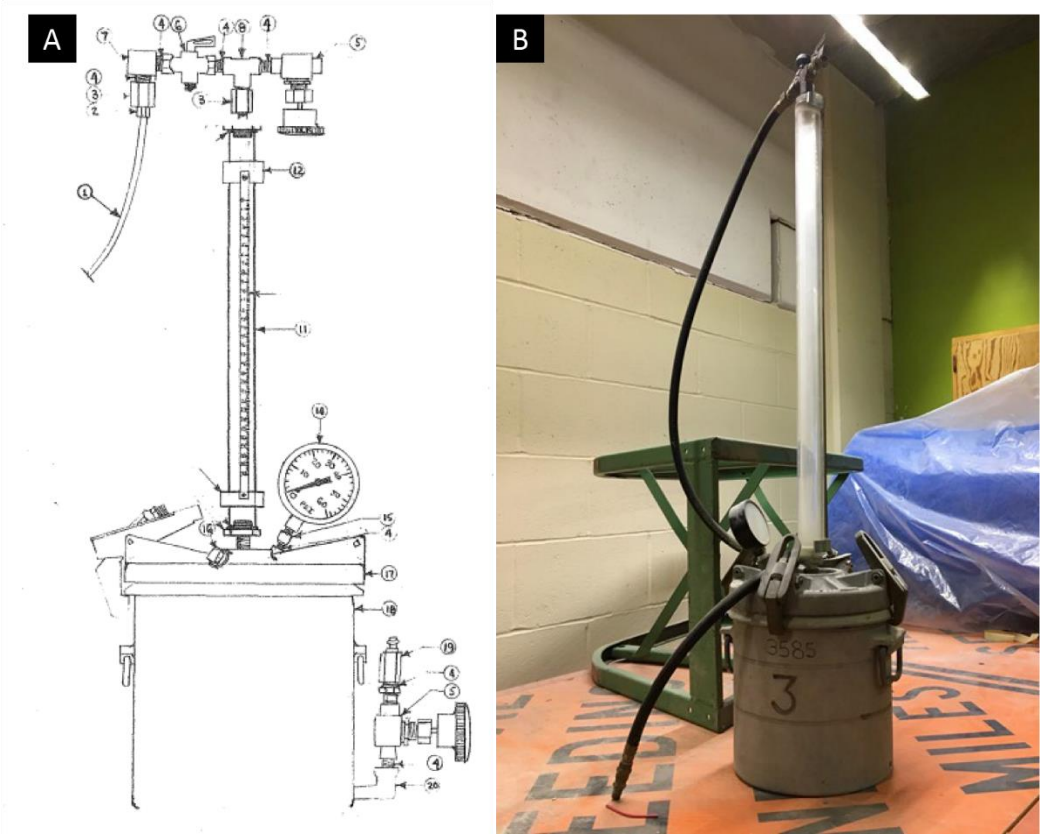

(a) Myers and Dubberke 1980 and (b) personal communication with M. Bob Dawson, Iowa DOT

Figure 4. (a) Original IPI device and (b) later device

Within this chamber, water would intrude CA pores at a constant 35 psi (240 kPa) and water level readings within the chamber would be measured after 1 and 15 minutes of intrusion. These indices were interpreted to relate to a lithology's macropore and micropore abundances (Myers and Dubberke 1980, Marks and Dubberke 1982), respectively. To achieve this, the chamber would first be loaded with 9,000 g of CA. Next, cold tap water would fill the chamber and Plexiglas water meter to the 0 mm mark. Once water and vent valves are closed, air pressurized to 35 psi would be applied to the chamber. At this moment, a stopwatch is initialized. After one minute of intrusion, the decrease in water level in the sight glass would be recorded. This volume would be known as the primary load index (PLI). Subsequently, a water level reading would be recorded after 15 minutes, and the volume of intrusion between the two readings would be called the secondary load index (SLI). The secondary load index was used to define aggregate durability and was related to the abundance of micron-sized pores in a sample. Myers and Dubberke (1980) classified carbonate CA possessing SLI values of 27 or more as the inability of aggregate pore systems to withstand freeze/thaw cycles. The standard operating procedure (SOP) developed by Dubberke is located in Appendix A.

After being used for nearly two decades to assess aggregate, the initial, or first generation (1G), IPI device was abandoned in the early 2000s, when a new, more automated IPI device, second generation (2G), was developed (Figure 5).

Gustafson et al. 2015, Iowa DOT

Figure 5. Second-generation IPI device

This second-generation automated device intrudes water from each of three cylinders (numbered 1, 2, and 3 in Figure 5) during prescribed time intervals (60 s, 60–900 s, and 900–1,800 s, respectively). The volumes that remain in the cylinders determine a source's PLI, SLI, and leakage factor, respectively.

This device utilized a decreased CA sample size of 4,500 g to assess IPI indices. Instead of manually assessing the point at which to record PLI and SLI intrusion volumes, this device incorporated a controller and three separate graduate cylinders to record intrusion into the sample-filled pot (i.e., primary load intrusion, secondary load intrusion, 15-minute leakage test volume). With these components, the automated controller would automatically draw liquid from each graduated cylinder during each time interval (i.e., 0–1 minutes, 1–15 minutes, and 15–30 minutes). In addition to improved automation and decreased sample size, this new device incorporated an amended procedure. With the new chamber, the introduction of pot expansion calibration emerged. Prior to each test, a no-sample trial would take place to estimate the volumetric expansion of the sample pot due to the pressure change to ensure the test was only measuring intrusion volumes into the CA and not expansion of the sample pot itself. As both PLI and SLI measurements are directly proportional to the weight of a sample, such indices would be standardized to a 9,000 g sample in the following manner:

$$PLI = V_1 \times (9000/W) \quad (1)$$

$$SLI = V_2 \times (9000/W) \quad (2)$$

where,
PLI: Primary load index (mL)
SLI: Secondary load index (mL)
V_1: Intruded volume between 0–1 minutes (mL)
V_2: Intruded volume between 1–15 minutes (mL)
W: Sample weight (g)

The SOP for the 2G device is in Appendix B. Not only has the 2G IPI testing device and method been adopted by other state agencies, but it was accepted as an American Association of State Highway and Transportation Officials (AASHTO) standard in August 2016 (AASHTO TP 120-16).

In this study, the research team analyzed the next phase of the IPI evolution. This third generation IPI device, known as the 3G IPI, incorporates improved automation, increased precision, and more possibilities in assessing CA pore volume distributions. Although the actual IPI device has greatly evolved since its initial conception (Figure 4), the basic concept relating cumulative liquid intrusion to pore size distributions and their connection to predicted road durability, has remained unchanged.

Prior Studies

Through the transition among the three IPI devices, studies have challenged the accuracy and repeatability of this petrophysical method and its links to freeze/thaw durability. However, although countless studies incorporate the Iowa Pore Index into evaluating aggregate sources, only a few actually contest its effectiveness.

In 2015, the Iowa DOT funded a project that aimed to determine the effect of grain size and the repeatability of test results utilizing the 2G IPI device (Gustafson et al. 2015). Traditionally, the IPI was standardized to assess pore distributions of 4,500 g of ½ by ¾ in. aggregate passing through ¾ in. sieve size and withheld by ½ in. sieve. This study also analyzed ½ by 3/8 in. and #4 by 3/8 in. aggregate to determine a preferential size. Through testing 21 sources in these three size fractions (i.e., ½ by ¾, ½ by 3/8 in., and #4 by 3/8 in.), the study broadly concluded that as aggregate particle size decreases so do secondary load indices. With this correlation, a correction factor was established that enables the use of particle sizes other than the standard IPI size. However, little evidence supports the favoring of one specific particle size over another (Gustafson et al. 2015). Therefore, ½ by ¾ in. particle sizes remained in use in the 2G IPI analysis.

To complement the grain size and repeatability study, the Iowa DOT funded a project to determine the geological basis of CA's IPI index test results (Gustafson et al. 2015). This study used the 2G testing device and visual lithological properties (i.e., depositional textures, facies, grains, pore types) to explain specific source results. Through rock typing and thin section microscopy, Ridzuan et al. (2017) uncovered that most aggregate sources contain at least three distinct rock types with corresponding varying porosity. As a result, it was concluded that a

specific sources' performance and IPI test results are dictated by aggregate source heterogeneity (Ridzuan et al. 2017).

Rationale for Continued Study

Unlike similar methods that analyze porosity (i.e., helium pycnometry, mercury intrusion porosimetry), the IPI is quick, inexpensive, easily utilized with crushed rocks, and non-destructive toward samples. Although this method has been utilized for several decades, correlation between IPI results and proven durability has been not always been predictive for some sources. These discrepancies suggest our understanding of the IPI test remains incomplete. Prior studies utilizing the IPI method incorporated the 2G IPI intrusion device.

With this current study, the researchers aimed to test the efficiency and repeatability, and explore more information through the introduction of the new 3G IPI fluid intrusion device that can measure the volume of intruded water at various time intervals ranging from 0.1–2.0 seconds, as well as measure intrusion at variable pressures up to 70 psi (480 kPa) (Figure 6).

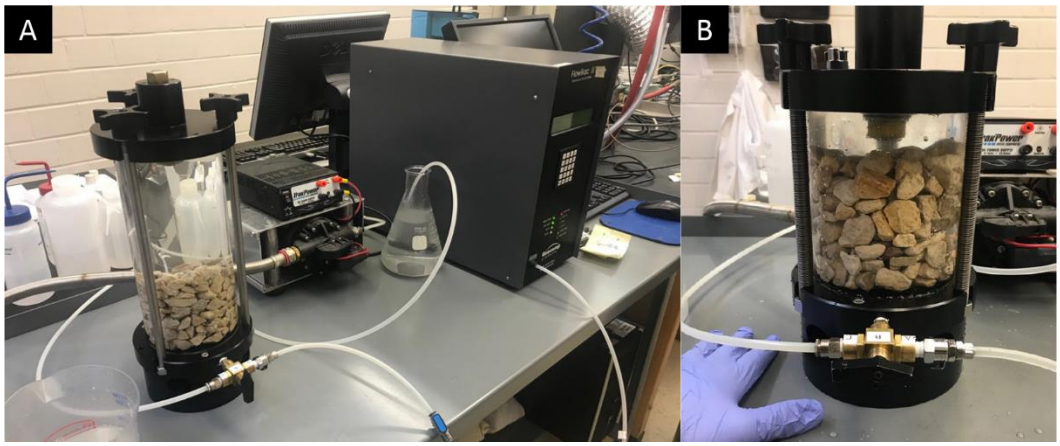

Figure 6. Third-generation IPI device (a) with 1,650 cm^3 chamber and (b) with 1,100 cm^3 chamber

The FlowTrac-II fluid intrusion device (Geocomp Corp., Acton, MA, US) was initially equipped with the 1,650 cm^3 chamber (Figure 6a). The device automates the intrusion of water into the sample-filled chamber at a set (or variable) pressure chosen by the operator. This device has the capacity to measure the volume of intruded water over much shorter time intervals (0.1–2.0 seconds), as well as measuring intrusion at pressures up to 70 psi (480 kPa). The chamber size was decreased to 1,100 cm^3 (Figure 6b) to decrease the initial soak time to improve accuracy of IPI indices.

Through utilizing a more automated device and pairing results with traditional petrophysical methods, the IPI results may be more indicative of individual lithologies, which may have been miscategorized in the past. Additionally, through petrographic thin section analysis, the researchers sought to link IPI test results and qualitative rock properties (e.g., pore types). With

this information, the IPI test may yield more reliable and accurate results that may be more useful when assessing the durability of a particular CA sample.

METHODS

After obtaining samples of aggregate sources from the Iowa DOT, the FlowTrac II fluid intrusion device was used to determine the rate and amount of intruded water into each sample of CA utilizing an amended 2G IPI method. With this new device, subsequent tests were conducted using varying instrumental parameters. The new data were compared to both prior studies (Gustafson et al. 2015, Ridzuan et al. 2017) and historical records to determine performance of the new device and efficacy of test methods.

Next, rock typing of these sources was utilized to distinguish lithological variation within one particular aggregate source or rock bed (Ridzuan et al. 2017). Of each specific rock type, two pebbles were collected; one for petrographic thin section analysis and one for mercury porosimetry. Helium pycnometry was utilized for grain density analysis of both pebbles.

Source Selection

For this study, the Iowa DOT provided 21 different sources for analysis. These CA samples weighed approximately 3 kg and were of ½ by ¾ in. size material. These sources were all analyzed previously in the Gustafson et al. (2015) report. Of these sources, 11 were primarily limestone and 10 were primarily dolostone (Table 1).

Table 1. Source information for the 21 carbonate coarse aggregate samples studied

Marker	Source	County	Series	System	Stage	Member	Formation	Group	Beds	Lith.	EOD	Facies	Reference
A	Alden Quarry	Hardin	Lower - Middle	Mississippian	Osagean	Undiff	Gilmore City	Sub-Augusta	0,1,3	LS	Inner Ramp	Skeletal shoal	Witzke and Bunker 2001
B	Ames Mine	Story	Upper	Devonian	Upper Frasnian	Owen	Lime Creek	Yellow Spring	47	LS	Inner Ramp	Peritidal /Supratidal	Day et al. 2013
C	Behr Quarry	Clinton	Lower	Silurian	Lland.- Wenlockian	Welton	Scotch Grove	Undifferentiated	1,2	DS	Open Marine	Deep Subtidal	Ludvigson et al. 1992
D	Bowser-Springville Quarry	Linn	Lower - Upper	Silurian	Wenlockian	Anamosa	Gower	Undifferentiated	6-7	DS	Open Marine	Lagoon	Ludvigson et al. 1992
E	CBJ Mine	Louisa	Lower	Mississippian	Kinderhookian	Wassonville	Maynes Creek	Sub-Augusta	16-19	DS	Middle Ramp	Subtidal	Witzke and Bunker 2001
F	Dotzler Quarry	Howard	Middle	Devonian	Upper Eifelian	Unknown	Spillville /Otis	Wapsipinicon	7-10A	DS	Open Marine	Subtidal	Witzke et al. 1988
G	Duenow Quarry	Mitchell	Middle	Devonian	Upper Givetian	Gizzard Creek?	Coralville	Cedar Valley	13	LS	Inner Ramp	Peritidal	Witzke et al. 1988
H	Durham Mine	Marion	Lower	Mississippian	Kinderhookian	Starrs Cave	Maynes Creek	Sub-Augusta	101	LS	Inner-Mid Ramp	Skeletal shoal	Witzke and Bunker 2001
I	Dyersville-Sundheim Quarry	Dubuque	Lower	Silurian	Llandoverian	Upper (Farmers Creek?)	Hopkinton	Undifferentiated	5-12	DS	Open Marine	Deep Subtidal	Ludvigson et al. 1992
J	Elwood-Yeager	Clinton	Lower	Silurian	Lland.- Wenlockian	Welton	Scotch Grove	Undifferentiated	1-2	DS	Open Marine	Deep Subtidal	Ludvigson et al. 1992
K	Griffith Quarry	Humboldt	Lower - Middle	Mississippian	Osagean	Undiff	Gilmore City	Sub-Augusta	1-4	LS	Inner Ramp	Ooid shoal	Witzke and Bunker 2001
L	Jones Quarry	Floyd	Middle	Devonian	Lower Frasnian	Idlewild	Lithograph City	Cedar Valley	1-4	LS	Inner Ramp	Peritidal /Supratidal	Witzke et al. 1988
M	Lacoste Quarry	Floyd	Middle	Devonian	Upper Givetian	Iowa City?	Coralville	Cedar Valley	1-4	LS	Inner Ramp	Peritidal /Supratidal	Witzke et al. 1988
N	Linwood Mine	Scott	Middle	Devonian	Upper Eifelian	Cedar Rapids	Otis	Wapsipinicon	27-30b	LS	Inner Ramp	Lagoon /Peritidal	Witzke et al. 1988
O	Morgan Quarry	Black Hawk	Middle	Devonian	Lower Givetian	Spring Grove	Pinicon Ridge	Wapsipinicon	5	LS	Restricted Ramp	Peritidal /Supratidal	Witzke et al. 1988
P	Portland West Quarry	Cerro Gordo	Middle	Devonian	Middle Frasnian	Nora /Mason City	Shell Rock	Cedar Valley	1-8	DS	Open Marine	Shallow subtidal	Witzke et al. 1988
Q	Stone City Quarry	Jones	Lower	Silurian	Wenlockian	Anamosa /Waubeek	Scotch Grove	Undifferentiated	2B-3	DS	Open Marine	Lagoon /Intermound	Ludvigson et al. 1992
R	Sully Mine	Jasper	Lower	Mississippian	Kinderhookian	Eagle City	Maynes Creek	Sub-Augusta	36-41	DS	Inner-Mid Ramp	Ooid Shoal?	Witzke and Bunker 2001
S	Warnholtz Quarry	Floyd	Middle	Devonian	Upper Givetian	Gizzard Creek?	Coralville	Cedar Valley	17-18	DS	Inner Ramp	Peritidal	Witzke et al. 1988
T	Waucoma Quarry	Fayette	Lower	Silurian	Llandoverian	Waucoma	Hopkinton	Undifferentiated	2-5	LS	Open Marine	Lagoon	Ludvigson et al. 1992
U	Weeping Water Mine	Cass (NE)	Upper	Pennsylvanian	Virgillian	Plattsmouth	Oread	Shawnee	9-10b	LS	Open Marine	Deep Subtidal	This study

Note: Marker values correlate with the geological map of Iowa (Figure 7). Lithology: LS – limestone, DS – dolostone

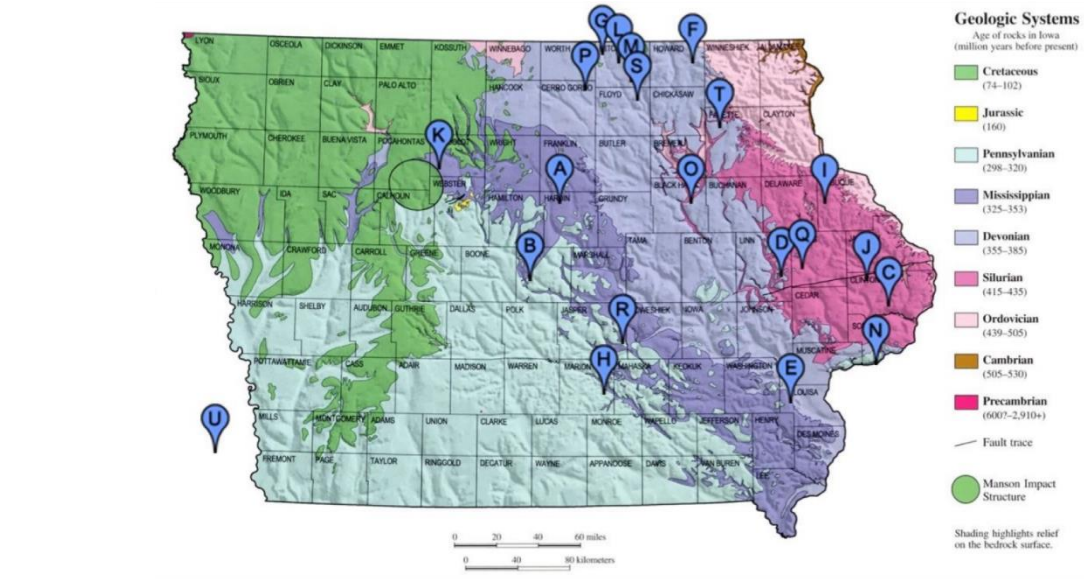

Gustafson et al. 2015, from the Iowa Geological Survey

Figure 7. Source locations of the 21 studied samples

The sources shown in Figure 7 are composed of Devonian, Silurian, Mississippian, and Pennsylvania aged strata, in decreasing abundancy by age. Letters indicated on the map correspond to the sources within Table 1.

Most CA used by the Iowa DOT originates within the state and ranges from Ordovician to Pennsylvanian in age. The sample origins from markers A to U are as follows:

- Alden Quarry (Hardin County) produces from the Lower-Middle Mississippian (Osagean) Gilmore City Formation (Sub-Augusta Group). The sample came from beds 0,1,3 and was mostly limestone.
- Ames Mine (Story County) produces from the Upper Devonian (Upper Frasnian) Owen Member of the Lime Creek Formation (Yellow Spring Group). The sample came from bed 47 and was mostly limestone.
- Behr Quarry (Clinton County) produces from the Lower Silurian (Llandoverian-Wenlockian) Welton Member of the Scotch Grove Formation. The sample came from beds 1 and 2 and was mostly dolostone.
- Bowser-Springville Quarry (Linn County) produces from the Lower-Upper Silurian (Wenlockian) Anamosa Member of the Gower Formation. The sample came from beds 6–7 and was mostly dolostone.
- CBJ Mine (Louisa County) produces from the Lower Mississippian (Kinderhookian) Wassonville Member of the Maynes Creek Formation (Sub-Augusta Group). The sample came from beds 16–19 and was mostly dolostone.
- Dotzler Quarry (Howard County) produces from the Middle Devonian (Upper Eifelian) Spillville/Otis Formation (Wapsipinicon Group). The sample came from beds 7–10A and was mostly dolostone.
- Duenow Quarry (Mitchell County) produces from the Middle Devonian (Upper Givetian)

Gizzard Creek? Member of the Coralville Formation (Cedar Valley Group). The sample came from bed 13 and was mostly limestone.

- Durham Mine (Marion County) produces from the Lower Mississippian (Kinderhookian) Starrs Cave Member of the Maynes Creek Formation (Sub-Augusta Group). The sample came from bed 101 and was mostly limestone.
- Dyersville-Sundheim Quarry (Dubuque County) produces from the Lower Silurian (Llandoverian) Farmers Creek(?) Member of the Hopkinton Formation. The sample came from beds 5–12 and was mostly dolostone.
- Elwood-Yeager (Clinton County) produces from the Lower Silurian (Lland.-Wenlockian) Welton Member of the Scotch Grove Formation. The sample came from beds 1–2 and was mostly dolostone.
- Griffith Quarry (Humboldt County) produces from the Lower-Middle Mississippian (Osagean) Undiff Member of the Gilmore City Formation (Sub-Augusta Group). The sample came from beds 1–4 and was mostly limestone.
- Jones Quarry (Floyd County) produces from the Middle Devonian (Lower Frasnian) Idlewild Member of the Lithograph City Formation (Cedar Valley Group). The sample came from beds 1–4 and was mostly limestone.
- Lacoste Quarry (Floyd County) produces from the Middle Devonian (Upper Givetian) Iowa City Member? Member of the Coralville Formation (Cedar Valley Group). The sample came from beds 1–4 and was mostly limestone.
- Linwood Mine (Scott County) produces from the Middle Devonian (Upper Eifelian) Cedar Rapids Member of the Otis Formation (Wapsipinicon Group). The sample came from beds 27–30b and was mostly limestone.
- Morgan Quarry (Black Hawk County) produces from the Middle Devonian (Lower Givetian) Spring Grove Member of the Pinicon Ridge Formation (Wapsipinicon Group). The sample came from bed 5 and was mostly limestone.
- Portland West Quarry (Cerro Gordo County) produces from the Middle Devonian (Middle Frasnian) Nora/Mason City Member of the Shell Rock Formation (Cedar Valley Group). The sample came from beds 1–8 and was mostly dolostone.
- Stone City Quarry (Jones County) produces from the Lower Silurian (Wenlockian) Anamosa/Waubeek Member of the Scotch Grove Formation. The sample came from beds 2B–3 and was mostly dolostone.
- Sully Mine (Jasper County) produces from the Lower Mississippian (Kinderhookian) Eagle City Member of the Maynes Creek Formation (Sub-Augusta Group). The sample came from beds 36–41 and was mostly dolostone.
- Warnholtz Quarry (Floyd County) produces from the Middle Devonian (Upper Givetian) Gizzard Creek(?) Member of the Coralville Formation (Cedar Valley Group). The sample came from beds 17–18 and was mostly dolostone.
- Waucoma Quarry (Fayette County) produces from the Lower Silurian (Llandoverian) Waucoma Member of the Hopkinton Formation. The sample came from beds 2–5 and was mostly limestone.
- Weeping Water Mine (Cass County, Nebraska) produces from the Upper Pennsylvanian (Virgillian) Plattsmouth Member of the Oread Formation (Shawnee Group). The sample came from beds 9–10b and was mostly limestone.

Iowa Pore Index (Second Generation or "Traditional")

All 21 carbonate sources were tested utilizing the second generation (2G) IPI method (Appendix B). These samples were analyzed previously (Gustafson et al. 2015), and these results were used as benchmarks for this study.

Iowa Pore Index (Third Generation)

Subsequent to testing with the 2G IPI device, all 21 samples were subjected to 3G IPI testing using a FlowTrac II device (Geocomp Corp., Acton, MA, US). As opposed to utilizing graduated cylinders to measure incremental intruded volumes, the 3G IPI device uses a metered pump to quantify cumulative intrusion volumes. This device has a smaller sample chamber size that led to a sample size decrease from 4.5 kg to 1 kg. CA samples (½ in. to ¾ in.) were analyzed at a constant pressure of intrusion (35 psi [240 kPa]). To ensure precise and repeatable results, the effect of expansion of the Plexiglas chamber was determined through repeated tests with an empty chamber. After establishing chamber expansion, the 21 samples were analyzed according to a new 3G IPI operating procedure (Appendix C).

In concordance to the initial SOP, CA samples were oven-dried for ~8 hours at 100°C to ensure desiccation. Prior to each sample analysis, a one-minute no-sample test trial was conducted to determine a correction factor for each sample. In other words, to adjust recorded intrusion, no-sample tests were utilized prior to each sample test to establish volume changes associated with Plexiglas expansion to ensure volumes were solely a result of aggregate porosity. The intruded volume was deduced from sample test volumes of intrusion as a correction factor. First, the chamber with a 1,650 cm^3 nominal capacity was filled with a 1,000 g sample of CA. Deionized (DI) water was then introduced into the chamber using a 12 V water pump, taking ~8 s to fill the vessel completely. During this time, conditions within the chamber remained at atmospheric pressure (15 psi [103 kPa]). Once filled with DI water, a constant pressure of water intrusion (35 psi) was applied to chamber. At this time, pressure and cumulative intruded volume began to be recorded in 0.5 s intervals, unlike the IPI 2G that recorded intruded volume after 60 s, 900 s, and 1,800 s. After 15 minutes, or 900 s, of recording, the test was terminated.

These data were initially recorded within the proprietary FlowTrac II Diags software but later exported into Microsoft Excel. Within Excel, data were corrected for chamber expansion and cumulative intrusion was converted to incremental intrusion over 0.5 s intervals. Finally, the PLI and SLI of each source was determined and compared to prior and historical data. The volume of intruded water after the first minute of intrusion was attributed to the PLI, or the macropore volume. The SLI was quantified from the volume of intruded water between minutes 1 and 15 of intrusion, which is associated to capillary or micropores. Due to the sample size decrease between the 2G and 3G versions of the IPI chamber, a conversion factor was applied. Both the PLI and the SLI volume measurements were standardized to 9,000 g according to the 2G IPI method (Appendix B).

After testing these samples utilizing a chamber with a 1,650 cm^3 capacity, the Plexiglas sample chamber was decreased to 14 cm in height in order to decrease the initial soak time while filling

the chamber. It was hypothesized that reducing the soak time would increase the total recorded intruded volume and result in more accurate porosity measurements. The volume of the chamber was decreased to 1,100 cm^3. Initial soak time was decreased to 5 s, potentially diminishing unrecorded pore intrusion. Results from the initial testing of both chamber sizes (1,650 cm^3 and 1,100 cm^3) were compared to historical IPI data. To reveal more information of CA petrophysical properties, the 21 CA samples also were run at 15 psi (103 kPa, approximately atmospheric pressure) and 60 psi (414 kPa) within the short chamber.

Rock Typing

Prior studies suggested each sample would be a mix of rock types (Ridzuan et al. 2017). Rock typing of these sources distinguished lithological variation within one particular aggregate source or rock bed. Since 10 of the 21 sources had been previously characterized (Ridzuan et al. 2017), only 11 aggregate samples were analyzed in this study. In order to ensure a representative sample from each source, each bag of aggregates was inverted and mixed; this would eliminate any segregation within the larger sample bag as a result of individual pebble densities. After mixing, 1,000 g of each source was arranged on an examination tray to measure heterogeneity. Using a stereoscopic microscope, each pebble was categorized based on the following characteristics: color, pore appearances (size, shape, and visual connectivity), dissolution enhanced pore geometry, clasts, and matrix. Upon sorting and differentiating within each rock type, each group was weighed, and percent abundances were calculated. Of each specific rock type, two pebbles were collected: one sample for petrographic thin section analysis and one for pebble mercury intrusion porosimetry analysis. However, to ensure each pair of pebbles constitutes similar lithologies, helium pycnometry was employed for each pebble to determine its grain density.

Helium Pycnometry

Helium pycnometry, or more generally gas pycnometry, uses gas to measure a sample's grain density. For this study, this concept was used not only to verify that pebble pairs identified during rock typing represented similar lithologies but also in an attempt to determine a grain density relationship with IPI results. For this analysis, the Micromeritics AccuPyc II 1340 was employed. Helium, with an atomic diameter ranging between 0.18 and 0.24 nm, is typically chosen for such analysis due to its ability to intrude into the smallest possible void spaces (Kalashnikov and Pevzner 2001). With most gas pycnometers, two chambers exist: one empty chamber (reference chamber), and one sample chamber. In practice, gas is injected into the sample-filled chamber to determine grain volume based on gas pressure fluctuations between chambers. These gas injections are often referred to as purges. For this study, five gas purges were conducted on each pebble to measure granular volume each time. Through incorporating the mass, grain density and grain volume are determined (Couto et al. 2012):

$$Vg = Vca - \frac{Vce}{\left(\frac{P1}{P2}\right)-1} \tag{3}$$

where,

V_g: Grain volume of solid (mL)
V_{ca}: Volume of sample chamber (mL)
V_{ce}: Volume of expansion chamber (mL)
P_1: Initial pressure within chamber (psi)
P_2: Pressure reached upon gas equilibrium (psi)

Mercury Intrusion Porosimetry

To compare the IPI to a more commonly used test method for determining the relative abundance of pore sizes, mercury porosimetry was employed. This method can intrude pores between 500 µm and 5.6 nm in size using increasing pressure (Giesche 2006). The efficacy of mercury used for this analysis is governed by high contact angles on high energy surfaces (i.e., quartz, calcite, and dolomite) (Ellison et al. 1967). In other words, mercury is highly cohesive so adhesive forces between mercury and mineral surfaces are minimal, resulting in little spontaneous imbibition into the porous medium, so the volume of mercury intruded is a function of pressure applied to the sample. Hence, this is one of the most accurate manners for determining pore-throat size distributions.

With increasing pressure of mercury intrusion, smaller and smaller pore throats are intruded, and therefore, resulting in a pressure-driven pore-throat size distribution. This relationship was explained by the following equation, known as Washburn's equation (Washburn 1921, Brabazon and Raffer 2015):

$$D = \frac{-4\gamma cos\theta}{P} \quad (4)$$

where,
D: Pore-throat diameter (µm)
γ: Surface tension of mercury (erg/cm^2)
θ: Contact angle
P: Applied pressure (psi)

Pore-throat size distributions were measured on a Quantachrome PoreMaster 33. Each sample was oven-dried for 6 hours at 135°C and stored in a desiccator at room temperature for 24 hours before being analyzed. Mercury intrusion was conducted at 26° to 28°C. A penetrometer with a stem volume of 2.0 cm^3 was used for all samples. For all experiments, mercury contact angle was set at 140°, mercury surface tension at 480 erg/cm^2. During the low-pressure phase of the experiment, fine evacuation was performed for one minute followed by coarse evacuation for five minutes. Low pressure analysis proceeded from approximately 2 psi to 50 psi. The start pressure of 2 psi limited the maximum size pores that the instrument was able to measure; however, this pressure was required to ensure that mercury had completely enveloped the pebble (also called conformance) before analysis began. Conformance was visually confirmed for each pebble during analysis because the penetrometer cell was transparent. After the low-pressure analysis, the penetrometer was prepared for the high pressure analysis by replacing a small amount of mercury from the stem (~1 cm) with hydraulic oil. Then, the total height of mercury

was used to apply a head-pressure correction in the instrument's control software. High pressure analysis then proceeded from 20 psi to a maximum pressure of approximately 33,000 psi (~230 MPa). Using Washburn's equation, maximum and minimum pressures (20 psi and 33,000 psi) equate to a pore-throat diameter range of 100 µm to 5.6 nm, respectively.

Thin Section Petrography

To link lithological and petrographic properties, the second pebble was sent to TPS Enterprises (Houston, TX) for thin section preparation. The polished thin sections were prepared with a blue-dyed epoxy to aid in the visualization of the sample's pore network. Examination of these samples occurred in plane-polarized light on an Olympus BX53 petrographic microscope, equipped with a 17-megapixel Olympus DP73 camera. Photomicrographs of each sample were taken to document the composition/matrix, pore structures, and textures. Additionally, a relative mud index value was attributed to each rock type. Each rock type was given a value from 1 to 3, with 1 indicating a minimum mud component and 3 indicating a large relative proportion of mud.

RESULTS

Iowa Pore Index

After multiple no-sample test trials, chamber expansion volumes were inconsistent and unpredictable due to volume change of the sample chamber. Through analyzing five chamber expansion cycles, a negative trend between the number of consecutive tests and total intruded volume was observable. As more no-sample IPI tests were performed, intruded volumes associated with chamber expansion decreased. It was observed that 95% of expansion occurs within first minute of analysis at 30 psi (Figure 8).

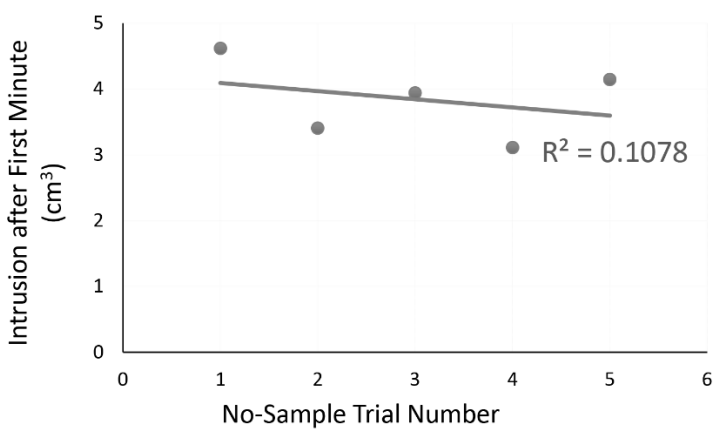

Figure 8. Intrusion decreases as the number of no-sample test trials increases

Five no-sample trials were repeated within an 81-minute time period. Intrusion observed during this test was attributed to expansion of the Plexiglas chamber and results in variation of cumulative intrusion among the tests. The first minute of cumulative intrusion was utilized because on average, 95.5% of the total intrusion within a run occurred within the initial minute. Although a strong relationship is absent, this negative trend influenced the adoption of a chamber expansion pretest prior to each sample trial.

Next, proceeding with IPI testing on the 21 samples, it was observed that as initial soak time increased, PLI and SLI values both deviate from historical trends (Figure 9).

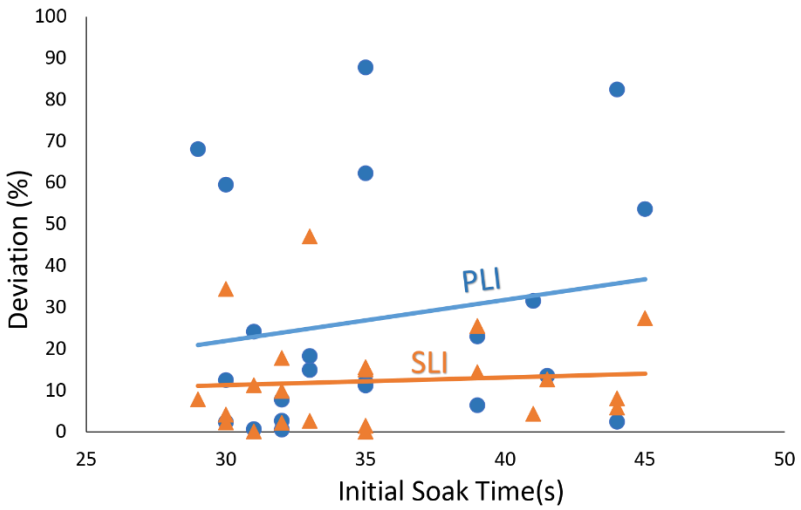

Figure 9. Recorded initial soak time, which varied randomly

Recall initial soak time is defined by the time an aggregate sample is submerged in water prior to recording of intrusion volumes. This occurs while the chamber is being filled with water. As initial soak time increased, the deviation from previously analyzed results (Gustafson et al. 2015) increased slightly for PLI and negligibly for SLI. Hence, increasing soak time results in elevated macropore intrusion prior to measurements and lower calculated PLI values.

Primary load indices ranged between 13 and 225, while SLIs ranged between 8 and 39. PLI and SLI indices are unit-less but relate to intruded volumes after 1 and 15 minutes of intrusion, respectively. Among the 21 samples, slight deviation from historical data occurred, as more total intrusion was recorded with the 3G device (Figure 10).

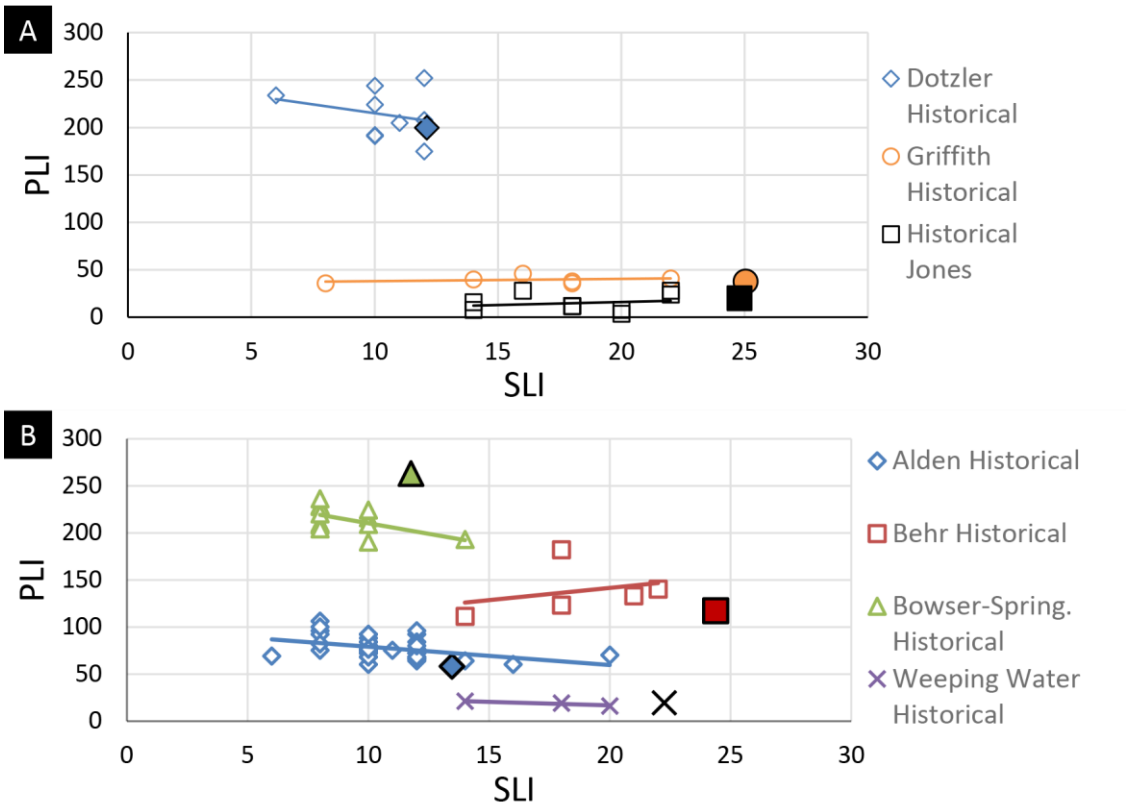

Figure 10. (a) Historical data from Dotzler, Griffith, and Jones samples and (b) from Alden, Behr, Bowser-Springville, and Weeping Water CA sources

After testing 21 CA samples, most results utilizing the 3G IPI (the closed symbols in Figure 10) correlated with historical data (the open symbols in Figure 10). Historical trends were determined through analyzing archived 2G IPI data that was provided by the Iowa DOT. Among these sources, most SLI values generated using the 3G device were greater than the historical data. This is due to more total recorded intrusion with the 3G device.

However, this study observed similar trends (Table 2) to previous work (Gustafson et al. 2015).

Table 2. Data from 2G IPI device compared to 3G IPI device large and small chamber

		Gustafson 2015		Large chamber		Small chamber	
Source	**Lith.**	**PLI**	**SLI**	**PLI**	**SLI**	**PLI**	**SLI**
Alden	LS	75	11	58	13	81	13
Ames Mine	LS	13	13	4	12	43	16
Behr	DS	133	21	117	24	139	26
Bowser-Spr.	DS	229	8	263	12	307	11
CBJ Mine	DS	191	20	187	21	166	22
Dotzler	DS	205	11	200	12	188	14
Duenow	LS	16	22	6	22	38	50
Durham	LS	147	12	120	12	135	15
Dyersville	DS	72	18	70	18	50	27
Elwood Yeager	DS	112	11	103	12	127	14
Griffith	LS	41	22	39	25	75	27
Jones	LS	24	22	21	25	45	30
Lacosta	LS	16	20	2	20	29	180
Linwood	LS	21	8	10	6	32	10
Morgan	LS	112	10	126	13	124	12
Portland West	LS	28	14	19	15	36	18
Stone City	DS	245	8	246	9	267	10
Sully	DS	172	17	174	17	192	18
Warnholtz	DS	79	44	88	45	98	46
Waucoma	LS	14	10	5	12	22	13
Weeping Water	LS	16	20	19	22	38	32

Lithology: LS – limestone, DS – dolostone

Although values differ significantly for numerous sources, IPI indices still record within historical ranges. Decreasing chamber size resulted in elevated PLI and SLI values compared to Gustafson et al. (2015) and large chamber results. This indicates intrusion was captured, resulting in more accurate pore volumes. Small chamber SLI values for limestone range between 10 and 50, while SLI indices for primarily dolostone sources range between 10 and 46. Small chamber PLI values are more indicative of lithology as limestone and dolomitic ranges vary (i.e., limestone PLI range or 22–135, dolostone PLI range of 36–307).

Additionally, with cumulative intrusion plotted for the first five minutes, it is apparent that the sources plot in two distinct groups (Figure 11).

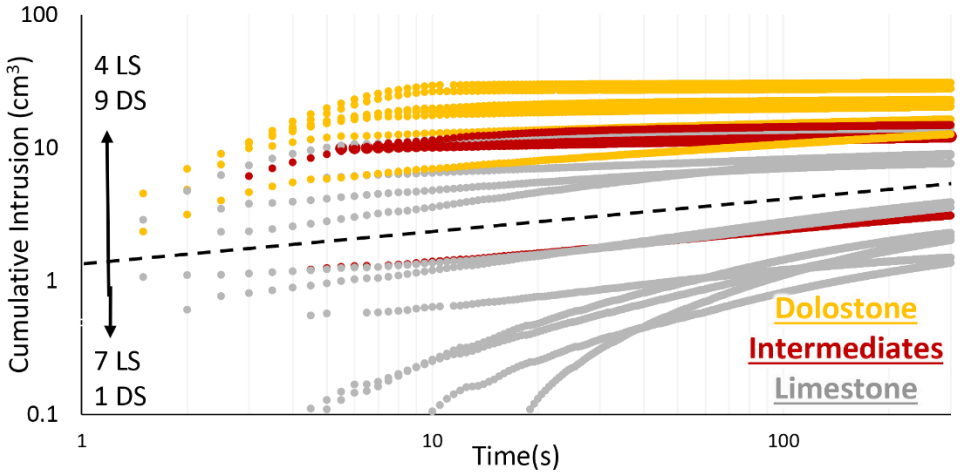

Figure 11. Cumulative intrusion curves plotted for studied samples with 1,650 cm^3 chamber

In the figure, lithological categories can be differentiated (i.e., primarily limestone sources versus primarily dolostone sources). This is possible because dolostone lithologies are more macroporous (so they have higher PLIs) while limestones are more nonporous or microporous (so they have lower PLIs).

After decreasing the chamber size, retesting of the 21 samples occurred using the 3G IPI SOP. Large chamber and small chamber PLI values plotted against 2G IPI data revealed similar indices, but overall there was more primary load intrusion with the use of the smaller chamber. To portray the origin of this relationship, 2G, large chamber, and small chamber IPI indices were compiled (Table 2). Utilizing the smaller chamber, PLI values ranged from 22–135 among primarily limestone samples and 36–307 among dolomitic samples. For SLI values, less differentiation between limestone (ranging from 10 to 50) and dolostone (10 to 46) occurred. Although analyzing cumulative intrusion with the large chamber differentiated lithology well, utilizing the smaller chamber separated primarily macroporous and microporous aggregate better (Figure 12).

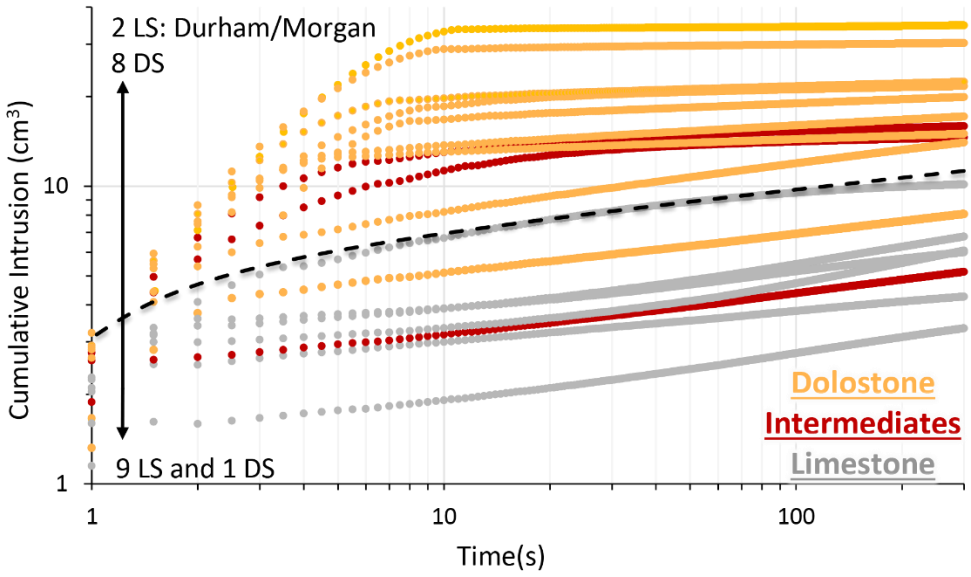

Figure 12. Cumulative intrusion curves for 1,100 cm^3 chamber

Decreasing chamber size to 1,100 cm^3, resulted in a greater spread in cumulative intrusion curves compared to the 1,650 cm^3 chamber. This allowed individual curves to be more easily read and lithologies were better separated. This can be attributed to recording more total intrusion by decreasing initial soak time.

With both PLI and SLI, values recorded with the small chamber were larger than those measured with the larger chamber, but large chamber IPI values were rather dissimilar to Gustafson et al. (2015) (Figure 13).

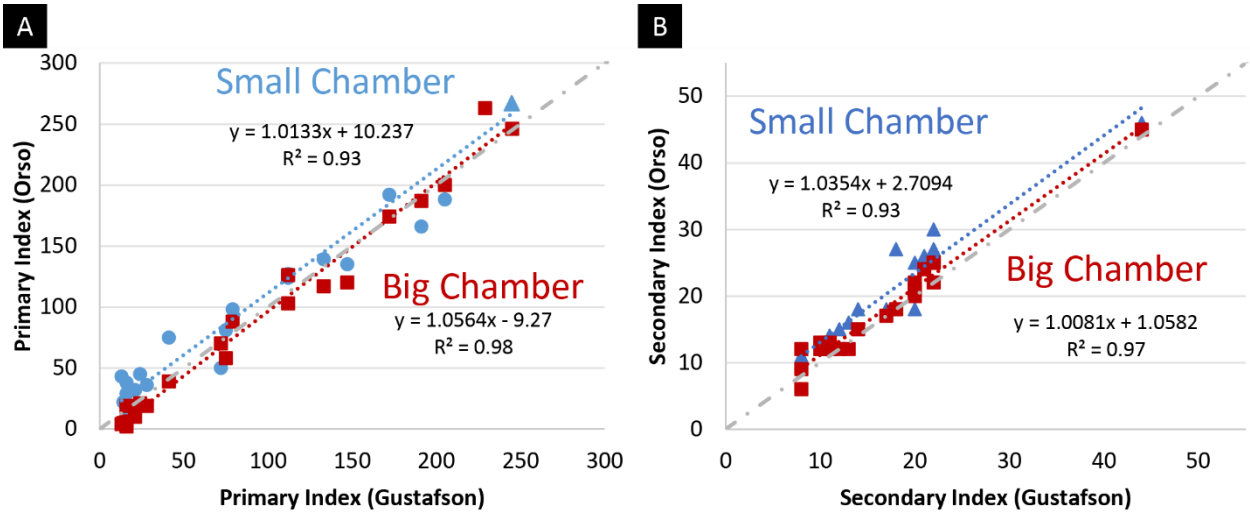

Figure 13. (a) Primary and (b) secondary load indices with the small chamber vs. big chamber

Note in Figure 13a that the PLI recorded with the small chamber deviated from prior data more than the large chamber. The trend line of the small chamber lies above the unity line and implies a positive deviation in PLI, or more macropore intrusion. A similar trend is observable with SLI (Figure 13b).

Through decreasing apparatus size, IPI indices for all 21 samples record higher pore volumes than with the larger 3G IPI chambers or with the 2G IPI graduated cylinders. This likely arose from the decrease in initial soak time. Small chamber and big chamber apparatus PLI and SLI values were compared to Gustafson et al. (2015) data.

Initially, five lithologically distinct samples were tested with the 3G IPI device procedure with other pressures: 15 psi (approximately atmospheric) and 60 psi. Prior to each test, chamber expansion volumes were recorded to reduce chamber-related volume changes. Table 3 lists the PLI and SLI values of each source (i.e., Bowser-Springville, Jones, Morgan, Sully, and Waucoma) derived from these various pressures.

Table 3. PLI and SLI calculated for five lithologically diverse sources

	PLI			SLI		
Source	**15 psi**	**35 psi**	**60 psi**	**15 psi**	**35 psi**	**60 psi**
Bowser-Springville	176	303	373	14	16	19
Jones	31	45	71	28	30	28
Morgan	52	92	140	31	45	41
Sully	124	175	192	37	35	35
Waucoma	5	14	19	19	21	24

Table 3 shows that PLI increases significantly as pressure increases, while SLI appears unaffected by an increase of fluid pressure.

To determine the effect of various rates of pressure, both PLI and SLI were plotted against pressure. With increasing pressure, PLI increased (Figure 14a).

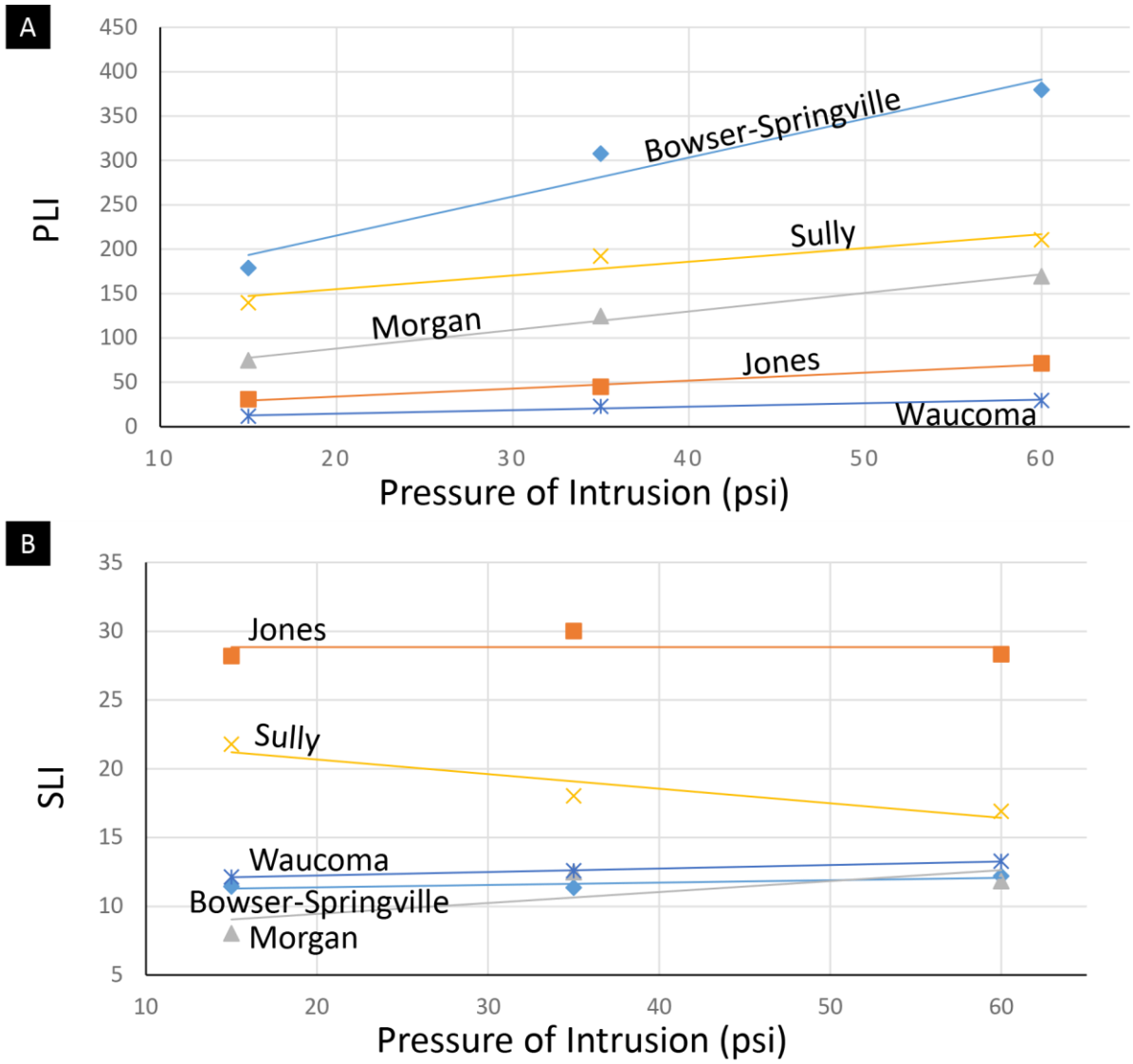

Figure 14. Pressure of intrusion for (a) PLI and (b) SLI for each source

As pressure of intrusion increased from 15 to 60 psi, PLI values increased (Figure 14a). However, this increase did not occur at the same rate in all samples but increased corresponding to macropore porosity in each sample. Increasing the pressure from 15 psi to 60 psi, the largest increase in PLI values occurred with Bowser-Springville, while the only a minute increase in PLI values was observed with Waucoma CA.

A dissimilar relationship between pressure of intrusion and SLI is visible (Figure 14b), implying that the majority of pore intrusion occurs within the initial minute of testing. No trend is observable between increasing pressure and SLI measurements. As pressure was increased, SLI values decreased for Sully CA, increased for Morgan CA, and remained relatively constant for Jones, Bowser-Springville, and Waucoma CA (Figure 14b).

To help derive more information from variable pressure tests, the remaining 16 CA samples were analyzed under 15, 30, and 60 psi intrusion conditions. Incremental intrusion plots were constructed for all sources that compare the deviation among these three pressures of intrusion (Figure 15a–u).

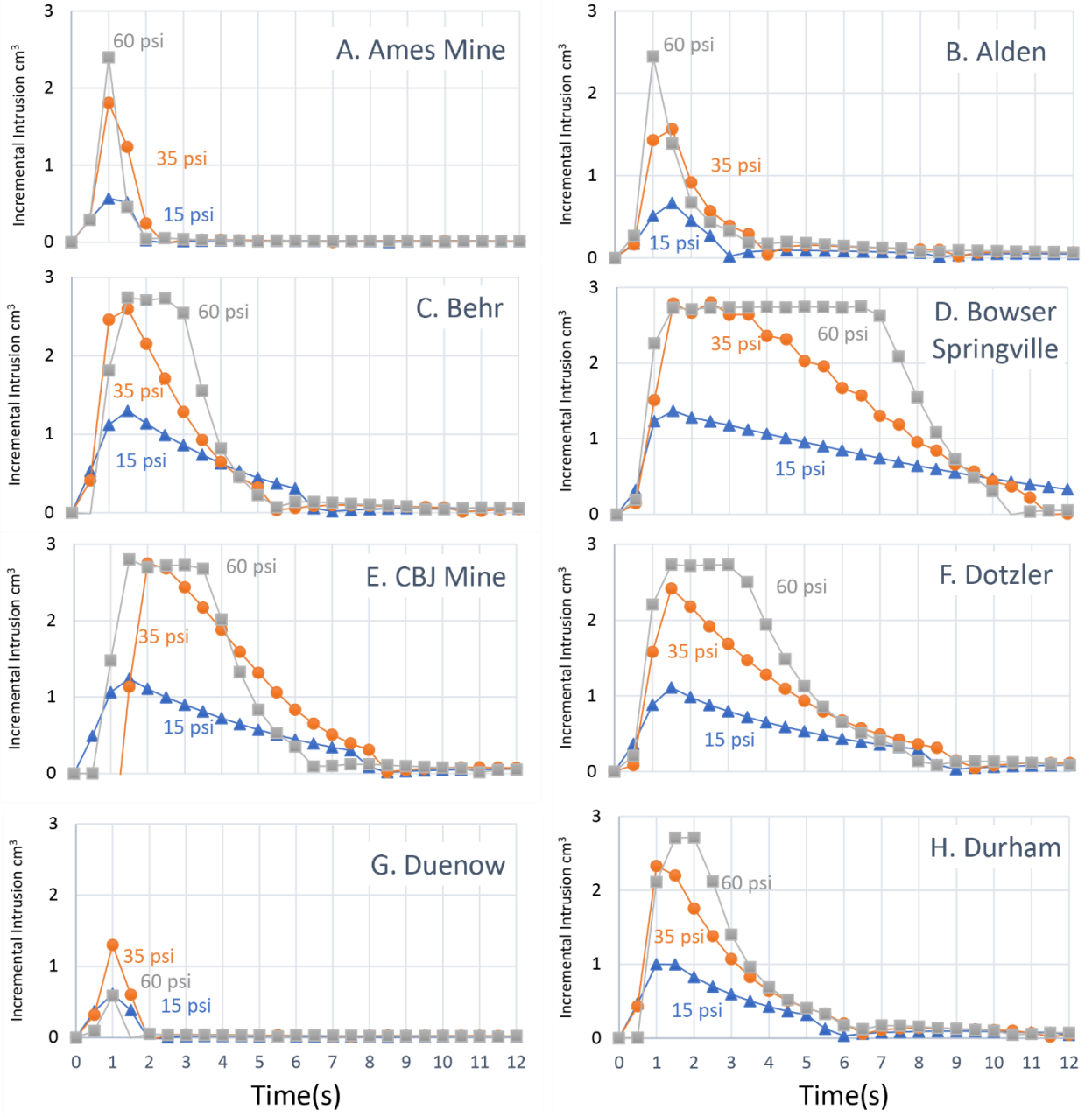
A. Ames Mine
B. Alden
C. Behr
D. Bowser Springville
E. CBJ Mine
F. Dotzler
G. Duenow
H. Durham
60 psi
35 psi
15 psi
Incremental Intrusion cm³
Time(s)

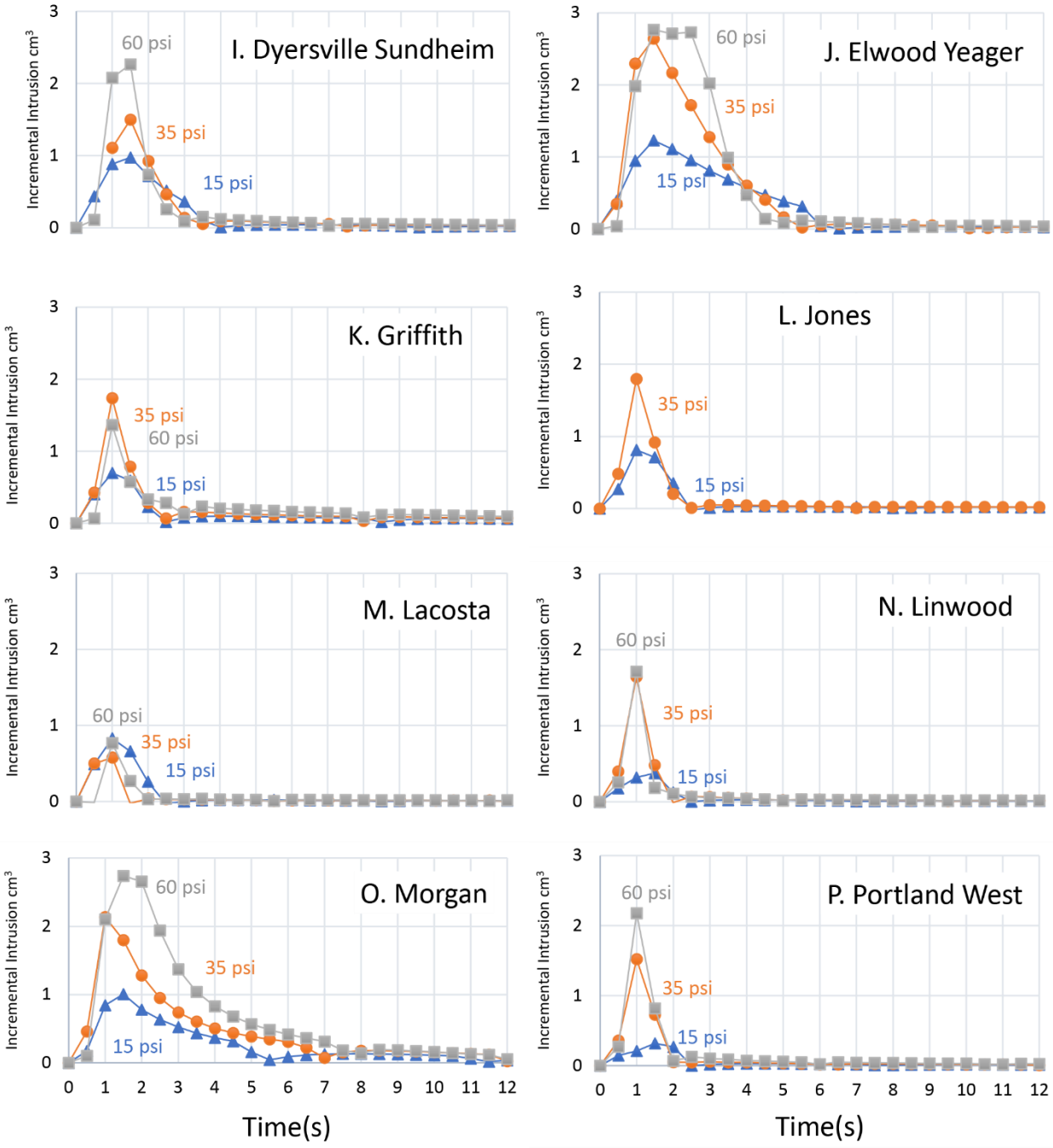
I. Dyersville Sundheim
J. Elwood Yeager
K. Griffith
L. Jones
M. Lacosta
N. Linwood
O. Morgan
P. Portland West
60 psi
35 psi
15 psi
Incremental Intrusion cm³
Time(s)

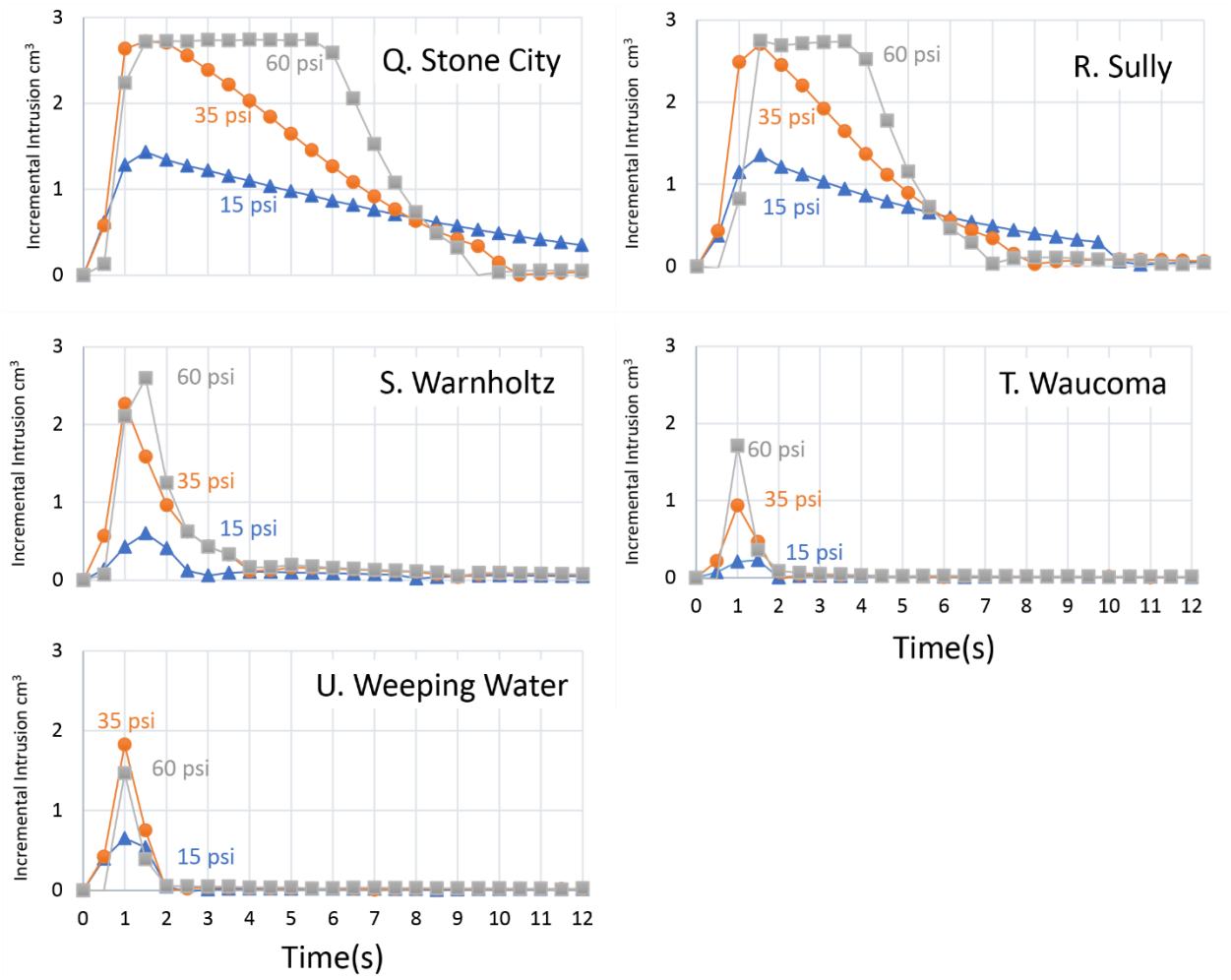

Figure 15. Incremental intrusion plots for the 21 CA samples at various pressures

Due to operational error, Jones 60 psi test failed to yield accurate results (Figure 15l). Incremental intrusion plots were created through calculating volumes of intrusion every 0.5 s during the testing procedure. The 3G IPI records cumulative intrusion, but computing the change of intruded volume every 0.5 second yields incremental rates. It is important to note that axes scales remain uniform among plots. Through plotting incremental intrusion of the samples, the transition point at which macropore intrusion concludes and micropore intrusion commences is source-specific and is visible by rate of change in intrusion. Transition points were determined through the plots and shown in Table 4.

Table 4. Transition points of each source

Source	Lithology	Transition point(s)
Alden	LS	2
Duenow	LS	2
Lacosta	LS	2
Linwood	LS	2
Waucoma	LS	2
Weeping Water	LS	2
Griffith	LS	2.5
Jones	LS	2.5
Portland West	INT	2.5
Ames Mine	LS	4
Dyersville	DS	4
Warnholtz	DS	4.5
Behr	DS	5.5
Elwood Yeager	INT	5.5
Durham	LS	6
Morgan	INT	7
Sully	DS	8
CBJ Mine	DS	8.5
Dotzler	DS	9.5
Stone City	DS	10.5
Bowser-Springville	DS	11.5

Lithology: LS – limestone, DS – dolostone

The time at which intrusion of macropores concluded was source-specific and ranged between 2 s and 11.5 s. Similarly, the initiation of micropore intrusion varied as a result.

After analyzing pressure- and intrusion-related trends among sources, a transition point between micropore and macropore intrusion was determined. Incremental intrusion data were analyzed to identify transition points where intrusion plateaued to a relatively constant value. The point at which macropore intrusion concludes and micropore intrusion commences varies according to source but is visible within incremental intrusion plots (Table 4). With these new transition points chosen for each source, new 3G PLI and 3G SLI values were calculated (Table 5) where intrusion prior to this transition point is attributed to macropore intrusion (i.e., PLI), while the remaining intruded volume for 15 minutes is indicative of micropore intrusion (i.e., SLI).

Table 5. PLI and SLI recalculated with individualized transition points

	Operational method		Special method		Deviation		
Source	**PLI**	**SLI**	**PLI**	**SLI**	**PLI**	**SLI**	**Lithology**
Alden	81	13	37	66	55%	394%	Limestone
Ames Mine	43	16	33	27	23%	67%	Limestone
Behr	139	26	117	48	16%	87%	Dolostone
Bowser-Spr.	307	11	303	16	1%	41%	Dolostone
CBJ Mine	166	22	149	40	10%	83%	Dolostone
Dotzler	188	14	166	35	12%	157%	Dolostone
Duenow	38	50	20	68	47%	36%	Limestone
Durham	135	15	109	41	19%	171%	Limestone
Dyersville	50	27	29	43	42%	62%	Limestone
Elwood Yeager	127	14	112	28	12%	96%	Intermediate
Griffith	75	27	30	73	60%	168%	Limestone
Jones	45	30	31	44	31%	47%	Limestone
Lacosta	29	180	10	199	65%	11%	Limestone
Linwood	32	10	23	19	29%	98%	Limestone
Morgan	124	12	92	45	26%	261%	Intermediate
Portland West	36	18	24	30	34%	63%	Intermediate
Stone City	267	10	260	18	3%	72%	Dolostone
Sully	192	18	175	35	9%	94%	Dolostone
Warnholtz	98	46	62	82	37%	79%	Dolostone
Waucoma	22	13	14	21	38%	67%	Limestone
Weeping Water	38	32	27	43	29%	35%	Limestone

All sources concluded macropore intrusion within the first 12 s. Hence, PLI values decreased, while SLI values increased. As a result, the 1-minute transition point that has been previously used with the 2G IPI would result in PLIs that incorporate a significant proportion of SLI intrusion. Although deviation from both historical and prior data is significant, individualized PLI and SLI values calculated for individual rock types ("special method") may better represent individual pore distributions.

Rock Typing

Rock typing was carried out on the 11 CA sources that had not been analyzed previously (cf. Gustafson et al. 2015). While many of these sources appeared to be homogenous to the naked eye, most sources contain at least three distinct rock types (Figure 16) based on color, visual porosity, dissolution, clasts, and matrix.

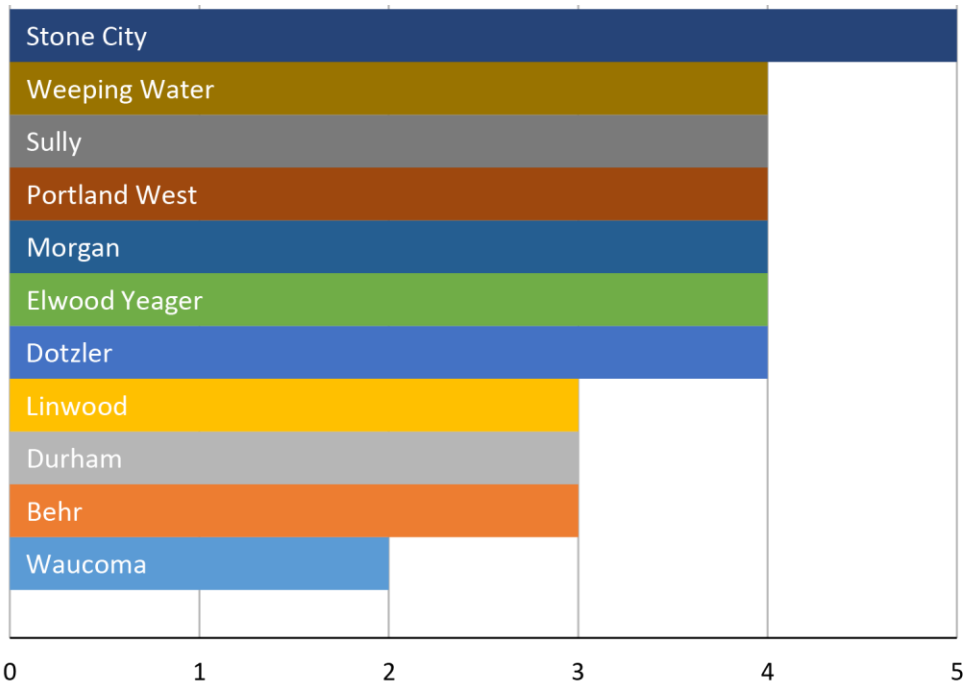

Figure 16. Rock types for the 11 CA sources

Note that most sources contained at least three different lithologies.

Each rock type was ranked by abundance, or weight percent (e.g., Type 1, the most abundant and Type 5, the least abundant). Among the CA sources, Waucoma aggregate was the most homogenous, containing only two distinct lithologies. On the other hand, Stone City aggregate was the most heterogeneous source analyzed, containing five rock types. In total, 40 pairs of aggregate pebbles were labeled and desiccated for subsequent analysis.

Helium Porosimetry

To verify similar lithological pairs were categorized through rock typing and retained for additional analysis, grain density was calculated for each CA sample for correlation purposes (Table 6).

Table 6. Grain density by source as measured by helium pycnometry

Source	Grain density (g/cm^3)					Weighted grain density (g/cm^3)
	Type 1	Type 2	Type 3	Type 4	Type 5	
Waucoma	2.71	2.71				2.71
Behr	3.14	2.84	3.17			3.07
Durham	2.73	2.74	2.75			2.73
Linwood	2.71	2.88	2.73			2.74
Dotzler	2.89	2.91	2.86	3.32		2.96
Elwood Yeager	2.87	2.82	2.83	2.88		2.86
Morgan	2.71	2.72	2.72	2.77		2.71
Portland West	2.72	2.82	2.82	2.71		2.77
Sully	2.87	3.05	2.88	2.88		2.93
Weeping Water	2.72	2.73	2.72	2.74		2.72
Stone City	2.87	2.86	2.85	2.87	2.93	2.87

In order to determine accurate rock type pairs, as well as variations within an individual source, helium pycnometry was utilized to determine grain density. The grain density of all 80 aggregate samples were measured and the data were normalized based on rock type abundance to calculate an average for the sample. Through using grain density as a determining factor, the heterogeneity within a particular coarse aggregate source is evident. However, dolomitic aggregate grain densities were elevated compared to limestone lithologies based on mineral compositions.

Of the 40 aggregate pairs, the average deviation in grain density between aggregates of each pair was 0.036 g/cm^3. However, most aggregate pairs deviated less than 0.01 g/cm^3. The two largest outliers from this trend that significantly affected the average were Behr CA with pairs deviating 0.23 and 0.28 g/cm^3. The grain density of the aggregate pairs ranged from 2.71 g/cm^3 and 3.32 g/cm^3. The densest aggregate pair was recorded as Type 4 Dotzler CA (3.32 g/cm^3), while the least dense was observed as Type 1 aggregate originating from Morgan quarry (2.71 g/cm^3).

However, due to differences in abundance among the aggregate types, each grain density measurement was standardized to the aggregate's percent abundance. Therefore, among the 40 aggregate pairs, the normalized grain density of all lithologies ranged from 2.71 g/cm^3 to 3.07 g/cm^3 (i.e., Waucoma sourced and Behr sourced, respectively). It was assumed that normalizing each grain density by rock type abundance representative grain densities would be produced for each source.

Generally speaking, CA sources that have been primarily characterized as limestone possessed lower grain densities among the sample set (Figure 17).

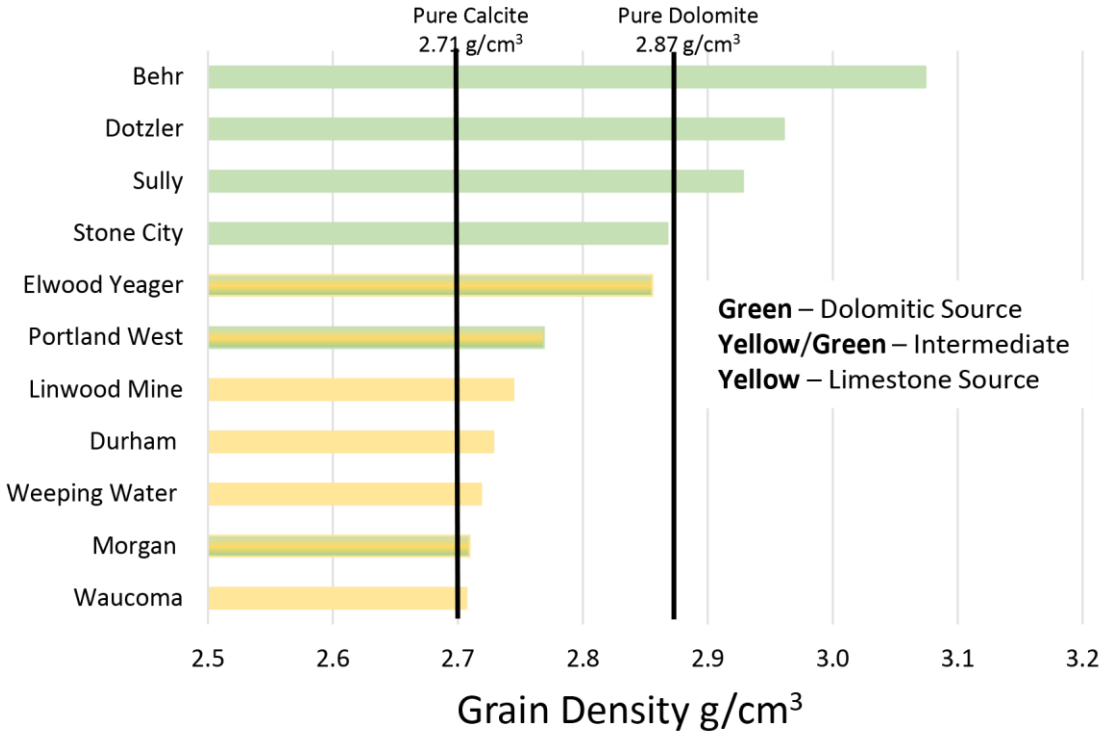

Figure 17. Grain density for 11 sample sources

Although grain density fluctuates among these sources, the variation is dictated by mineralogical compositions. The primary mineral within limestone is calcite (2.71 g/cm^3), while dolomite (2.87 g/cm^3) is dominant within dolostone. However, as indicated with source grain densities, both limestone and dolomitic sources stray from their primary mineral grain density. Impurities, secondary mineralization, and alteration likely contributed to these results.

The average grain density of the limestone sources analyzed was 2.72 g/cm^3, essentially the density of pure calcite, 2.71 g/cm^3. In contrast, dolomitic sources had an average of 2.94 g/cm^3, close to the density of pure dolomite, 2.84 g/cm^3. Impurities, secondary mineralization, and mineral alterations (e.g., clay, iron oxide, metallic carbonate minerals) within these dolomitic sources likely influenced these higher grain densities.

Mercury Intrusion Porosimetry

Mercury intrusion porosimetry (MIP) provides a more detailed measurement of pore network by providing a pore-throat size distribution curve, which ultimately quantifies effective porosity. Eleven CA sources were analyzed via MIP to identify their modal pore-throat sizes and assess whether they were within the critical range. The critical range is a range of pore-throat sizes that cause deterioration within aggregates (Ridzuan et al. 2017). This range has been disputed, but the general consensus exists within a 0.005 to 0.2 µm range (Kaneuji 1978, Marks and Dubberke 1982, Ridzuan et al. 2017). For the purpose of this study, the critical pore range of investigation

was 0.02–0.1 µm, as previously determined from studying similar CA with similar methods (Ridzuan et al. 2017).

Mean, median, and mode of pore-throat sizes within each rock type were determined. In addition, a normalized mean, median, and mode was determined for each rock type that incorporated rock type abundances. In conclusion, 13 of these rock type samples possessed a modal pore-throat distribution within this critical range (Table 7).

Table 7. Modal pore-throat diameters measured via mercury intrusion porosimetry

Source	Mean (um)	Mode (um)	Median (um)	Rock type (%)	Normalized mean (um)	Normalized mode (um)	Normalized median (um)
Behr-1	0.0179	0.0071	0.0431	72%	0.0185	0.0076	0.0394
Behr-2	0.0190	0.0094	0.0242	23%			
Behr-3	0.0249	0.0064	0.0519	6%			
Dotzler-1	0.9441	0.0476	2.7390	31%	0.5741	0.0227	1.6781
Dotzler-2	0.1839	0.0101	0.3710	30%			
Dotzler-3	0.6397	0.0088	1.7220	22%			
Dotzler-4	0.5069	0.0179	2.0190	17%			
Durham-1	0.3095	0.0381	0.8236	89%	0.3062	0.0367	0.8414
Durham-2	0.1065	0.0390	0.1597	6%			
Durham-3	0.4772	0.0109	1.9260	5%			
Elwood Yeager-1	0.1021	0.0412	0.1144	61%	0.0912	0.0280	4.6746
Elwood Yeager-2	0.0157	0.0080	0.0172	21%			
Elwood Yeager-3	0.1461	0.0065	27.7700	16%			
Elwood Yeager-4	0.0883	0.0077	2.0110	2%			
Linwood-1	0.0646	0.0430	0.0671	78%	0.0853	0.0369	0.0961
Linwood-2	0.1589	0.0148	0.2000	18%			
Linwood-3	0.1614	0.0148	0.2000	4%			
Morgan-1	0.2627	0.0074	0.5609	75%	0.2003	0.0065	0.4303
Morgan-2				17%			
Morgan-3	0.0434	0.0136	0.1378	6%			
Morgan-4	0.0172	0.0064	0.0206	1%			
Portland West-1	0.1495	0.0481	0.2632	41%	0.2916	0.1017	6.9301
Portland West-2	0.0801	0.0090	23.7500	28%			
Portland West-3	0.8913	0.2950	1.1380	22%			
Portland West-4	0.1602	0.1657	0.2119	9%			
Stone City-1	0.8372	0.0295	4.7990	82%	0.7336	0.0276	4.5625
Stone City-2	0.1817	0.0071	6.3140	6%			
Stone City-3	0.3924	0.0156	1.8680	6%			
Stone City-4	0.2172	0.0105	3.8450	3%			
Stone City-5	0.1711	0.0617	0.3174	3%			
Sully-1	1.6010	0.0130	17.7000	32%	1.3890	0.0174	12.6376
Sully-2				31%			
Sully-3	0.7932	0.0347	3.6980	24%			
Sully-4	5.3720	0.0374	47.6800	13%			
Waucoma-1	0.0332	0.0108	0.0600	85%	0.0600	0.0143	0.8220
Waucoma-2	0.2136	0.0345	5.1920	15%			
Weeping Water-1	0.0234	0.0073	0.0296	82%	0.0552	0.0119	2.8912
Weeping Water-2	0.0613	0.0384	0.0610	7%			
Weeping Water-3	0.4522	0.0125	46.6500	6%			
Weeping Water-4	0.0835	0.0543	0.0622	5%			

Note: Relative abundances of rock types were used to calculate source-standardized values.

In an attempt to connect mercury porosimetry data to IPI results, normalized values of each source were compared to PLI and SLI indices. Large chamber and small chamber indices were incorporated. Although little correlation can be observed between PLI and mercury data, a trend can be identified between modal pore throats and large chamber SLI values (Figure 18).

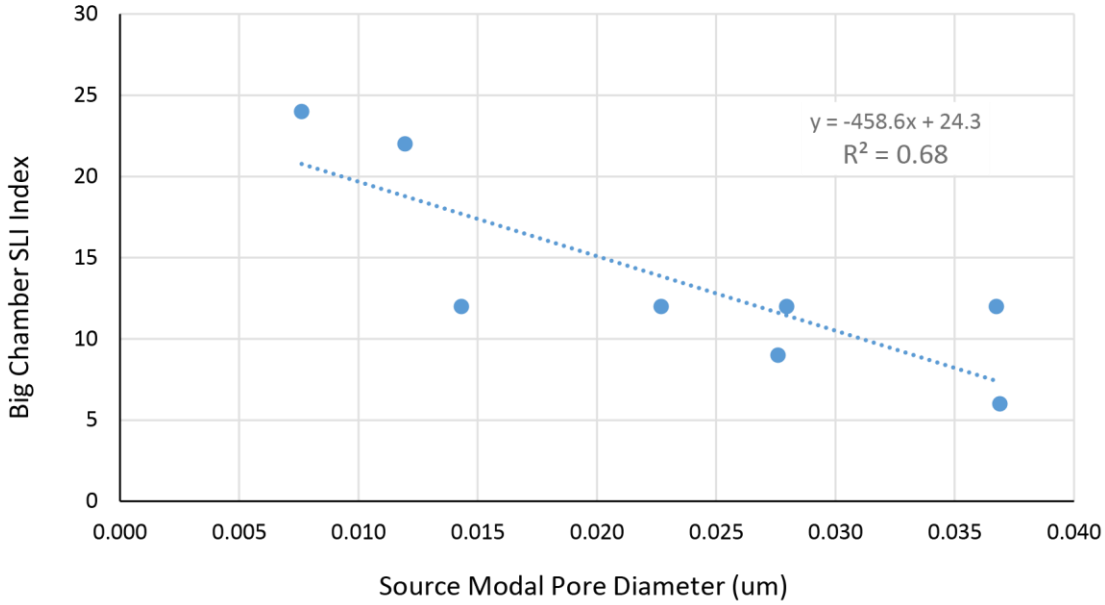

Figure 18. Comparison between source modal pore diameter and big chamber SLI index

Through determining mean, median, and modal pore-throat diameters of each rock type utilizing mercury porosimetry, as better understating of the bulk behavior of each source was pursued. By comparing these parameters to PLI and SLI indices in both current and recent studies, a moderate correlation is shown between large chamber SLI and source-standardized modal pore-throat diameters. It is suggested that as modal pore-throat diameters decrease, SLI index values increase. Hence, these smaller pore throats are what has been associated with a higher susceptibility to ice segregation deterioration within individual aggregate grains. Among the 11 sources, Morgan, Portland West, and Sully CA results were omitted due to incomplete mercury porosimetry data.

Thin Section Petrography

Thin-section petrography was used to document the composition/matrix, pore structure, and texture of each sample as well as to attribute a relative mud index value ranging from 1 to 3 (with 1 indicating a minimum mud component and 3 indicating a large relative proportion of mud). On this basis, the likely environment of deposition for each was inferred (Table 8).

Table 8. Lithological features and inferred corresponding environments of deposition

Source	Mode (um)	Limestone vs. Dolostone	Grain Size	Grain Type	Texture	Pore type	Mud index	Grain- vs. Mud-dominated	Interpreted EOD
Behr-1	0.0071	Dolostone	M	Dolomite	Crystalline	Interparticle / Vuggy	2	Grain-dominated	Deep Subtidal
Behr-2	0.0094	Dolostone	F	Dolomite	Crystalline	Interparticle	3	Grain-dominated	
Behr-3	0.0064	Dolostone	F	Dolomite	Crystalline	Imtercrystalline	1	Grain-dominated	
Dotzler-1	0.0476	Dolostone	F	Microcrystalline	Dolomicrite	Interparticle / Vuggy	3	Mud-dominated	Subtidal
Dotzler-2	0.0101	Dolostone	F	Microcrystalline	Dolomicrosparite	Intercrystalline / Vuggy	2	Mud-dominated	
Dotzler-3	0.0088	Dolostone	F-C	Microcrystalline	Dolomicrite	Intercrystalline	2	Grain-dominated	
Dotzler-4	0.0179	Dolostone	F	Dolomite	Dolomicrosparite	Intercrystalline	2	Mud-dominated	
Durham-1	0.0381	Limestone	C	Skeletal / Peloids	Peloidal Packstone	Interparticle	2	Grain-dominated	Skeletal Shoal
Durham-2	0.039	Limestone	C	Peloids / Skeletal	Peloidal Grainstone	Interparticle	1	Grain-dominated	
Durham-3	0.0109	Limestone	C	Skeletal Packstone	Skeletal	Interparticle	1	Grain-dominated	
Elwood Yeager-1	0.0412	Dolostone	F	Dolomite	Dolomicrite	Intercrystalline	3	Mud-dominated	Deep Subtidal
Elwood Yeager-2	0.008	Dolostone	F	Dolomite	Dolomicrite	Intercrystalline	1	Grain-dominated	
Elwood Yeager-3	0.0065	Dolostone	M	Dolomite	Crystalline	Intercrystalline / Vuggy	1	Grain-dominated	
Elwood Yeager-4	0.0077	Dolostone	F	Dolomite	Dolomicrite	Intercrystalline	2	Mud-dominated	
Linwood-1	0.043	Limestone	M	Sparry Calcite	Crystalline	Breccia	1	Grain-dominated	Lagoon/ Peritidal
Linwood-2	0.0148	Limestone	F	Microcrystalline	Micrite	Intergranular Microporosity	3	Mud-dominated	
Linwood-3	0.0148	Limestone	F	Peloids	Peloidal Packstone	Intergranular Microporosity	2	Mud-dominated	
Morgan-1	0.0074	Limestone	F	Peloids / Skeletal	Peloidal Wackestone	Intergranular Microporosity	3	Mud-dominated	Peritidal/Supratidal
Morgan-2		Limestone	F	Microcrystalline	Micrite	Intergranular Microporosity	3	Mud-dominated	
Morgan-3	0.0136	Limestone	M	Calcite	Crystalline	Intercrystalline	2	Grain-dominated	
Morgan-4	0.0064	Limestone	M	Calcite	Crystalline	Intercrystalline	1	Grain-dominated	
Portland West-1	0.0481	Limestone	F	Microcrystalline	Micrite	Intergranular Microporosity	2	Mud-dominated	Shallow Subtidal
Portland West-2	0.009	Dolostone	F	Dolomite	Crystalline	Interparticle / Vuggy	1	Grain-dominated	
Portland West-3	0.295	Limestone	M	Microcrystalline	Micrite	Interparticle / Vuggy	1	Grain-dominated	
Portland West-4	0.1657	Limestone	F	Skeletal	Skeletal Micrite	Intergranular Microporosity	3	Mud-dominated	
Stone City-1	0.0295	Dolostone	F	Dolomite	Crystalline	Intercrystalline	2	Grain-dominated	Lagoon/ Intermound
Stone City-2	0.0071	Dolostone	F	Dolomite	Crystalline	Intercrystalline / Moldic	1	Grain-dominated	
Stone City-3	0.0156	Dolostone	F	Dolomite	Crystalline	Intercrystalline	1	Grain-dominated	
Stone City-4	0.0105	Dolostone	F	Dolomite	Crystalline	Intercrystalline / Shelter	2	Grain-dominated	
Stone City-5	0.0617	Dolostone	F-M	Dolomite	Crystalline	Intercrystalline	2	Grain-dominated	
Sully-1	0.013	Dolostone	M	Dolomite	Crystalline	Intercrystalline	1	Grain-dominated	Inner-Mid Ramp
Sully-2		Dolostone	M	Dolomite	Crystalline	Intercrystalline / Vuggy	1	Grain-dominated	
Sully-3	0.0347	Dolostone	F-M	Dolomite	Crystalline	Intercrystalline	2	Grain-dominated	
Sully-4	0.0374	Dolostone	M	Dolomite	Crystalline	Intercrystalline / Vuggy	1	Grain-dominated	
Waucoma-1	0.0108	Limestone	F	Skeletal	Skeletal Packstone	Interparticle Microporosity	3	Mud-dominated	Lagoon
Waucoma-2	0.0345	Limestone	F	Skeletal	Biomicrite	Interparticle Microporosity	3	Mud-dominated	
Weeping Water-1	0.0073	Limestone	F-M	Skeletal	Skeletal Wackestone	Interparticle Microporosity	2	Mud-dominated	Deep Subtidal
Weeping Water-2	0.0384	Limestone	F-M	Skeletal	Skeletal Packstone	Interparticle Microporosity	2	Mud-dominated	
Weeping Water-3	0.0125	Limestone	F-M	Skeletal	Skeletal Packstone	Interparticle Microporosity	1	Mud-dominated	
Weeping Water-4	0.0543	Limestone	F-M	Skeletal	Skeletal Packstone	Interparticle Microporosity	2	Mud-dominated	

Note: Among the outline features are grain size, grain type, texture, pore types, and relative mud indices. Combining these attributes, a general depositional environment was assigned to each aggregate source as a whole.
Grain size: F = Fine, M = Medium, C = Coarse

Behr

Type 1 Behr CA (Figure 19a), 72% of the sample, contained primarily very-fine to medium crystalline dolomite (10 µm to 70 µm crystal diameter).

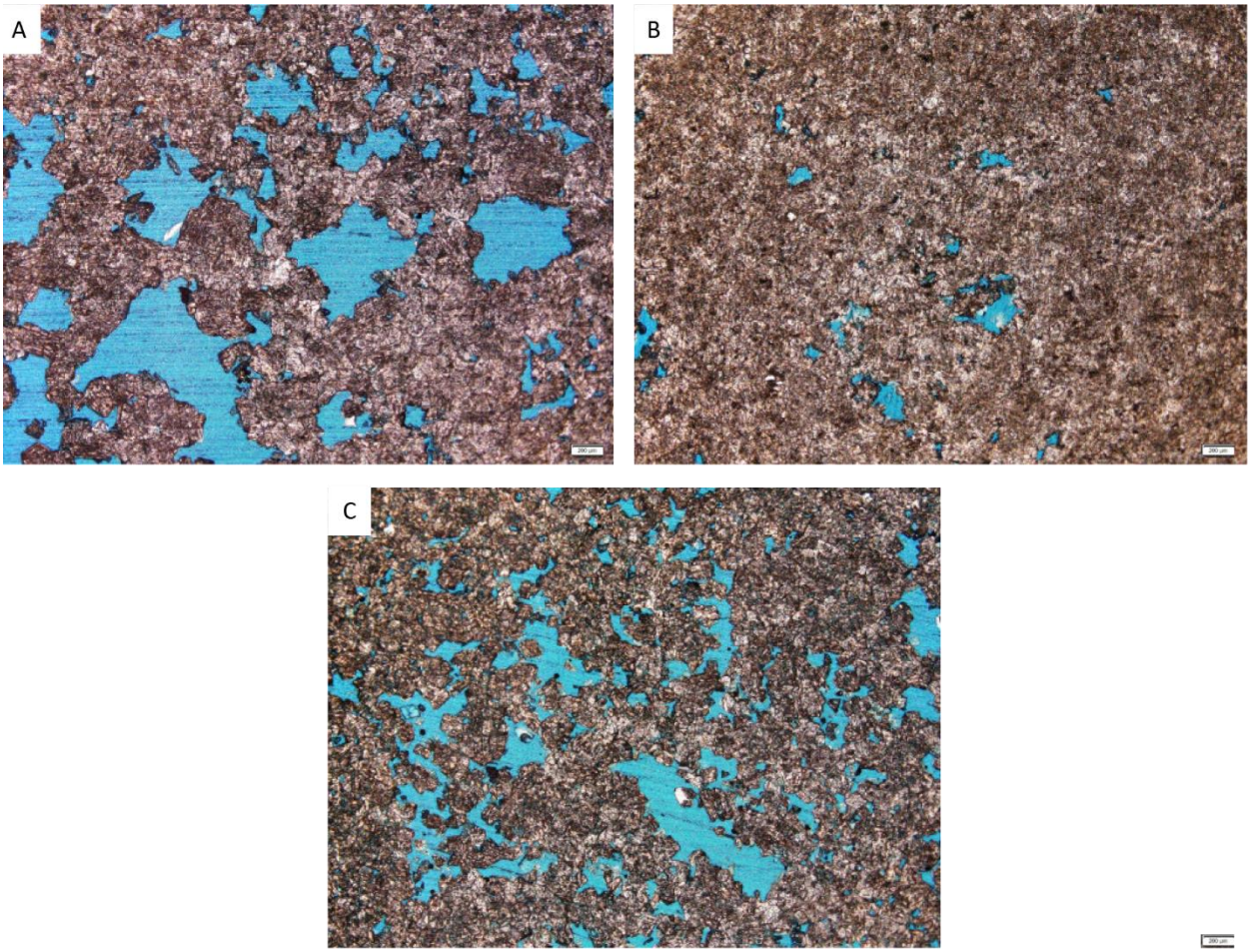

Figure 19. Behr (a) Type 1, (b) Type 2, and (c) Type 3

Type 1 (Figure 19a) appears to contain an abundance of large (>300 µm) touching vugs (cavities inside aggregate), but possess a modal pore diameter of 7.13 nm. Decreasing in visible porosity, Behr Type 2 (Figure 19b) contains a modal pore diameter of 9.44 nm. Lastly, at only 6% source abundance, Type 3 (Figure 19c) contains a pore diameter mode of 6.44 nm. Visible as brown, nearly opaque occurrences, other secondary mineralization led to higher grain densities than Type 1 and 3.

This facies is dominated by planar-s crystals and are mostly subhedral. Primary fabric does not appear to have been preserved. Pores are present in the form of interparticle pores and touching vugs with a visual estimation of approximately 20–35% porosity. Dissolution seems present on vug surfaces and to have partially connected vugs. Most vugs are at least 250 µm in diameter. Trace, partially opaque, or dark brown minerals are also visible within Type 1 Behr CA. Type 2

Behr CA (Figure 19b) is primarily composed of very-fine to fine crystalline dolostone with anhedral crystal forms. Type 2 CA comprises 23% of Behr-sourced rock. The presence of increased mud is implied by non-distinctive granular material and visual porosity decreases as a result. Pores are mostly present as fine (i.e., < 5µm), interparticle pores with occasional medium-sized vugs (i.e., 300 µm). Lastly, Type 3 CA (Figure 19c) has a similar fabric as Type 1. However, porosity in Type 3 is described as intercrystalline and fenestral porosity. All three rock types of Behr CA show evidence of dissolution (Figure 19). This sample was likely deposited within an open marine, deep subtidal setting (Ludvigson et al. 1992).

Dotzler

Dotzler aggregate (Figure 20) is composed of four distinct rock types with varying abundances (i.e., 31%, 31%, 22%, and 17%, respectively).

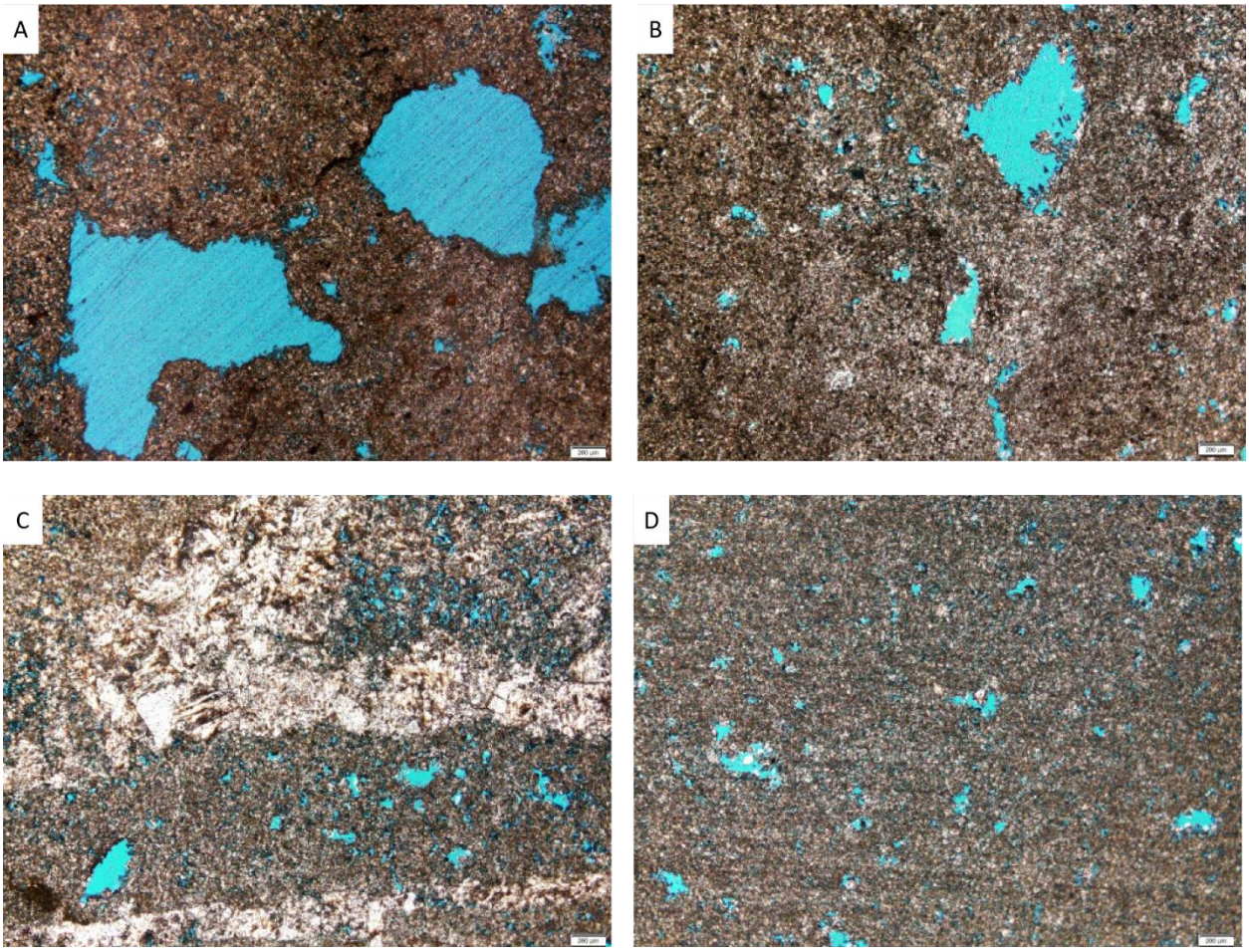

Figure 20. Dotzler (a) Type 1, (b) Type 2, (c) Type 3, and (d) Type 4

As a result, although this source has multiple lithologies, they occur in approximately similar proportions. This uniformity is unique to the Dotzler CA. Dotzler Type 1 sourced CA is composed of primarily very-fine to fine crystalline dolomicrite with occasional fracture-filling

dolomite that is medium to coarse grained. Most pores are located between dolomicrite crystals, so they fit into the interparticle pore class. Fracture-filling dolomite precipitated as anhedral poly-modal crystals with minimal porosity. Few large vugs (600–800 µm) are present, but dissolution surfaces appear to line these bodies. Within Type 2 CA, mineral composition is dominated by fine grains of dolomite, which results in a rock type of dolomicrosparite. These grains are rather euhedral and display planar-e type fabrics (i.e., clearly defined intercrystalline boundaries). Pores within Type 2 occur primarily as intercrystalline pores (i.e., <10 µm), and occasional vuggy secondary porosity. Type 3 Dotzler CA mineralogy consists of a very fine-grained dolomicrite with abundant fractures filled with coarse dolomite cement ranging in size from approximately 15 µm to 350 µm. All crystals within this rock type are anhedral and nonplanar. A visual estimate of porosity is in the range of 10–15% as intercrystalline pores. Rock Type 4 comprises 17% of the Dotzler sample and is rather muddy with very fine grained, anhedral, nonplanar dolomite. Pores within this type are predominantly intercrystalline though some appear to be products of dissolution (Figure 20D). The interpreted environment of deposition for Dotzler CA was likely an open marine, subtidal setting (Witzke et al. 1988).

Durham

Durham aggregate has historically been categorized as an intermediate source, where both dolostone and limestone beds are mined for aggregate (Figure 21).

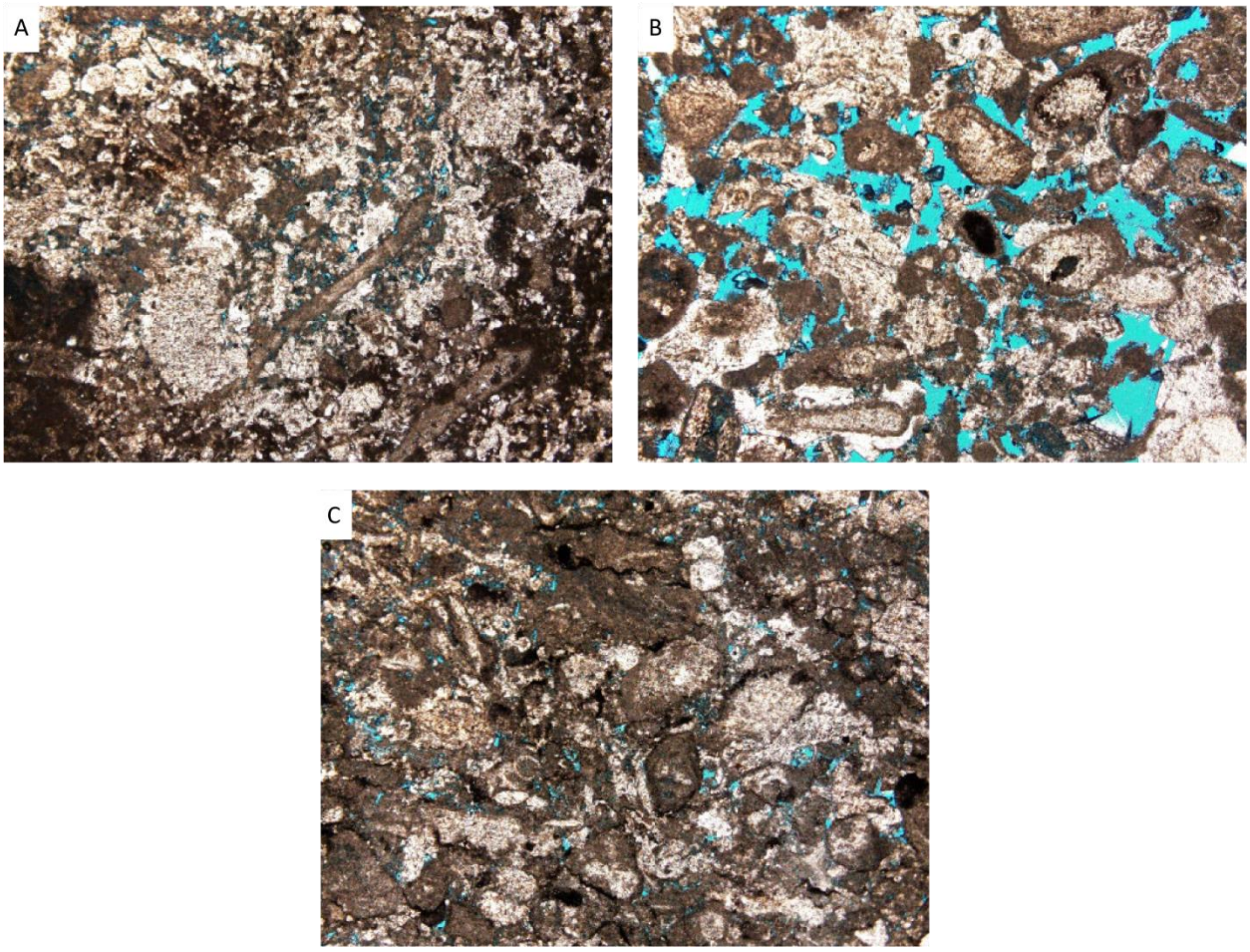

Figure 21. Durham (a) Type 1, (b) Type 2, and (c) Type 3

Modal pore diameters are 38.1, 38.9, and 10.8 nm, respectively.

This sample was derived from a primarily pure limestone bed (i.e., North Hill Group). Through rock typing, it was concluded that Durham contains three rock types, but is dominated by Rock Type 1 with an 89% abundance. This rock type contains skeletal fragments (e.g., crinoid), peloids, and a minute proportion of mud. Therefore, this lithology is classified as a crinoidal peloidal packstone. Approximately 30% of the grains appear to be dolomitized at grain boundaries. Stylolites are present within this rock type. A visual porosity estimation of 5–7% comes from the presence of 10–50 µm interparticle pores. Type 2, which only constitutes 6% by abundance, is a peloidal grainstone with occasional crinoid debris with grains approximately 150–300 µm in diameter. Little dolotimization is visible, but dissolution within interparticle pores is apparent as grain boundaries appear to be receding. Hence, these rims can be interpreted as intergranular pressure dissolution. This rock type yielded a visual porosity estimation of 10–15%. Lastly, Rock Type 3 is a coarse skeletal packstone. Grains range from 200 µm to 1 mm with interparticle pores. Stylolites are present and larger grains possess dissolution rims that aid in pore connectivity. With highly abundant fossilized material, the hypothesized depositional environment for Durham aggregate was a skeletal sand shoal located within the inner-mid ramp setting (Witzke and Bunker 2001).

Elwood Yeager

This source contains four rock types with the following abundances: 61%, 21%, 16%, and 2% (Figure 22).

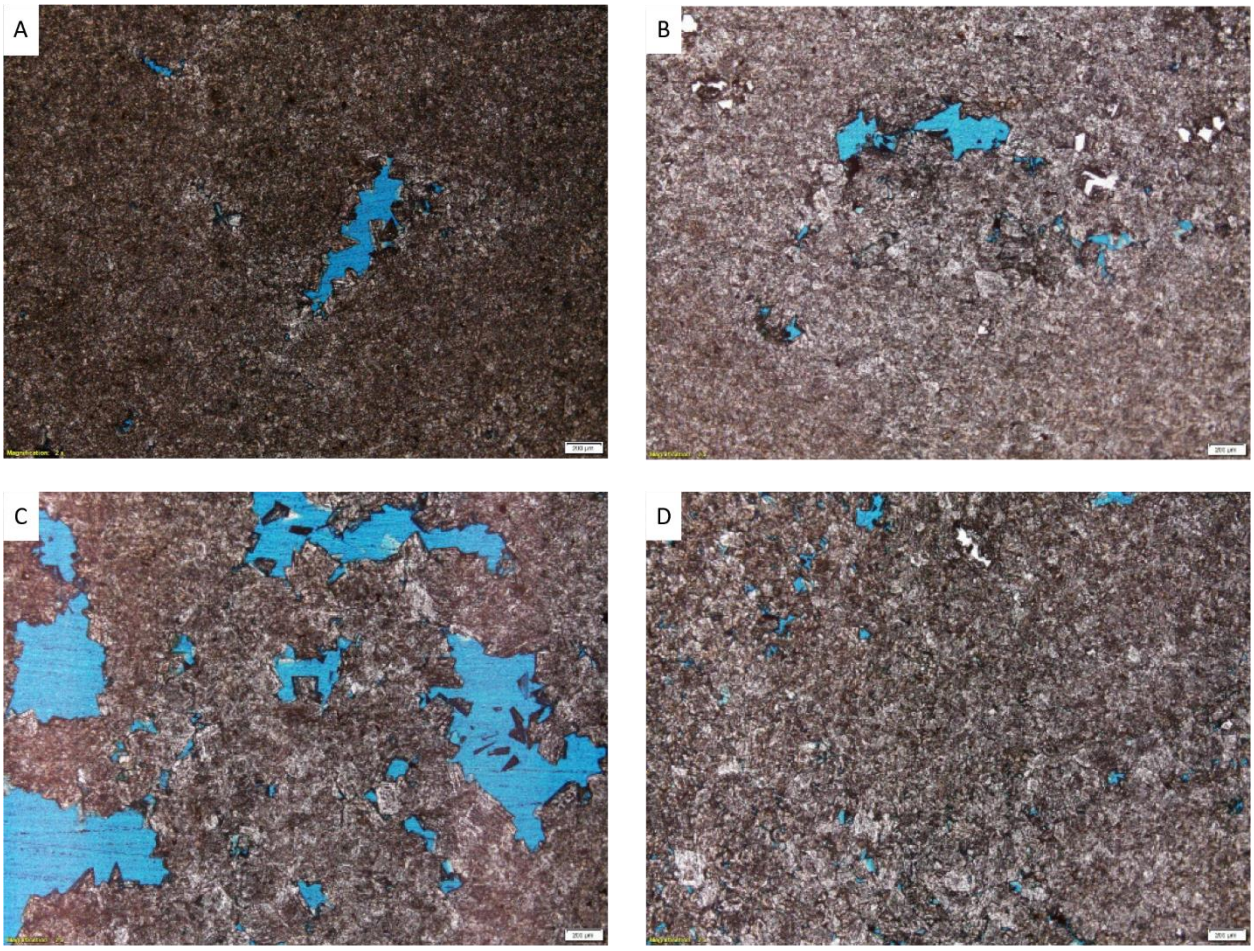

Figure 22. Elwood-Yeager (a) Type 1, (b) Type 2, (c) Type 3, and (d) Type 4

Note that Type 3 (Figure 22c) appears to possess the most visual porosity among this source with roughly 20–30%. Modal pore throats vary among rock types (41.2, 8.8, 6.5, and 7.7 nm, respectively).

Type 1 CA is a non-planar dolomicrite with minimal intercrystalline porosity resulting in low visual macroporosity. However, secondary pores are present in the form of large, occasionally connected vugs that range from 150 µm to 1.2 mm in diameter. Similarly, Type 2 and Type 4 CA are composed of very fine and fine anhedral dolomite crystals forming a dolomicrite. Intercrystalline pores are imperceptible, but occasional 100–200 µm sized vugs are visible. Visible porosity of these rock types is less than 3%. Type 3 is unique among other Elwood Yeager rock types because it includes rare intercrystalline pores and an extensive pore system of large vugs (i.e., 0.2–3 mm) and few connecting channels (touching vugs). Additionally,

dolomitic grain sizes range from fine nonplanar anhedral crystals to medium euhedral crystals. Through comparing photomicrographs, an approximate visual porosity of 20–30% was determined. Elwood Yeager CA was deposited in an open marine, deep subtidal environment (Ludvigson et al. 1992).

Linwood

Linwood CA (Figure 23) is principally composed of Type 1 lithologies (78%), while Types 2 and 3 contribute to only 18% and 4%, respectively.

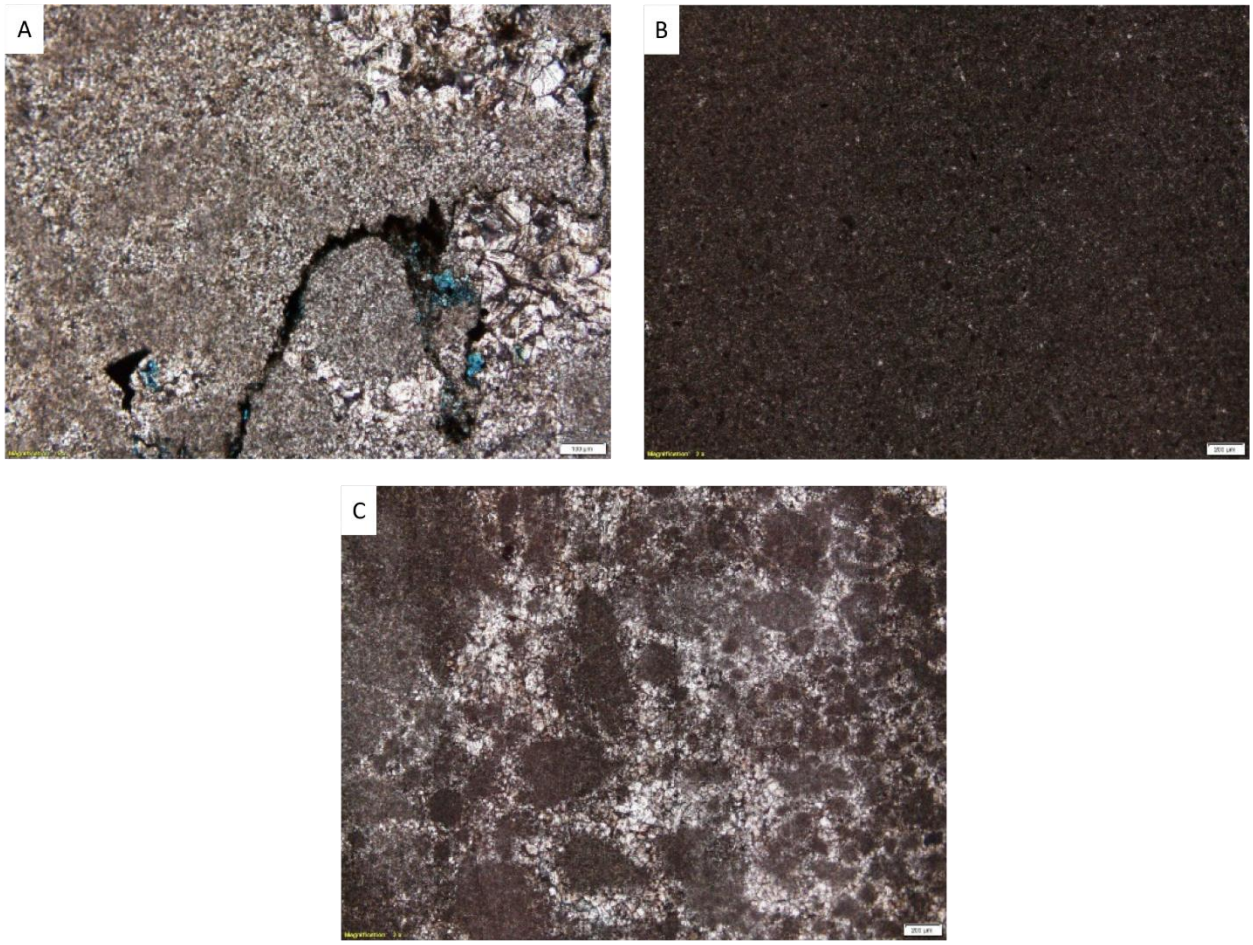

Figure 23. Linwood CA (a) Type 1, (b) Type 2, and (c) Type 3

Modal pore-throat diameters are 43.0, 14.8, and 14.8 nm, respectively.

Grain size within Type 1 ranges widely from < 5 µm to 150 µm. Within both the fine and coarse calcite lithologies, intercrystalline pores are rare. Most pores occur along stylolites and at the interface between coarse and fine-grained areas. Along these planes, dissolution occurred and created small pores (i.e., <50 µm in diameter). As a result, due to the angularity of the coarser clasts as well as the fine sparry calcite cement, the sample is described as a brecciated limestone.

Type 2 differs significantly; its composition is predominantly very fine-grained lime mudstone. Its component crystals are relatively undistinguishable due to diminutive size and they host minimal porosity, none of which was observed through thin section microscopy. At only 4% weight abundance, Type 3 is classified as a peloidal packstone, or biopelmicrite, with pore-forming micro-fractures. Abundant clay-sized particles supported an interpreted depositional setting of lagoonal/peritidal on an inner ramp (Witzke et al. 1988).

Morgan

Rock Type 1 CA (Figure 24) constitutes 75% of this source.

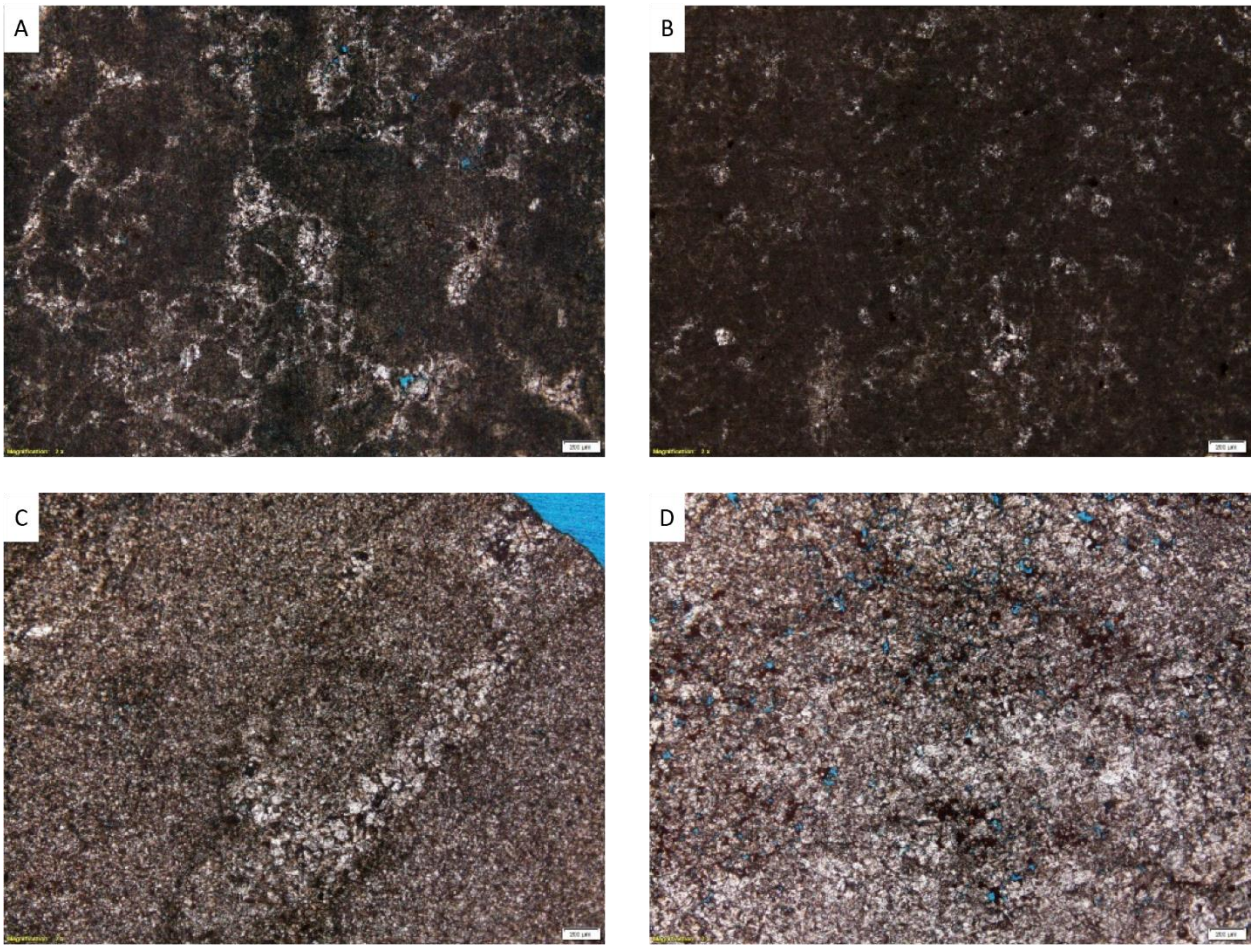

Figure 24. Morgan CA (a) Type 1, (b) Type 2, (c) Type 3, and (d) Type 4

The average grain size of Type 1 is approximately 275 µm and grains are peloidal and skeletal in origin (e.g., ostracoda). Micropores are visible at grain boundaries and are less than 10 µm in size. Micropore throats occasionally connect these pore bodies and result in a visual porosity of around 3–5%. This rock type is a peloidal skeletal wackestone. Rock Type 2 is composed of very fine matrix material with an occasional euhedral calcite crystal; it is best described as a micritic limestone or a lime mudstone. The euhedral crystal forms are approximately 100–200 µm in

diameter and are 5–10% of the thin section composition, while the muddy matrix is <5 µm. Pores are indescribable due to nanoscale pores. Rock Type 3 contains mainly fine, subhedral calcite crystals with common coarse-grained calcite mineralization in fractures. Coarser grains appear to be more euhedral in form with rare intercrystalline pores. On the other hand, within the finer matrix, intercrystalline pores are abundant, resulting in a visual estimate of approximately 15% porosity. At only 1% weight abundance within Morgan sourced aggregate, Type 4 samples are a fine to medium grain crystalline grainstone with intercrystalline pores and vugs with approximately 15% visual porosity. A plausible depositional environment for this source is a restricted ramp; peritidal/supratidal facies (Witzke et al. 1988).

Portland West

This aggregate source (Figure 25) has traditionally been referred to as primarily limestone with a minor dolomitic component.

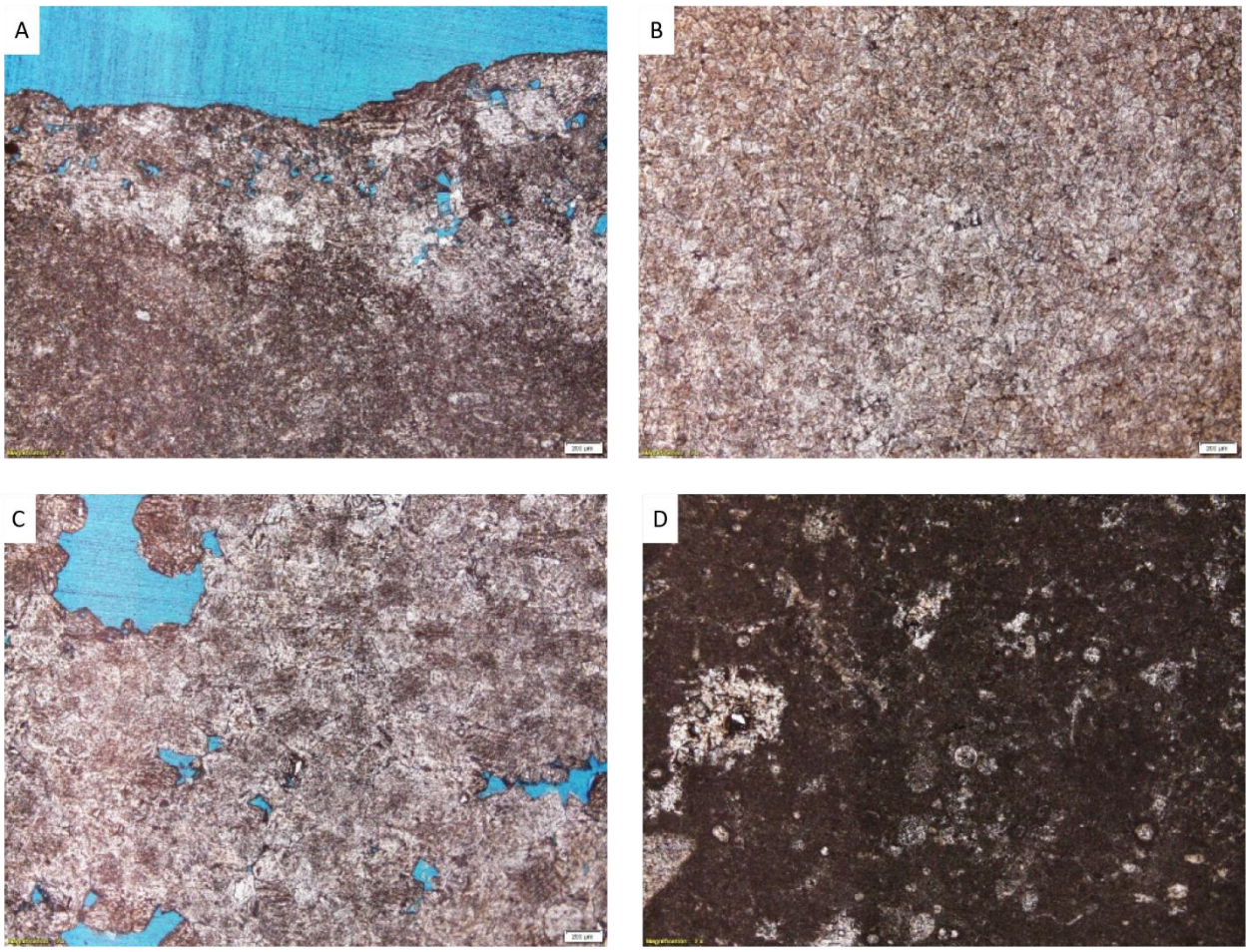

Figure 25. Portland West (a) Type 1, (b) Type 2, (c) Type 3, and (d) Type 4

Modal pore diameters are 48.1, 9.0, 295, and 165 nm, respectively.

The sample analyzed contained four distinct rock types with the following abundances: 41%, 28%, 22%, and 9%. Through thin section analysis, Type 1 is described as primarily a micritic limestone (lime mudstone) with void-filling and surficial dolomite cementation. Dolomitic rhombs are distinguishable with {021} twinning orientation compared to calcite twins (e.g., {012} twins). Visual porosity decreases in abundance and size as grain size decreases, as well as further from the dolomitization fronts. Contrary to Type 1, Rock Type 2 is mainly nonplanar, polymodal dolomite that is approximately 100 μm in size. Vugs solely attribute to a visual porosity of around 5%. Type 3 is primarily composed of very fine grains and is considered a micritic limestone. However, within voids, dolomite mineralization is common. Occasional vugs contribute to a visual porosity of 6%. Type 4 aggregate is composed of an argillaceous micrite with abundant crinoid debris and trace ostracod and amphipora fragments. Porosity appears minimal within this rock type. Portland West CA was deposited within an open marine, shallow subtidal environment (Witzke et al. 1988).

Stone City

Stone City contains five rock types (Figure 26) and is the most heterogeneous source analyzed within this study.

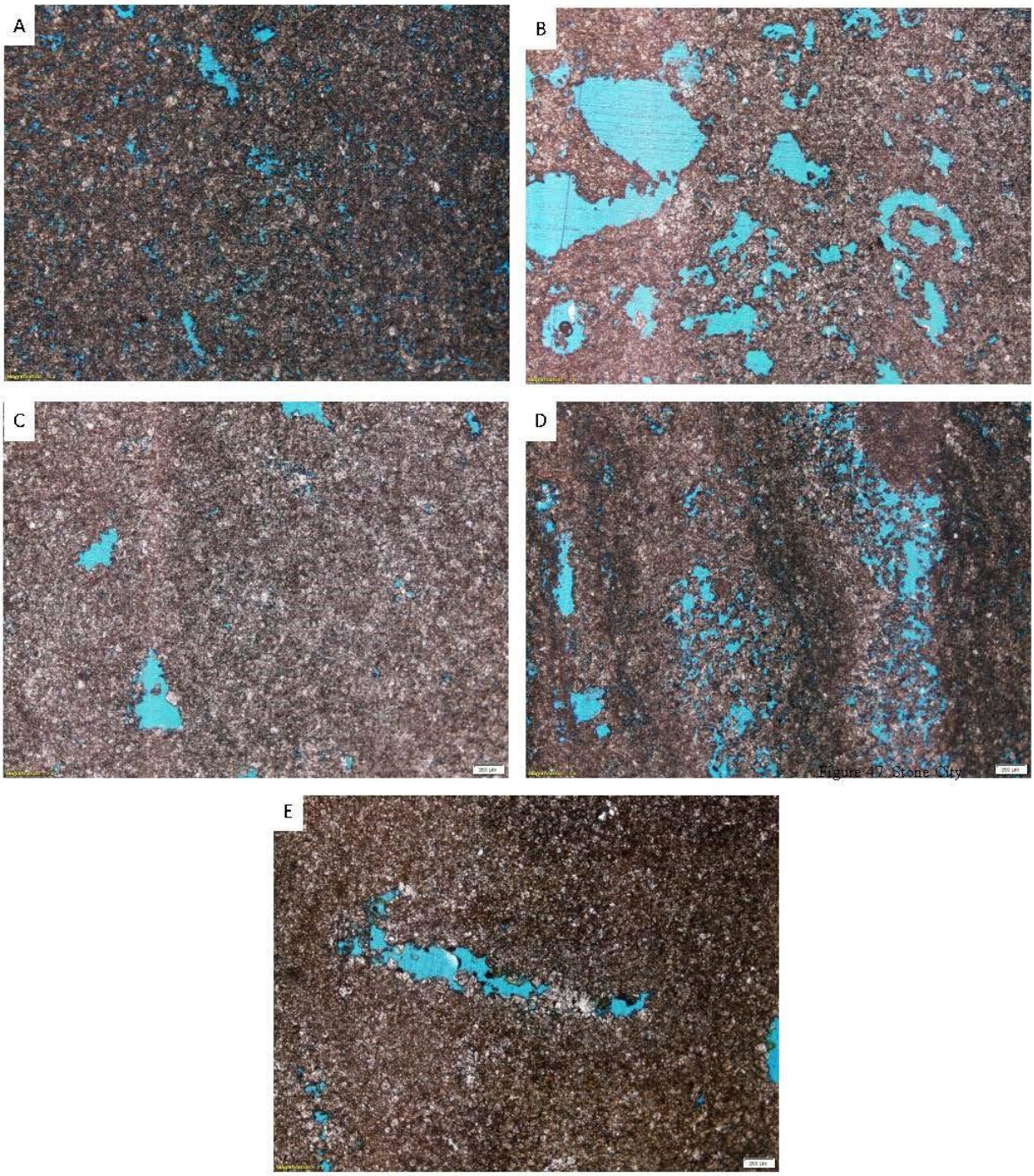

Figure 26. Stone City (a) Type 1, (b) Type 2, (c) Type 3, (d) Type 4, and (e) Type 5

Stone City's modal pore-throat diameters are 29.5, 7.1, 15.6, 10.5, and 61.7 nm, respectively. Note that Type 4 CA (Figure 26d) is unique among this source as it appears to be a product of the dolomitization of a stromatoporoid fossil.

Despite this diversity, the majority of pebbles were categorized as Type 1 with 82% abundance. Type 1 is highly porous with a grain composition of fine-grained polymodal, planar-e, euhedral, dolomitic rhombs. Abundant intercrystalline pores and the rare vug (approximately 200 µm) contribute to a visual porosity of about 25%. Type 2 Stone City CA is similarly porous with an estimated visual porosity of 20%. This fine-grained polymodal dolostone appears to possess pores that have resulted from fossil dissolution (i.e., moldic pores). Of these organisms, crinoids and goniophyllum (e.g., square corals) have been removed preferentially during fabric-selective dissolution. Type 3 is comparable to Type 2 CA with a fine-grained polymodal dolomitic arrangement. However, pores are reduced due to rarer vugs and intercrystalline pores. The presence of previous organism (e.g., crinoids and goniophyllum) is unclear. A visual porosity estimation of 15% was found for Rock Type 3. At only 3% abundance, Type 4 CA is unique compared to prior Stone City CA. Thick (i.e., 200–400 µm) linear, fine-grained, features were observed. Coarse-grained polymodal dolomite crystals line these features and the majority of vugs and intercrystalline pores are contained in the dolomitic layer; a visual porosity of 20–30% is applicable. As a result, this rock type is interpreted to be the product of dolomitization of a stromatoporoid. Lastly, at only 3% weight abundance, Type 5 CA is a fine-grained unimodal, planar-s dolomite with large vugs ranging from 0.1 to 8 mm in diameter. The lining of these vugs appeared smooth in texture. This suggests that these are dissolution features. As a result, the visual porosity of this rock type is estimated at 20–35%. These lithologies were deposited in a lagoon or intermound setting (Ludvigson et al. 1992).

Sully

Aggregates from this locality are composed of four specific rock types, but are all dolomitic in lithology (Figure 27).

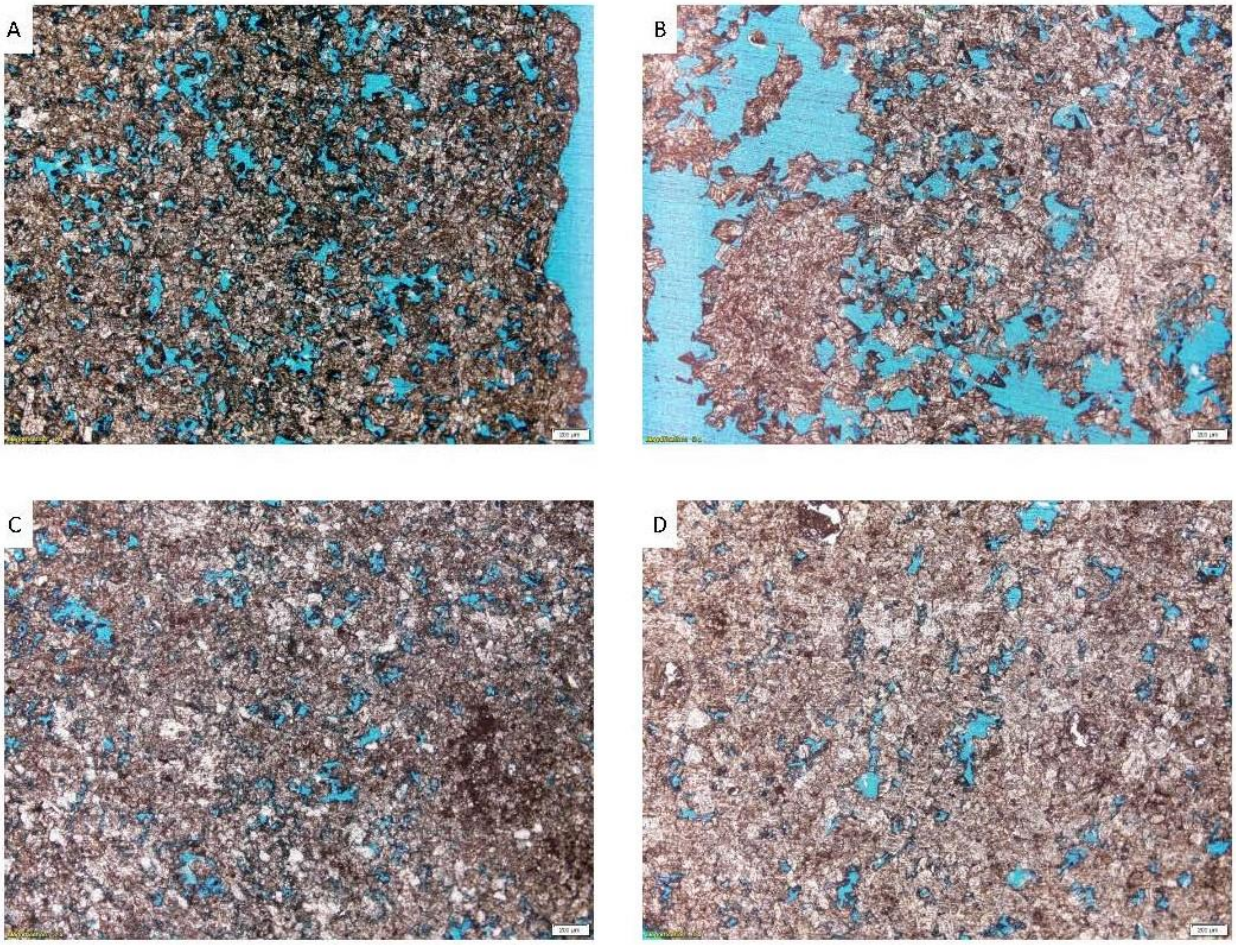

Figure 27. Sully sourced aggregate (a) Type 1, (b) Type 2, (c) Type 3, and (d) Type 4

Modal pore-throat diameters within this source range from 13–37 nm, with Type 2 aggregate possessing the greatest visual porosity (i.e., approximately 30–40%).

Type 1 comprises 32% of the sample and is a homogenous dolostone composed of medium unimodal, planar-e dolomite crystals. Intercrystalline pores are abundant; some of which show evidence of dissolution with smooth pore surfaces. This dolomite is very porous with a visual porosity estimate of 30%. Type 2 was similar to Rock Type 1 with medium unimodal, planar-e dolomite crystals, but there were also frequent nonplanar, fine dolomite crystals. Intercrystalline pores are more abundant in the coarser-grained constituents, while rare in the micro-dolomitic features. Within this rock type, channels and vugs increase the connectivity of various pore types and suggest past dissolution. Within an occasional vug or channel, rare slightly opaque minerals are present (likely iron oxides). Porosity of 30–40% was estimated visually for this rock type. Compared to previously discussed Sully CA, Rock Type 3 (24%) is finer in grain size and possessed less abundant macropores. This dolostone was composed of poly-modal, planar-e dolomite crystals. Pores in this sample were located between crystal interfaces. Rare slightly opaque minerals are present within voids. Rock Type 4 was a dolostone composed of nonplanar anhedral crystals. Intercrystalline pores are minimal, but vugs are common. Vugs and frequent channels are mostly less than 150 µm in diameter, but due to abundance create a sample with

around 15% porosity. The depositional environment was interpreted as an inner-mid ramp setting, perhaps an ooid sand shoal (Witzke and Bunker 2001).

Waucoma

The sample contained only two rock types (Figure 28), making this source the least diverse.

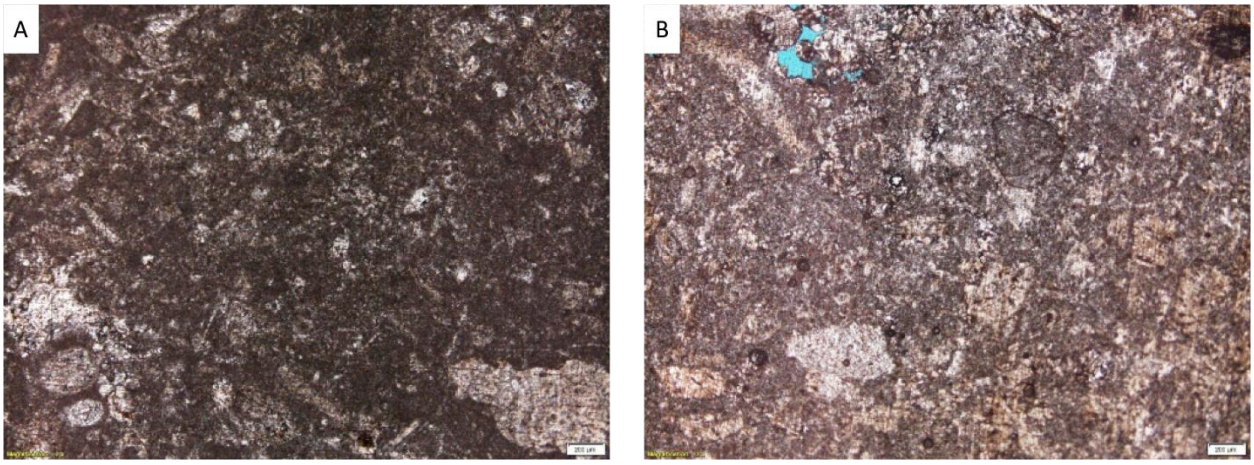

Figure 28. Waucoma (a) Type 1 and (b) Type 2

Modal pore diameters are 10.8 and 34.5 nm, respectively.

Rock Type 1 was a skeletal packstone, or biomicrite. This rock is mud-dominated and has an abundance of fossil material (e.g., crinoids, brachiopods, horn corals, and tabulate corals). Due to its mud matrix, this rock type possesses minimal porosity that is visually identifiable. Type 2 CA differs greatly from the former rock type. This lithology was micrite, or lime mudstone. Rare skeletal material was present, none of it identifiable. Intercrystalline/interparticle pores are absent, while rare vugs were present and result in approximately 3–5% total visual porosity. Waucoma CA, possessing a large proportion of both clay-sized particles and fossil fragments, was interpreted to have been deposited within an open marine, lagoon locality.

Weeping Water

Four rock types were identified in the Weeping Water sample (Figure 29), which is the only Pennsylvanian-aged coarse aggregate source.

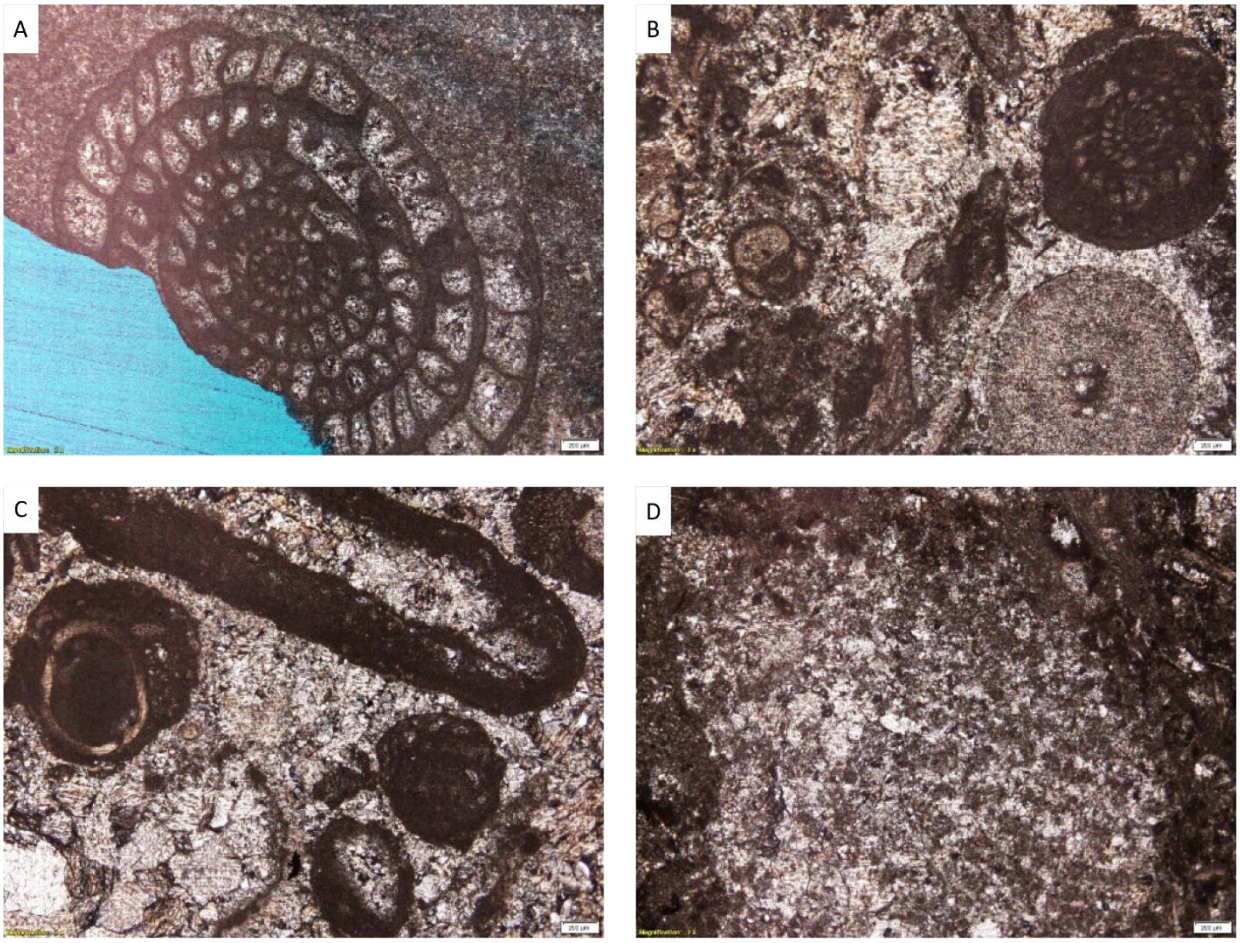

Figure 29. Weeping Water (a) Type 1, (b) Type 2, (c) Type 3, and (d) Type 4

Modal pore diameters are 7.3, 38.3, 12.5, and 54.3 nm, respectively.

Type 1 aggregate comprises 82% of the sample and was classified as a skeletal wackestone (biomicrite). The sole skeletal material within this lithology is a species of foraminifera (e.g., ozawainellidae, neoschwagerininae, schubertellidae, or verbeekininae) (BouDagher-Fadel 2008). These average approximately 2 mm in size. Micropores are indiscernible. Type 2 aggregate (7%) had more abundant fauna and granular material as a result. Therefore, this rock type is a skeletal packstone (biomicrite) and possessed low total porosity with no visual pores. Type 3 aggregates are similarly skeletal packstones (biomicrite), but with less mud; cement appears to be enriched in calcite mineralization. This is indicative of increasing energy of deposition. Crystal re-mineralization is observable within rare vugs. Visually identifiable pores were also rare in this rock type. Type 4 is composed of primarily skeletal packstones (biomicrite) with dolomite-filing fractures. No pores are visible within this sample. Through thin section analysis, an open marine depositional environment was interpreted.

DISCUSSION

3G IPI Test Method and Device

Numerous benefits were achieved through the development of the 3G IPI testing device that overcame challenges with 2G device testing:

Automation reduces operator error. First, the 2G device relies on the operator's perception of intruded volumes through measuring fluid levels by eye within graduated cylinders. With this procedure, inherent error is prevalent and precision in fluid measurements can be variable. Incorporating the FlowTrac II automated fluid intrusion device in the 3G IPI, many of these issues were mitigated. In addition, the improved automation can measure fluid intrusion in time increments varying from 0.1 s to 2 s. Hence, user error in assessing intruded volumes is reduced.

Smaller sample size offers greater flexibility. Sample size has typically remained constant for the IPI devices with 4.5 kg of aggregate are analyzed. However, with the decreased chamber size of the 3G device, sample size was decreased to 1 kg. While samples from producer stockpiles are easy to obtain, using a smaller samples size makes it possible to run the IPI test on shorter sections of core that may not be long enough for the 2G measurement. For example, with the 3G device, a 2.5 in. diameter core sample needs to be only 9 in. long to yield 1 kg of crushed aggregate (assuming 0% porosity and 50% loss to fines on crushing) and 12 in. long if it is 20% porosity. With the 2G device, these lengths need to be 4.5 times longer (40.5 in. and 54 in., respectively).

Reduced soak time. The 2G device required longer to fill the sample chamber prior to measurement. During this time, water was able to intrude the CA's pore system due to spontaneous imbibition without being measured in the PLI graduated cylinder. This likely resulted in PLI measurements being lower than they actually were. With the 2G device, it takes approximately one minute to completely fill the sample-filled chamber and initialize the test. With the 3G device, initial soak time decreased. As determined from experimental data with this study, initial soak time has an influence on the IPI indices that are recorded. Although more prevalent within macroporous sources, both limestone and dolostone samples PLI and SLI deviate based on varying initial soak time because as water is filling the chamber prior to the recording of fluid intrusion, fluid is entering large pores. Through, analyzing the sample and decreasing the chamber volume from 1,650 cm^3 to 1,100 cm^3, pretest soak time decreased 56% and now takes approximately 20 s to completely fill the chamber prior to measurement. With this change, total recorded intrusion increased slightly, which suggests prior measurements may not have accurately measured the macropore volume. Therefore, through decreasing soak time, PLIs that are more representative of actual lithologies are determined.

More accurate PLI and SLI. Because of the automation of intrusion volume measurement, it was possible to track fluid intrusion as a function of time with greater accuracy. From this it was found that a transition was made from PLI-type intrusion to SLI-type intrusion much sooner than 60 seconds, the boundary between primary and secondary intrusion in the 2G device.

In the first stage of this research, 21 CA samples were analyzed using the 2G IPI test method but with the 3G device. These same samples were previously studied for the effect of CA pebble size with the 2G IPI device (Gustafson et al. 2015) and these PLI and SLI values were used as control data for this study. Through analyzing PLI and SLI indices from both studies, it was determined that the 3G device result yielded comparable micro- and macropore ratios. On average, both PLI and SLI indices of these sources increased slightly from results using the 2G device. As recently discussed, this is associated with decreased initial soak time that increased total intruded volumes. Although these indices may deviate from both prior data, this simple difference alone provides more accurate estimations of macropore and micropore volumes.

Along with improved automation, the nature of measuring intrusion with the 3G device permits a higher resolution of intrusion data. Because incremental intruded volumes can be recorded as quickly as every 0.1 s, more information can be derived than through using the 2G device, which only measures the volume of intrusion after 60 s and 900 s. Incremental intrusion can be determined from cumulative intrusion data that is output by the device.

With the ability to analyze incremental intrusion, the rate of intrusion can be calculated and inferred from plots. When plotting the cumulative intrusion for the 21 CA samples, a visual separation of sources that are primarily limestone and sources that are primarily dolostones is present (Figure 12). This differentiation is portrayed within the first 10 seconds of intrusion and is indicative of the PLI (predominantly from macropores). Intuitively, one could expect this relationship, as dolostones are typically more macroporous than limestones. Nonetheless, this provides an additional method to categorize and compare IPI results through incorporating other lithologies.

Faster operation and leak detection. Additionally, the device reads out variation in pressure, which can be used to determine if intrusion is a result of a leak or flawed seal. The previous 2G device included a third graduated cylinder that would analyze potential leaks for 15 minutes after testing. Not needing the additional 15 minutes to run the leak detection cylinder makes the 3G device more time efficient.

Higher pressure can investigate smaller pore sizes. One aspect of the IPI that has remained rather constant through the evolution is the pressure of intrusion utilized to quantify the pore ratios. A water pressure of 35 psi, or 240 kPa, has been the standard since its development in the 1980s. However, with the capabilities of this new device, pressure of intrusion can be varied up to 70 psi. Therefore, in efforts to better understand IPI results, the pressure of testing was initially decreased to 15 psi, then increased to 60 psi. Through this testing, a PLI index relationship with pressure was determined. Through plotting incremental intrusion data for all samples, it was apparent that the rate of intrusion is impacted by the pore structure, which can be indicative of individual lithology. An incremental intrusion plot was created for each source with all three pressure (i.e., 15, 35, and 60 psi) tests specified. By comparing all plots, each incremental intrusion plot appeared rather unique, but collectively, the incremental rate of intrusion seemed to plateau sooner for samples with low macropore abundances. This phenomenon can be explained as water easily intruding larger pores, but as pore-throat diameters decrease, intraparticle forces (e.g., surface tension) increase and result in slower rates of

intrusion. The contact angle of the liquid and the surface tension of the sample rock ultimately dictate the wettability of the fluid/CA pair. However, due to similar chemical and lithological makeup among these sources, the connectivity of pores and pore diameters are the primary components in the rate change of liquid intrusion (Yuan and Lee 2013). With this realization, which was only achieved through the evolution of the IPI device, the times at which PLI and SLI are measured may need revision to shorter time intervals.

Rock Typing

Petrography showed that most CA samples were heterogeneous. Similar to previous studies (Ridzuan et al. 2017), all sources contained more than one rock type. Not only were these differences visually identifiable, but they were also evident petrophysically in the helium pycnometry and mercury porosimetry results. Although some rock types only may be present in small quantities, it is important to assess all rock types because even a small relative abundance of a certain rock type may lead to poor performance. Marks and Dubberke (1982) established that a small quantity (≈ 15%) of flawed aggregate may cause the occurrence of D-cracks within concrete, although the exact proportion has not been defined and indeed may vary depending on the CA's properties.

Critical Pore-Throat Diameters

As previously defined by Marks and Dubberke (1982), the micropores, or capillary pores, that are associated with premature deterioration, range between a pore diameter of 0.04–0.2 μm. It was hypothesized that CA sources possessing a modal distribution of pores within this range would cause D-cracks (Marks and Dubberke 1982). Similarly, if 15% or more of the CA sample possessed this modal size, the source as a whole was regarded as unsound (Marks and Dubberke 1982). Later, this critical range of pore throats was revised to 0.02–0.1 μm through additional analysis with mercury porosimetry data (Ridzuan et al. 2017).

Through using this range, 13 of the 40 distinct rock types analyzed in this study would be deemed lower quality with modal pore-throat diameters within the critical range (Table 7). Additionally, assuming this critical pore-throat range, 5 of these 11 CA sources (i.e., Dotzler, Durham, Elwood Yeager, Linwood, Portland West, and Stone City) would be categorized as non-durable with the most abundant rock types possessing this modal pore size. Within these CA sources, the questionable rock types compose more that 15%. However, this is not the case as all of these sources are categorized with a durability classification of 3 or 3i (i.e., only minimal deterioration in non-interstate roads in 25 and in 30 years, respectively) (Iowa DOT 2019). Based on the premise that the relationship between pore volumes within this critical range and the frequency of D-cracks is still unspecified, this modal differentiation may not truly indicate non-durable CA. However, through a more comprehensive testing approach, the critical range may be able to be re-evaluated with the incorporation of 3G IPI results.

Depositional and Post Depositional Controls on Aggregate Pore Systems

Numerous factors, both depositional and post-depositional, affect the pore system of a carbonate rock. As a result, to understand the capillary pores within aggregate that have been shown to facilitate premature concrete deterioration, it is necessary to account for the depositional and post-depositional features of a carbonate. Dunham (1962) and Folk (1959) both provided classification schemes for the depositional fabric of carbonate rocks based on field and/or petrographic analysis. However, with petrophysics, modern rock fabrics influence fluid/rock interactions. Therefore, in order to fully understand how the lithology of an aggregate influences its IPI results, it is imperative to understand how these properties emerge from the aggregate's depositional and diagenetic history. Through pairing textural features observed through thin section microscopy and IPI indices, a more extensive correlation between lithological and petrophysical properties may be uncovered.

Carbonate Sediment Types

Within carbonate rock, pore types and distributions can be classified as products of primary or secondary processes. Primary pores are dominantly formed during deposition. Murray (1960) defines carbonate primary pores to originate within a combination of framework, mud, and sand-sized sediments. Framework pores occur as intercrystalline pores within precipitated interlocking calcite crystals that can be either organically or inorganically generated. Besides intercrystalline pores, primary vugs are typically prevalent as framework is often formed imperfectly and fragmented. Carbonates with framework texture form predominantly in reef settings where autochthonous carbonate accumulation rates are rapid and result in thick carbonate platforms. Although inorganically generated carbonate contributes to such systems, fauna (e.g., echinoids, bivalves, sponges) provide the majority of carbonate framework textures (Perry et al. 2011). Besides reef settings, hot springs, karst/cave deposits, and ground water generate such framework textures.

Another type of sedimentation that affects carbonate primary pores involves the deposition of transported carbonate sand- and gravel-sized particles. Typically, such material is deposited within high-energy environments that prevent finer particles from settling out of suspension (e.g., shorelines, areas adjacent to reefs). Ooids, peloids, and skeletal fragments are among the most prevalent deposited material within this category of carbonate sediments. Although such material may generate in situ, longshore-transported sediments typically result in poorly sorted carbonate rocks. In contrast, localized well-sorted, sand-sized carbonate accumulations do occur, but are typically rare and limited to small-scale isolated depositional environments (Murray 1960). Broadly, these poorly sorted carbonate sand and gravel deposits typically lack extensive pore networks.

Lastly, mud abundance greatly influences the primary pore network in carbonate rocks. These fine-grained carbonate particles, typically < 10 μm in diameter, can originate in situ as precipitants or are transported debris from mechanical breakdown of sand and skeletal material (i.e., autochthonous or allochthonous). Carbonate mud can accumulate within an array of environments of deposition but are primarily limited to low-energy settings where settling from

suspension is possible (Murray 1960). Therefore, the most common depositional settings are located within protected carbonate platforms or distal, deep-water settings (e.g., shelf, basin). Although these three broad categories of carbonate sediments deposit within particular environments, migration of depositional environments means that they can be juxtaposed vertically in a sedimentary succession over very short length scales.

Dolomitization

Typically, dolostones have higher porosity than similarly originated limestones. Although dolostones often possess more macropores than limestone, it is important to understand its origin in order to estimate abundance of microporosity effectively (Wang et al. 2015). Although dolomite can precipitate directly out of solution or as a metamorphic phase mineral, the majority of dolomitization in the sedimentary rock record occurs as the replacement of calcite and/or aragonite (Warren 2000). These minerals are less thermodynamically stable than dolomite and with the introduction of magnesium-rich fluids, will convert to dolomite (Al-Awadi et al. 2009). Dolomite is considered a metastable mineral and will transform its mineralogical structure based on non-equilibrium with incorporated conditions (Warren 2000). As a result, the substitution of magnesium for calcium will occur, as well as the reordering of these elements to decrease reactivity of mineralization. Replacement and reordering typically result in modification of the crystal lattice (Althoff 1977). However, this transition is not instantaneous; therefore, contemporary units may represent only partially dolomitized carbonate lithologies. The dolomitization process often erases any vestige of the original depositional texture, making interpretation of lithology or depositional environment difficult.

In the early 19th century, it was first proposed that through dolomitization, porosity increases by approximately 12% based on unit cell volume differences between calcite and dolomite (De Beaumont 1837). While others have argued more recently that dolostone porosity resembles the pore structure of its calcite parent (Lucia 2004). Lucia (2004) argues that porosity of dolomitized layers is similar to its limestone precursor or less as a result of "over dolomitization." Regardless, the complexity of the dolomitization process suppresses the possibility of completely delineating its depositional and diagenetic history based on textural features alone.

Cementation and Compaction

Among these carbonate sediment types, cementation can greatly decrease pore space and the connectivity of pores. Cementation, which can be initiated at various times based on depositional setting, occurs when fine cementing material occupies intergranular/intercrystalline pore space. In other words, cement present within carbonate rocks may be evidence of depositional or diagenetic processes. Typically, within carbonate rock, cements are commonly composed of calcite, dolomite, or chert (Murray 1960). However, based on origin, two specific types of cement exist; cements that grew into pore space and cements that are created through carbonate mud replacement or recrystallization (Bathurst 1961). Based on petrographic properties, these two scenarios can be distinguished for interpretation. It is important to note that although porosity decreases as a function of cementation, an increase in capillary pores is typically observed with an increase of fine material (Murray 1960). Therefore, elevated cementation may

result in the generation of capillary pores, which are associated with increased freeze/thaw susceptibility.

Similarly, compaction usually results in the reduction of total porosity with carbonate rock. The three main factors that influence compaction are overburden stress, grain size, and clay content (Croize et al. 2013). Such occurrences typically increase with age and burial depth and may affect the entirety of a formation or only a single bed or lamina. Due to the stability differences between dolomite and calcite previously mentioned, limestone facies are typically more prone to compaction and porosity reduction. Similarly, because reworking of crystalline and granular material is initiated with compaction, fine-grained material requires more stress for deformation and is therefore less prone to compaction. This is supported by increased adhesion and friction with decreasing sediment size (Coogan and Manus 1975). Upon lithification and burial, contemporary carbonate facies initially experience a 30–40% porosity reduction. However, with increased burial, mechanical and chemical compaction contribute to an exponential reduction of primary porosity with depth.

Pressure Solution and Dissolution

Chemical compaction is another important diagenetic process that results in porosity decrease during carbonate rock burial. Chemical compaction is often referred to as pressure solution or pressure dissolution. With the introduction of non-hydrostatic stress (e.g., overburden pressure), grains with higher solubility begin to dissolve at intergranular/intercrystalline boundaries. Intergranular pressure solution (i.e., granular-scale) and stylolitization (i.e., facies-scale) are the main types of this diagenetic feature. However, stylolitization is more common (Tada and Siever 1989). This associated stress decreases porosity and pore sizes by forcing a tighter arrangement of particles (Murray 1960). Pressure solution not only decreases total porosity, it also decreases bed thickness by ~10% while providing an avenue for diagenetic cementation (Tada and Siever 1989). It has also been observed that although cement and clay content are not necessary, often such components advance stylolitization (Heald 1959). Evidence for pressure solution is rather uncomplicated as stylolites are visible as either columnar, lenticular, or hummocky, dark-colored, linear features where carbonate material has since dissolved and solely insoluble clay minerals remain (Bathurst 1972).

Diagenetic Secondary Vugs

Numerous mechanisms occur post-deposition that result in the creation of secondary vugs, which ultimately may increase porosity. The most common within carbonate rocks, which was briefly mentioned previously, is carbonate dissolution. Dissolution can occur among an array of selected carbonate materials (e.g., skeletal fragments, lime mud, cements). In addition, incomplete dolomite replacement, fractures, and preserved pores are also common mechanisms of secondary vugs (Murray 1960). Lucia (1995) categorizes such pores, but emphasizes their orientation with other rock components.

Depending on the rock fabric and the connectivity of pores, or lack thereof, units possessing similar porosity and pore size distribution can behave differently with respect to fluid flow.

Vuggy porosity is classified by non-connected and interconnected vugs within either a grain- or mud-dominated matrix. Conceptually, such scenarios may possess similar pore volumes but may vary greatly in terms of permeability. In other words, connected vugs encourage fluid flow, while isolated vugs remain detached from the connected pore network (Lucia 1995). As a result, petrographic analysis may be helpful in characterizing the connectedness of vugs through interparticle pores and the microporous matrix (as illustrated by Choquette and Pray 1970 and Scholle and Ulmer-Scholle 2003).

Observed Fabrics and Petrophysical Properties

As previously discussed, aggregate durability is assessed by the Iowa DOT in part by utilizing the Iowa Pore Index test method. In addition, the Iowa DOT analyzes aggregate for clay content due to its swelling and water absorbing properties through using X-ray fluorescence. Hence, the presence of clay can significantly speed up the deterioration process. However, it has been questioned whether other specific lithological properties may be useful in assessing aggregate rock quality. Mercury porosimetry and IPI data will be paired with petrographic thin section observations in an effort to better understand aggregate pore systems and the lithological properties that govern them.

It has been observed that a modal pore-throat diameter range of 0.04–0.2 µm is associated with poor performing aggregates (Ridzuan et al. 2017). In the current study, it was concluded that 13 rock types are susceptible to freeze/thaw damage (7 limestones and 6 dolostones). As a whole, rock types possessing this modal pore-throat size distribution typically contained elevated proportions of mud, or very fine-grained material. Specifically, through analyzing relative mud proportions based on lithology (i.e., limestone and dolostone) and assigning values of 1, 2, or 3, indicating increasing amounts of mud, respectively, 10 rock types were given mud index values of 2 or 3. These features, as well as mercury porosimetry data are paired and found in Table 9.

Table 9. Pore-throat diameters paired with lithological rock properties

Source	Mean (um)	Mode (um)	Rock type (%)	Limestone vs. Dolostone	Mud index	Grain- vs. Mud-dominated
Behr-1	0.0179	0.0071	72%	Dolostone	2	Grain-dominated
Behr-2	0.019	0.0094	23%	Dolostone	3	Grain-dominated
Behr-3	0.0249	0.0064	6%	Dolostone	1	Grain-dominated
Dotzler-1	0.9441	0.0476*	31%	Dolostone	3	Mud-dominated
Dotzler-2	0.1839	0.0101	30%	Dolostone	2	Mud-dominated
Dotzler-3	0.6397	0.0088	22%	Dolostone	2	Grain-dominated
Dotzler-4	0.5069	0.0179	17%	Dolostone	2	Mud-dominated
Durham-1	0.3095	0.0381*	89%	Limestone	2	Grain-dominated
Durham-2	0.1065	0.039*	6%	Limestone	1	Grain-dominated
Durham-3	0.4772	0.0109	5%	Limestone	1	Grain-dominated
Elwood Yeager-1	0.1021	0.0412*	61%	Dolostone	3	Mud-dominated
Elwood Yeager-2	0.0157	0.008	21%	Dolostone	1	Grain-dominated
Elwood Yeager-3	0.1461	0.0065	16%	Dolostone	1	Grain-dominated
Elwood Yeager-4	0.0883	0.0077	2%	Dolostone	2	Mud-dominated
Linwood-1	0.0646	0.043*	78%	Limestone	1	Grain-dominated
Linwood-2	0.1589	0.0148	18%	Limestone	3	Mud-dominated
Linwood-3	0.1614	0.0148	4%	Limestone	2	Mud-dominated
Morgan-1	0.2627	0.0074	75%	Limestone	3	Mud-dominated
Morgan-2			17%	Limestone	3	Mud-dominated
Morgan-3	0.0434	0.0136	6%	Limestone	2	Grain-dominated
Morgan-4	0.0172	0.0064	1%	Limestone	1	Grain-dominated
Portland West-1	0.1495	0.0481*	41%	Limestone	2	Mud-dominated
Portland West-2	0.0801	0.009	28%	Dolostone	1	Grain-dominated
Portland West-3	0.8913	0.295	22%	Limestone	1	Grain-dominated
Portland West-4	0.1602	0.1657	9%	Limestone	3	Mud-dominated
Stone City-1	0.8372	0.0295*	82%	Dolostone	2	Grain-dominated
Stone City-2	0.1817	0.0071	6%	Dolostone	1	Grain-dominated
Stone City-3	0.3924	0.0156	6%	Dolostone	1	Grain-dominated
Stone City-4	0.2172	0.0105	3%	Dolostone	2	Grain-dominated
Stone City-5	0.1711	0.0617*	3%	Dolostone	2	Grain-dominated
Sully-1	1.601	0.013	32%	Dolostone	1	Grain-dominated
Sully-2			31%	Dolostone	1	Grain-dominated
Sully-3	0.7932	0.0347*	24%	Dolostone	2	Grain-dominated
Sully-4	5.372	0.0374*	13%	Dolostone	1	Grain-dominated
Waucoma-1	0.0332	0.0108	85%	Limestone	3	Mud-dominated
Waucoma-2	0.2136	0.0345*	15%	Limestone	3	Mud-dominated
Weeping Water-1	0.0234	0.0073	82%	Limestone	2	Mud-dominated
Weeping Water-2	0.0613	0.0384*	7%	Limestone	2	Mud-dominated
Weeping Water-3	0.4522	0.0125	6%	Limestone	1	Mud-dominated
Weeping Water-4	0.0835	0.0543*	5%	Limestone	2	Mud-dominated

*Indicates measured modal pore diameters within the critical range of capillary pore sizes

Typically, for limestone units, this critical range was observed in either mud-dominated matrices, or within a mixed matrix with the presence of pressure dissolution. Within the dolostone rock

types, fine-grained crystalline fabrics or mud-dominated facies possessed this modal pore distribution.

Specifically for limestones, four of the seven these sources possessed a mud-dominated matrix (i.e., Portland West Type 1, Waucoma Type 2, and Weeping Water Types 2 and 3). On the other hand, two of the remaining three sources contained pressure solution seams, or stylolites (Durham Type 1 and Linwood Type 1). The remaining source, Durham 2, is a coarse-grained, peloidal grainstone with occasional dark-colored, intergranular pressure solution rims. Referring back to carbonate sediment types, these sources contained large proportions of carbonate mud in addition to sand-sized carbonate particles (e.g., fossil fragments, peloids) that suggests a low-energy, marine environment of deposition (perhaps in a marine shelf setting). Therefore, it could be suggested that increased mud content and pressure dissolution evidence may increase the abundance of capillary pores. Intuitively, this makes sense as intergranular pore-throat diameters within a well-sorted, fine-grained matrix are inherently smaller than similar pores within a larger-grained, well-sorted distribution of sediment. Additionally, although primary porosity of clast-dominated matrices involves larger pore-throat diameters than mud-dominated matrices, evidence of increased compaction, as well as cementation, may in turn result in decreasing the initial pores into the critical zone. However, it is important to note that the remaining 12 limestone rock types analyzed that do not possess the modal critical pore-throat range, 8 contain a mud-dominated matrix. When pairing the modal pore throats of these limestone sources to IPI values, it is determined that SLI indices range from 13 to 32.

Six dolostone rock types were categorized as possessing modal pore throats within the critical range (i.e., 0.04–0.2 µm): Dotzler Type 1, Elwood Yeager Type 1, Stone City Type 1 and Type 5, and Sully Types 3 and 4. Besides Sully Type 4 aggregate, mud indices of these rock types were recorded as either 2 or 3, indicating a large mud component. In other words, most of these dolomitic rock types possessed fine-grained material, with larger amounts of mud composition. Sully Type 3 and Type 4 aggregate possessed grain dominated matrices with decreased mud components compared to other sources. Secondary load indices of these units ranged between 10 and 18, which are moderate values compared to the total dolostone SLI range of 10–46. However, as previously addressed, these rock types compose various percentages of the entirety of sources utilized for testing, which is only reflected partially by IPI indices. However, through standardizing modal pore-throat sizes among sources by rock type percentages, a moderate correlation between modal pore diameter and SLI indices is observed.

In conclusion, based on pairing lithological textures and observations to IPI indices and modal pore diameters, it is broadly generalized that increased mud content results in an increased abundance of capillary pores within the critical zone (i.e., 0.04–0.2 µm). Similarly, although stylolitization was only evident in two rock types (i.e., Durham Type 1 and Linwood Type 1), it is suggested that pressure dissolution decreases pore-throat sizes and may result in pore-throat diameters associated with premature concrete deterioration. Within the scope of this study, which encompassed analyzing 11 Class 3 or Class 3i coarse aggregate sources, these generalizations are the extent through which pairing contemporary rock fabrics with such petrophysical data. However, through analyzing a wider variety of coarse aggregate sources (e.g., non-durable, Class 2, Class 3, and Class 3i sources), a broader understanding of this relationship may be delineated.

Heterogeneity-Aware IPI Method

The concept of heterogeneity has been discussed in terms of lithologies within individual CA samples. Not only was heterogeneity discovered within each source through qualitative visual inspection, but grain density and pore-throat size distributions varied within each sample. However, CA heterogeneity has not been addressed within the IPI testing procedure as a whole.

The fundamental basis of the IPI relies on the principle that fluid intrusion within the first minute of testing relates strictly to large pores (macropores), while the remainder of the 15-minute test is considered to measure the volume of small pores (micropores). This 1-minute transition point, between the intrusion of macro- and micropores, is dependent on the assumption that pore intrusion is reliant on time as opposed to petrophysical properties (i.e., pore connectivity, porosity, and pore types). However, visually analyzing incremental intrusion plots for each pressure and each sample, the time of macropore intrusion only deviated slightly (i.e., 1–4 seconds). Therefore, it can be concluded that this is not merely a time-dependent feature. Nonetheless, with the lack of automation and precision/resolution of volume measurements instilled in the 1G and 2G IPI devices, it is understandable to standardize all sources to a specific time to calculate estimations of pore indices. However, since freeze/thaw durability and IPI tests results have previously miscorrelated (Olsen et al. 1983, Richardson 2009, Davis 2011), it is imperative that maximum precision of this water intrusion porosimetry method is achieved.

With the data acquisition capabilities of the new 3G device, perhaps the procedure should be amended to account for overall heterogeneity instead of assuming a single threshold for the transition from macropore (PLI) to micropore (SLI) intrusion. The ability to plot intrusion rates, or incremental intrusion, allows for a better assessment of a more source-specific transition point. As dictated by pore connectivity and pore throat, current theory assumes that as intrusion rates plateau after the initial burst of intrusion, macropore intrusion is minimal and subsequent intrusion is associated with micropores. As determined from variable pressure of intrusion plots for each sample, most macropore intrusion occurs within the first 15 seconds. In other words, with this finding, it suggests that prior PLI values included the entirety of macropore volumes and a significant proportion of micropore intrusion. With each individualized, transition point (Figure 15A-U), PLI and SLI indices can be re-evaluated using the new time points rather than using the legacy 1-minute transition point, which will be more characteristic of individual lithological properties than previously determined (Table 5).

This suggestion may improve the predictive capability of IPI indices. However, assessing an individual source's effect on PLI and SLI values may be more complex because of the heterogeneity among CA sources. With the IPI, pore distribution results are a product of the bulk behavior of each source. Since each sample contained multiple rock types, the presence of poor quality rock types (which may cause D-cracks) could be masked by more abundant, higher quality rock types. Petrography, as well as petrophysical analysis utilizing mercury intrusion porosimetry, can reveal this heterogeneity with the presence of these non-ideal lithologies. Although this recommendation would lead to more laborious testing protocol, it may be attractive for the special investigations of CA with ambiguous IPI test results, other test properties, and/or field performance.

Special Investigation Method (Advanced Characterization)

When significant uncertainty exists about the quality of a CA sample, ledge, or source, the research team proposes that a special investigation method be employed. This method would test each rock type in the CA individually. In this manner it can be thought of as a Heterogeneity Aware IPI method. Initially, rock typing of the intended CA would differentiate its various component lithologies. As determined with this study, decreasing sample size from 4.5 kg of crush rock utilized with the 2G method, to 1 kg of CA with the 3G device, resulted in negligible differences in IPI indices. With this acknowledgement, one could assume an additional decrease in sample size would yield accurate results, but this would have to be supported by additional testing.

Therefore, with this precedent, rock typing of an entire "money bag" of CA (≈ 5 kg), would suffice for analyzing its component rock types. This would yield approximately 250 g of a rock type with 5% abundancy within the entire source. If sample quantity exists, 1,000 g of each rock type could be selected for analysis. Essentially, the operational 3G IPI method would be used for each rock type and a rock type-specific transition point between macropore and micropore intrusion would be identified. With transition points individualized by rock type, individual IPI indices could indicate low-quality rock types to avoid. In addition to this procedure, pairing prior or subsequent mercury porosimetry data, helium pycnometry results, and/or petrographic analysis could provide additional information on the link between the bulk behavior of a CA source and the heterogeneity that exists within an individual sample. Not only can this method aid in better understanding of non-durable CA and the 3G IPI, but this can improve source selection and re-evaluation.

Most aggregate sources are composed of numerous rock beds, or ledges (Iowa DOT 2019). Consequentially, individual rock types typically correspond to individual beds. Although many state departments of transportation choose aggregate sources based on locality and cost efficiency, these results can be utilized to implement better assessments of ledge quality to know when it may be worth it to pay more for higher quality material. In addition, with the success of this method, CA sources that have been previously categorized as non-durable could be re-evaluated to identify and mitigate problematic lithologies. Studies on the blending of aggregates could also be undertaken to identify CA mixes that produce optimal quality. This method may increase cost on the front end by requiring more testing but may improve the overall durability of road systems through more elaborate investigation.

Operational Method

Although the special investigation method may provide the most accurate IPI indices, it is likely impractical to employ for routine analysis and quality assessment and quality control (QA/QC). Therefore, an operational method can be adopted to improve the accuracy of IPI indices using more general transition points of intrusion based on lithology (i.e., dolostone, limestones, and intermediates).

As previously stated, all macropore intrusion (PLI) of the 21 studied sources concluded within the initial 12 s of water intrusion based on analyzing the rate of incremental intrusion for each source. Therefore, this finding suggests that the 2G IPI method for measuring PLI and SLI indices using a 60 s transition point does not accurately describe the water intrusion process. To better improve the 3G IPI method, lithological specific transition points have been determined as follows:

- LS Transition Point: Primarily Limestone CA Source (2.7 s)
- INT Transition Point: Intermediate (Mixed LS/DS CA Source) (5.0 s)
- DS Transition Point: Primarily Dolostone CA Source (7.8 s)

These values were determined through analyzing the transition point for all 21 sources (Figure 15A-U) and determining an average transition point for each lithological group (i.e., limestone, dolostone, and intermediates) (Table 4).

With these average transition points, PLI values among all source types will likely decrease and SLI values, the more indicative value for assessing freeze/thaw susceptibility, will likely increase. In other words, prior PLI values incorporated the entirety of macropore volume intrusion as well as a significant proportion of micropore intrusion. Due to varying macropore volumes among these three categories, the pattern of transition points is supported. Although the utilization of this method is solely applicable to the 3G IPI device, the additional improvements outlined in this discussion section, as well as this proposed operational method encourage the adoption of this device and operational method as the benchmark for future CA evaluation.

CONCLUSION AND RECOMMENDATIONS

In order to effectively assess CA quality for use in portland cement concrete, it is crucial to understand a source's petrophysical properties, as they influence the overall durability and longevity of the road systems of which they are a part. Capillary pores, or pores with throat diameters between 50 nm to 10 µm, impact premature deterioration of pavement in environments with repetitive freeze/thaw cycles that cause exerted pressures capable of forming D-cracks. To test for capillary pore abundances and porosity of a specific CA source, the original Iowa Pore Index test was created. The Iowa Pore Index is an effective tool to differentiate durable and non-durable CA sources using pressurized water intrusion. This method, which was initially created by Iowa DOT geologists, has been preferred by several state departments of transportation and accepted as an AASHTO standard due to its non-hazardous, quick, and simple procedure for quantifying pore distributions (e.g., macro- and micropores). However, occasionally aggregate samples perform satisfactorily with test, but underperform in the field.

With this study, a new, more automated water intrusion device (3G IPI device) was investigated for its applicability in analyzing pore distributions of carbonate coarse aggregate. Through replicating IPI tests using the 3G device, 21 previously analyzed CA samples yielded comparable results among devices. Hence, the 3G device is capable of providing similar PLI and SLI as its predecessor. Several benefits of utilizing this 3G device were highlighted:

- Automation removes operator error
- Smaller sample size offers greater flexibility
- Higher pressure investigates smaller pore sizes
- Reduced soak time yields more accurate PLI and SLI
- Faster operation and leak detection

With improved automation and data analysis capabilities with this device, it was determined that the traditional transition point between quantifying macro- and micropore intrusion may be too large and that different lithologies have different transition points. It was observed that most macropore intrusion concludes within 15 s of pressurized intrusion, as opposed to the transition point of 60 s for the 2G IPI device.

Therefore, three different methods (i.e., heterogeneity, special investigation, and operational methods) of using this IPI device and interpreting intrusion data were developed. It is recommended that the special investigation method be used to investigate sources that may show disagreement between IPI indices and observed performance. This method involves differentiating rock types within a particular aggregate source and analyzing each rock type utilizing the heterogeneity-aware IPI method, mercury porosimetry analysis, helium pycnometry, and petrographic thin section investigation. This process is intended to indicate specific non-durable coarse aggregate rock types that negatively affect the bulk behavior of the source as whole. With guidance from this method, CA can be mixed to produce optimal performance properties.

However, the special investigation method is probably too time intensive for routine quality assessment and quality control. Therefore, the operational method is recommended for using the 3G IPI device for measuring IPI indices on a routine basis. With this method, lithology-specific transition points have been calculated to use within the traditional IPI calculations. As determined by the studied sources, limestone, intermediate, and dolostone sources conclude macropore intrusion within different time intervals (i.e., 3, 5, and 8 s, respectively). With utilization of these calculated intervals, primary and secondary load indices should more accurately represent the water intrusion process and aid in a better understanding of coarse aggregate freeze/thaw susceptibility.

REFERENCES

Al-Awadi, M., W. J. Clark, W. R. Moore, M. Herron, T. Zhang, W. Zhao, N. Hurley, D. Kho, B. Montaron, and F. Sadooni. 2009. Dolomite: Perspectives on a Perplexing Mineral: *Oilfield Review*, Vol. 21, No. 3, pp. 32–45.

Althoff, P. L. 1977. Structural refinements of dolomite and a magnesian calcite and implications for dolomite formation in the marine environment. *American Mineralogist*, Vol. 62, No. 6–7, pp. 772–783.

Bathurst, R. G. C. 1961. Diagenetic Fabric in Some British Dinantian Limestones. *Geological Journal*, Vol. 2, No. 1, pp. 11–36.

Bathurst, R. G. C., 1972. *Developments in Sedimentology: Carbonate Sediments and Their Diagenesis, Vol. 12*. Elsevier Science, Amsterdam, Netherlands. https://www.elsevier.com/books/carbonate-sediments-and-their-diagenesis/bathurst/978-0-444-40891-4

Brabazon, D. and A. Raffer. 2015. Chapter 3 - Advanced Characterization Techniques for Nanostructures. In *Emerging Nanotechnologies for Manufacturing* (Second Edition). William Andrew/Elsevier, Oxford, pp. 53–85.

BouDagher-Fadel, M. K. 2008. Evolution and Geological Significance of Larger Benthic Foraminifera. *Developments in Paleontology and Stratigraphy*, Vol. 21, No. 5, pp. 215–295.

Choquette, P. W. and L. C. Pray. 1970. Geologic Nomenclature and Classification of Porosity in Sedimentary Carbonates. *AAPG Bulletin*, Vol. 54, No. 2, pp. 207–250.

Coogan, A. H. and R. W. Manus. 1975. Chapter 3. Compaction and Diagenesis of Carbonate Sands. *Compaction of Coarse-Grained Sediments*, Vol. 18, pp. 79–166.

Couto, H. J. B., P. F. A. Braga, and S. C. A. Franca. 2012. Use of Gas Pycnometry for Estimating the Iron Content in Mineral Samples. *Minerals Engineering*, Vol. 39, pp. 45–47.

Croizé, D., F. Renard, and J.-P. Gratier. 2013. Chapter 3 - Compaction and Porosity Reduction in Carbonates: A Review of Observations, Theory, and Experiments. *Advances in Geophysics*, Vol. 54, pp. 181–238

Davis, S. P. 2011. Influence of Particle Size and Sample Preparation on the Iowa Pore Index. MS thesis. Missouri University of Science and Technology, Rolla, MO.

Dash, J. G., A. W. Rempel, and J. S. Wettlaufer. 2006. The Physics of Premelted Ice and Its Geophysical Consequences. *Reviews of Modern Physics*, Vol. 78, No. 3, pp. 695–741.

Day, J. E., B. J. Witzke, and B. Bunker. 2013. Overview of Middle and Upper Devonian Northern Shelf Facies in the Iowa Basin. *Iowa Geological Survey Guidebook*, Vol. 29, pp. 1–40

De Beaumont, E. 1837. Application du calcul à l'hypothèse de la formation par epigenie desanhydrites, des gypses et des dolomies. *Bulletine la Société Géologique de France*, Vol. 8, pp. 174–177.

Detwiler, R., M. Nagi, and S. Bhattacharja. 2001. Identifying Combinations of Materials that Lead to Premature Deterioration in Concrete Pavements. Seventh International Conference on Concrete Pavements. *The Use of Concrete in Developing Long-Lasting Pavement Solutions for the 21st Century*, Vol. 1, pp. 209–223.

Dong, H., P. Gao, and G. Ye. 2017. Characterization and Comparison of Capillary Pore Structures of Digital Cement Pastes. *Materials and Structures*, Vol. 50, No. 154, pp. 1–12.

Drumm, E. C. and R. Meier. 2003. *NCHRP Web Document 60 (Project 20-50[7/12]): LTPP Data Analysis: Daily and Seasonal Variations in In Situ Material Properties*. National Cooperative Highway Research Program, Washington, DC.

Dubberke, W. 2002. Evaluating Aggregate for PCC: Observations, Comments and Opinion. Last accessed Jan 2019. www.angelfire.com/ia/concrete/page10.html.

Dunham, R. J. 1962. Classification of Carbonate Rocks according to Depositional Texture. In *Classification of Carbonate Rocks—A Symposium*. American Association of Petroleum Geologists Memoir, Vol. 1, pp. 108–121.

Ellison A. H., R. B. Klemm, A. M. Schwartz, L. S. Grubb, and D. A. Petrash. 1967. Contact Angles of Mercury on Various Surfaces and the Effect of Temperature. *Journal of Chemical and Engineering Data*, Vol. 12, No. 4, pp. 607–609.

Folk, R. L. 1959. Practical Petrographic Classification of Limestones. *American Association of Petroleum Geologists Bulletin*, Vol. 43, No. 1, pp. 1–38.

Giesche, H. 2006. Mercury Porosimetry: A General (Practical) Overview. *Particle & Particle Systems Characterization*, Vol. 23, No. 1, pp. 9–19.

Gustafson, K. J., R. Dawson, K. B. Jones, and N. Tieck. 2015. *Carbonate Rock Pore Size Distribution Determination through Iowa Pore Index Testing*. Iowa Department of Transportation Highway Division, Ames, IA.

Hallet, B. 2006. Geology: Why do Freezing Rocks Break? *Science*, Vol. 314, No. 5802, pp. 1092–1093.

Hanna, A. N. 2003. Aggregate Tests for Portland Cement Concrete Pavements: Review and Recommendations. *National Cooperative Highway Research Program Research Results Digest*, No. 281.

Hanson, T. D. 2009. *100 Years of Concrete Pavement in Iowa*. Iowa Department of Transportation Highway Division, Ames, IA.

Heald, M. T. 1959. Significance of Stylolites in Permeable Sandstones. *Journal of Sedimentary Petrology*, Vol. 29, No. 2, pp. 251–253.

Iowa DOT. 2015. *Iowa Transportation Improvement Program (2016–2020).* Iowa Department of Transportation, Iowa Transportation Commission, Ames, IA.

Iowa DOT. 2019. General Aggregate Source Information, Materials IM T203. Office of Construction & Materials, Iowa Department of Transportation, Ames, IA. https://maple.iowadot.gov/files/t203.pdf.

Kalashnikov, E. V. and B. Z. Pevzner. 2001. Motion of a Helium Atom through Comparable-Diameter Channel in the Frenkel–Kontorova Model. *Physics of the Solid State*, Vol. 44, No. 2, pp. 294–299.

Klieger, P., D. Stark, and W. Teske, 1978. *The Influence of Environment and Materials on D-Cracking*. Portland Cement Association, Skokie, IL.

Lucia, F. J. 1995. Rock-Fabric/Petrophysical Classification of Carbonate Pore Space for Reservoir Characterization. *American Association of Petroleum Geologists Bulletin.* Vol. 79, pp. 1275–1300.

Lucia, F. J. 2004. Origin and petrophysics of dolostone pore space. From *The Geometry and Petrogenesis of Dolomite Hydrocarbon Reservoirs*. Geological Society, London. Special Publications No. 235, pp. 141–155.

Ludvigson, G. A., B. J. Witzke, and L. González. 1992. Observations on the Diagenesis and Stable Isotopic Compositions of Silurian Carbonates in Iowa: Field Trip Guidebook to Silurian Exposures in Jones and Linn Counties. *Iowa Geological Survey Guidebook*, Vol. 11, pp. 73–83.

Marks, V. J. and W. Dubberke. 1982. Durability of Concrete and the Iowa Pore Index Test. *Transportation Research Record*, No. 853, pp. 25–30.

Miller, J. S. and W. Y. Bellinger. 2003. *Distress Identification Manual for the Long-Term Pavement Performance Program*. FHWA-RD-03-031. Federal Highway Administration Research and Technology, McLean, VA.

Murray, R. C. 1960. Origin of Porosity in Carbonate Rocks. *Journal of Sedimentary Petrology*, Vol. 30, No. 1, pp. 59–84.

Murton, J. B., R. Peterson, and J. C. Ozouf. 2006. Bedrock Fracture by Ice Segregation in Cold Regions. *Science*. Vol. 314, No. 5802, pp. 1127–1129.

Myers, J. D. and W. Dubberke. 1980. Iowa Pore Index Test. Interim Report. Iowa Department of Transportation Office of Materials, Ames, IA.

Olsen, M. P. J., D. J. Janssen, and B. J. Dempsey. 1983. *D-Cracking in Portland Cement Concrete Pavements*. University of Illinois and Illinois Department of Transportation, FHWA/IL/UI-199, Urbana, IL.

Perry, C. T., M. A. Salter, A. R. Harborne, S. F. Crowley, H. L. Jelks, and R. W. Wilson. 2011. Fish as Major Carbonate Mud Producers and Missing Components of the Tropical Carbonate Factory. *Proceedings of the National Academy of Sciences of the United States of America*, Vol. 108, No. 10, pp. 3865–3869.

Richardson, D. N. 2009. *Quick Test for Durability Factor Estimation*. Missouri Department of Transportation, Jefferson City, MO.

Ridzuan, M. F., F. Hasiuk, and P. Taylor. 2017. *Calibrating the Iowa Pore Index with Mercury Intrusion Porosimetry and Petrography*. National Concrete Pavement Technology Center and Midwest Transportation Center, Iowa State University, Ames, IA.

Scholle, P. A. and D. S. Ulmer-Scholle. 2003. Carbonate Classification: Porosity. From *A Color Guide to the Petrography of Carbonate Rocks: Grains, Textures, Porosity, Diagenesis*. AAPG Memoir 77. American Association of Petroleum Geologists, Tulsa, OK.

Schwartz, D. R. 1987. NCHRP Synthesis of Highway Practice 134: D-Cracking of Concrete Pavements. National Cooperative Highway Research Program, Washington, DC.

Stark, D. 1976. Characteristics and Utilization of Coarse Aggregates Associated with D-Cracking. In *Living with Marginal Aggregates*. STP597-EB. ASTM International, West Conshohocken, PA, pp. 45–58.

Tada, R. and R. Siever. 1989. Pressure Solution During Diagenesis. *Annual Review of Earth and Planetary Sciences*. Vol. 17, pp. 89–118.

Van Dam, T. J., L. L. Sutter, K. D. Smith, M. J. Wade, and K. R. Peterson. 2002. *Guidelines for Detection, Analysis, and Treatment of Materials Related Distress in Concrete Pavements—Volume 2: Guidelines Description and Use*. FHWA-RD-01-164. Federal Highway Administration, Turner-Fairbank Highway Research Center, McLean, VA.

Walder, J. and B. Hallet. 1985. A Theoretical Model of the Fracture of Rock During Freezing. *Geological Society of America Bulletin*, Vol. 96, No. 3, pp. 336–346.

Wang, G., P. Li, F. Hao, H. Zou, and X. Yu. 2015. Origin of Dolomite in the Third Member of Feixianguan Formation (Lower Triassic) in the Jiannan Area, Sichuan Basin, China. *Marine and Petroleum Geology*, Vol. 63, pp. 127–141.

Warren, J. 2000. Dolomite: Occurrence, Evolution, and Economically Important Associations. *Earth Science Reviews*, Vol. 52, No. 1–3, pp. 1–81.

Washburn, E. W. 1921. Note on a Method of Determining the Distribution of Pore Sizes in a Porous Material. *Proceedings of the National Academy of Sciences of the United States of America*, Vol. 7, No. 4, pp. 115–116.

Witzke, B. J. and B. J. Bunker. 2001. Comments on the Mississippian Stratigraphic Succession in Iowa, in Stratigraphy and Biostratigraphy of the Mississippian Subsystem (Carboniferous System) in its Type Region, the Mississippi River Valley of Illinois, Missouri, and Iowa. *International Union of Geological Sciences Subcommission on Carboniferous Stratigraphy Guidebook for Field Conference*. St. Louis, Missouri, pp. 63–75.

Witzke, B. J., B. J. Bunker, and F. S. Rogers. 1988. Eifelian through Lower Frasnian Stratigraphy and Deposition in the Iowa Area, Central Midcontinent, USA. *Devonian of the World: Proceedings of the 2nd International Symposium on the Devonian System*, Memoir 14, Vol. 1, pp. 221–250.

Yuan, Y. and T. R. Lee. 2013. Contact Angle and Wetting Properties. In *Surface Science Techniques*, Vol. 51, pp. 3–34.

APPENDIX A. IOWA PORE INDEX (GENERATION 1) OPERATING METHOD

After Myers and Dubberke 1980

Procedure

Chamber

A modified Press-Ur-Meter is used to perform the pore index test. The pump, valve, and gauge were removed from the lid and replaced by a 320 ml Plexiglas tube, graduated in 2 ml increments. The addition of a standard 60 psi pressure gauge completes the lid modifications. A hole was drilled through the side of the pot at the bottom, fitted with a valve, and is used for loading and unloading the pot with cold tap water. Two valves are located at the top of the Plexiglas tube. One valve is connected to a line supplying air at a constant 35 psi. The other valve is a vent valve and is opened while charging the unit with water.

Test Procedure

1. Place 9,000 g of oven dried, ½ x ¾ in. aggregate in the pot.

2. Attach the lid, open the vent valve, and fill the pot and Plexiglas tube with cold tap water to the 0 milliliter mark. The pressure gauge on the lid must remain at the 0 psi mark during this filling stage.

3. Close the water supply and vent valves and then open the 35 psi air supply valve as soon as possible. The air valve remains open throughout the duration of the test.

4. Take a water level reading at one minute. The amount of water injected during this first minute fills the aggregate's macropores and is referred to as the primary load. A large primary load is considered to be an indication of a high-quality limestone pore system. A well-developed macropore system probably functions in a manner similar to air entrainment voids in concrete paste. The primary load is not used in the Iowa Pore Index (IPI) test result calculations.

5. Take a water level reading at 15 minutes. The volume of water intruded between minutes one and 15 is the secondary load and represents the amount of water that has intruded into the aggregate's micropore system. A secondary load of 27 ml or more indicates a negative limestone property that correlates with a saturated aggregate's inability to withstand internal pressures caused by freezing. The secondary load in milliliters is reported out as the final IPI test result.

Notes

During the evaluation phase of the IPI test, samples ranging from 3,000 to 10,000 g were accepted for testing. Since the secondary load (pore index test result) is directly proportional to the size of the sample, we computer adjusted the test results to reflect a projected 9,000 g sample. Many of the adjusted test results were from short samples received from the districts, but, in a few cases, we were forced to use a half-sample because some high absorption, full samples exceeded the capacity of the 320 ml tube during the primary load phase of the test.

APPENDIX B. IOWA PORE INDEX (GENERATION 2) OPERATING METHOD

Scope

This test method covers the procedure to determine the Iowa Pore Index (IPI) of aggregates.

Procedure

Chamber

1. Balance – A balance having a capacity of 5,000 g or more and accurate to at least 0.5 g.

2. Iowa Pore Index chamber – For the first-time setup of the chamber, the following steps should be taken:

    a. A pressurized air line needs to be connected to the primary air regulator on the back of the chamber. The two air regulators should already be pre-set. The primary air regulator should be set to 65–70 psi (gauge on back of chamber) and the secondary air regulator should be set to 35 psi (gauge on front of instrument).

    b. The hose to the three-way valve near the sample pot water inlet needs to be connected to a water source with water at room temperature.

    c. A Tygon or water hose should be connected to the three-way valve water outlet and run into a drain or sink.

    d. The IPI chamber should be leveled using the bubble level mounted between the graduated cylinders.

3. Oven – Capable of maintaining a uniform temperature of 230 ± 9°F.

4. Sieves – Wooden box sieves of suitable size to get the proper sized materials as needed for testing.

System Check

The pore index chamber should be checked each day of operation by running only water in the sample pot. The results of this check will also be used to determine the amount of sample pot expansion when the system is under pressure (step 6 under Test Procedure that follows). To determine the amount of pot expansion, follow steps 1 through 5 of the Test Procedure. Stop the test after the primary load is determined (after one minute). Take and record the amount of pot

expansion from the primary load (first) graduated cylinder. Use this amount in the calculation in step 6 (usually about 40 ml).

Test Procedure

1. Place 4,500 g of oven-dried + ½ in. by ¾ in. aggregate in the sample pot. Push on the sample pot lid to snap it into place. Place the lever across the top of the sample pot lid and tighten with the threaded clamp to align the two indicator lines. It is important that the sample pot lid is clamped with the same clamp pressure for every test.

2. Ensure that compressed air and water are being supplied to the chamber.

3. Turn the power switch to ON and the green power indicator light should come on.

4. Turn the mode switch from OFF to LOAD. Push the Start button and the load indicator light should come on. To regulate the rate of fill to the graduated cylinders on the chamber, feather the three-way valve on the sample pot to the load position. Carefully fill until the water is at the zero mark on all three graduated cylinders and, then, turn the three-way valve to the RUN position. It is very important that the water is at the zero mark on the three graduated cylinders for every test. Failure to do so will affect the accuracy of this test.

5. Turn the mode switch clockwise to the RUN position and push the Start button. The run indicator light should come on and the load indicator light will turn off. The valve to the first (primary) graduated cylinder will open and the valves to the second (secondary) and third (system check) graduated cylinders will close. The primary load indicator light will come on and the primary load digital timer will begin. After one minute, the primary load indicator light and the primary load digital timer will turn off and the secondary load indicator light and secondary load digital timer will turn on. The secondary graduated cylinder valve will open, and the primary graduated cylinder valve will close. After 14 minutes, the secondary indicator light and digital timer will turn off and the system check indicator light and digital timer will turn on. The system check graduated cylinder valve will open and the secondary graduated cylinder valve will close. After 15 more minutes, the system check indicator light and digital timer will turn off and the system check graduated cylinder valve will close. After a short delay, the test done light will come on.

6. Take and record readings from all three graduated cylinders (in ml). Use the following equations to determine the primary and secondary pore indexes:

    - Primary pore index = (1-minute reading – pot expansion) × (9,000 g sample weight)

    - Secondary pore index = (14-minute reading) × (9,000 g sample weight)

7. Turn the Mode switch to the DRAIN position, push the Start button, and switch the three-

way valve on the sample pot to the DRAIN position. All three graduated cylinder valves will open.

8. After the water has drained, carefully loosen the threaded clamp securing the sample pot lid and allow the air pressure to unseal the sample lid. If necessary, close the drain valve to assist with lid removal.

9. Switch the Mode switch to the OFF position. All of the digital timers will be reset. Remove the sample.

Notes

- The secondary pore index number represents the amount of water injected into the aggregate capillary pore system (0.1 to 0.01 micrometer radius). A secondary load of 27 or greater indicates an inability of the aggregate to withstand saturated freeze/thaw pressures.

- If the system check graduated cylinder does not read less than six after the test, this indicates a leak in the pressurized system and the test is not valid.

- The Stop button can be activated at any time. This is the same as turning the Mode switch to OFF. This will open all of the graduated cylinder valves; the air-source valve will close, the vent valve will open, and the digital timers will be reset.

- The ground fault interrupt (GFI) on the electric plug will need to be reset if there is any interruption in power. This includes unplugging the power cord.

- The battery-powered digital timers are always lit. Batteries should last 10 years before needing replacement.

- A faint air noise will be present from the secondary air regulator. This is normal for a precision regulator as it adjusts pressure.

- If the chamber is overfilled with water, press Stop and open the small valve located on the lower left front panel.

- Clean and lubricate the O-ring (with petroleum jelly) in the sample pot lid as needed.

APPENDIX C. IOWA PORE INDEX (GENERATION 3) OPERATING METHOD

Procedure

1. Prepare a 1,000 g sample of aggregate that has been washed and oven-dried.

2. Turn on the computer and the FlowTrac-II System. Open the Diag.com software shortcut on the desktop of the computer. On the system menu, check the final pressure and sample recording sequence values:

    a. Pressure – 35 psi

    b. Sample Shot – 0.1–2 second

3. On the FlowTrac-II System, select fill pump. After the pump is full, initialize system/pump.

4. Apply petroleum jelly to the bottom of the Plexiglas cylinder chamber and the bottom O-ring to encourage a proper seal. Align the B symbol on the cylinder with the three-way valve located on the bottom section of the system.

5. Add the sample to the apparatus. Apply petroleum jelly to the top of the cylinder and the upper portion, and secure the chamber with the three bolts, washers, and nuts (max tightness with hands).

6. Inspect all polyflow lines and verify proper connections as shown in Figure 30 below.

7. Fill the 1,000 ml Erlenmeyer flask with approximately 750 ml of water. Turn the polyflow line valve between the Erlenmeyer flask and the water pump to open (parallel with the line).

8. Turn the water pump on. With the pressure release valve instituted (at the top of the cylinder), slowly turn the three-way valve to C to allow water flow into the apparatus. While filling, move/shift the apparatus around to aid air escape between aggregate fragments. Continue to fill the cylinder with water while attempting to allow all air bubbles to escape. Once completely filled, return the three-way valve to the B position. Close the polyflow line valve between the Erlenmeyer flask and the water pump. Open the polyflow line valve between the FlowTrac-II and three-way valve.

9. On the FlowTrac-II system, select the pressure over time tab. Click start (this will fill the polyflow line with water and accounts for flow line expansion). Allow the test to run for at least 5 seconds. Stop the test by selecting the ESC button. Turn the three-way valve to C. Close polyflow line valve between Erlenmeyer flask and water pump. Click Start. (Prior data will be overwritten.)

10. After selecting start, the test on the aggregate sample will now begin. FlowTrac-II will record data until manually turned off. After 15 minutes, stop the test by selecting ESC. Turn the three-way valve to B.

11. Close the polyflow valve between the cylinder and the FlowTrac-II. Disconnect the polyflow lines from the apparatus. Take the cylinder to the sink and connect the pressure release valve. Turn the three-way valve to the C position to allow water to drain. Empty the sample and disassemble the apparatus. Rinse off parts and dry with a towel. Empty/drain the system pump. Open the pump valves to eliminate potential wear (buttons 1 and 3).

12. Save the test results on the computer or an external hard drive to avoid test data from being overwritten. Analyze the results utilizing the IPI primary load index (PLI) and secondary load index (SLI) definitions and calculations as follows:

    Primary Pore Index Value = $\left[\frac{9000}{W_1}\right] \times (V_1 - Vs_1 - V_0)$

    Secondary Pore Index Value = $\left[\frac{9000}{W_1}\right] \times (V_{15} - Vs_{15} - Vs_1 - V_1)$

    where,
    W_1 = Initial sample mass, g
    Vs_1 = Water volume reading at 60 s from the standardization test, mL
    Vs_{15} = Water volume reading at 15 min from the standardization test, mL
    V_0 = Initial water volume reading, mL
    V_1 = Water volume reading at 60 s, mL
    V_{15} = Water volume reading at 15 min, mL

13. Run the calibration test before each sample test to determine expansion.

System Setup Reference

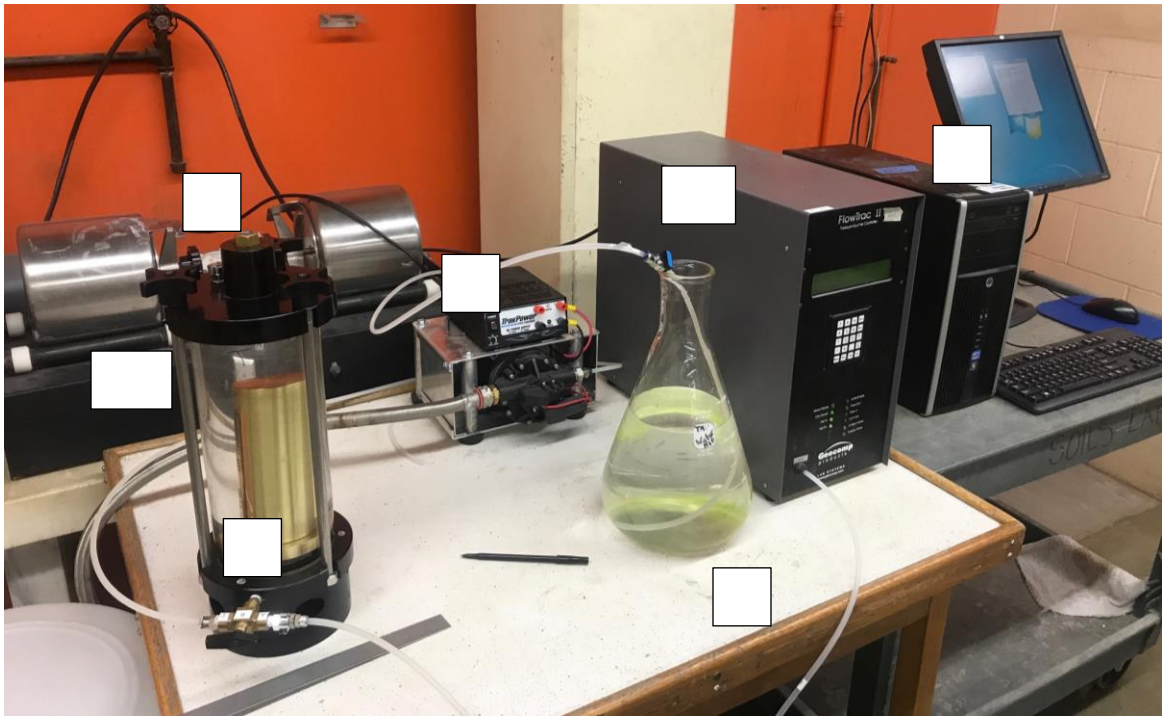

Figure 30. IPI (Generation 3) system setup

Chamber and Associated Equipment

- IPI Apparatus
  - FlowTrac-II system
  - Sample chamber
- Computer with FlowTrac-II triaxial software installed
- Calibration/pot expansion cylinder
- Water pump for initial filling of sample chamber
- Deionized water
- 1,000 ml Erlenmeyer flask
- Pressure release valve

THE INSTITUTE FOR TRANSPORTATION IS THE FOCAL POINT FOR TRANSPORTATION AT IOWA STATE UNIVERSITY.

InTrans centers and programs perform transportation research and provide technology transfer services for government agencies and private companies;

InTrans contributes to ISU's educational programs for transportation students and provides K–12 outreach; and

InTrans conducts local, regional, and national transportation services and continuing education programs.

IOWA STATE UNIVERSITY

Visit **InTrans.iastate.edu** for color pdfs of this and other research reports.